

# VISVESVARAYA TECHNOLOGICAL UNIVERSITY

“JNANA SANGAMA” BELAGAVI, KARNATAKA-590 018



2020-2021

## PROJECT REPORT ON

“ELECTRIC PROPULSION SYSTEM FOR POCKETQUBE AND CUBESATS”

*Submitted in the partial fulfilment of the award of the Degree in*

“B.E IN AEROSPACE ENGINEERING”

*Submitted by*

RUTHVIK VIJAYKUMAR JOSHI - 1AH17AS026

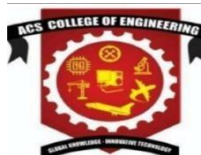
SARVESH J - 1AH17AS029

**Under the Guidance of**

**Mr. KARTHIKEYAN P**

Assistant Professor

Department of Aerospace Engineering.



**DEPARTMENT OF AEROSPACE ENGINEERING**

**ACS COLLEGE OF ENGINEERING,**

**Kambipura, Mysore Road, Bangalore-74**

**ACS COLLEGE OF ENGINEERING**  
**Kambipura Mysore Road, Bangalore 560 074**  
**DEPARTMENT OF AEROSPACE ENGINEERING**



**CERTIFICATE**

This is to certify that the dissertation work entitled "**ELECTRIC PROPULSION SYSTEM FOR POCKETQUBE AND CUBESATS**" is a bonafide work carried out by, **MR RUTHVIK VIJAYKUMAR JOSHI, MR SARVESH J** bearing university serial number **1AH17AS026, 1AH17AS029** respectively, in partial fulfillment of award of the degree of **Bachelor of Engineering in Aerospace Engineering**, from **Visvesvaraya Technological University, Belagavi** during the year **2020-2021**. The project report has been approved as it satisfies the academic requirement in respect of Project work prescribed for the degree.

---

**Signature of guide**

Mr. KARTHIKEYAN P  
Assistant Professor  
Dept. of Aerospace Engineering  
ACSCE- Bangalore

---

**Signature of HOD**

Dr. P R MUKESH  
Prof. & HOD  
Dept. of Aerospace Engineering  
ACSCE- Bangalore

---

**Signature of Principal**

Dr. M.S MURALI  
Principal  
ACSCE- Bangalore

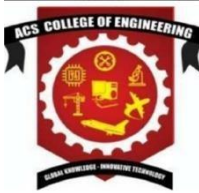
**Name of the Examiner**

1. \_\_\_\_\_  
2. \_\_\_\_\_

**Signature**

1. \_\_\_\_\_  
2. \_\_\_\_\_

**ACS COLLEGE OF ENGINEERING**  
**Kambipura Mysore Road, Bangalore 560 074**  
**DEPARTMENT OF AEROSPACE ENGINEERING**



**DECLARATION**

We, **RUTVHIK VIJAYKUMAR JOSHI, SARVESH J** the students of 8<sup>th</sup> semester of Aerospace Engineering, **ACS College of Engineering, Bangalore-560074**, declare that the work entitled "**ELECTRIC PROPULSION SYSTEM FOR POCKETQUBE AND CUBESATS**" has been successfully completed under the guidance of **Mr. KARTHIKEYAN P**, ACS College of Engineering, Bangalore. This dissertation work is submitted to Visvesvaraya Technological University in partial fulfillment of the requirements for the award of Degree of **Bachelor of Engineering in Aerospace Engineering** during the academic year **2020-2021**. Further the matter embodied in the project report has not been submitted previously by anybody for the award of any degree or diploma to any university.

RUTHVIK VIJAYKUMAR JOSHI (1AH17AS026)

SARVESH J (1AH17AS029)

Place: Bangalore

Date:

## **ACKNOWLEDGMENT**

The satisfaction and euphoria that accompany the successful completion of any task would be incomplete without the mention of the people who made it possible, because success is the epitome of hard work and perseverance, but steadfast of all encouraging guidance. So with gratitude I acknowledge all those whose guidance and encouragement served us as a beacon light and crowned our effort with success.

I would like to express our earnest appreciation to **Dr. M.S MURALI**, Principal ACSCE, for his valuable support

We would like to express our deep sense of gratitude to **Dr. P R MUKESH**, Prof. & Head of the Department, Department of Aerospace Engineering, ACSCE for providing good facilities, constant encouragement and valuable guidance.

We would also like to express our deep sense of gratitude to **Mr. KARTHIKEYAN P**, Assistant Professor, Dept. of Aerospace Engineering, who guided us to carry out this project, for their exemplary guidance, valuable suggestions, expert advice and encouragement

With immense pleasure, I would like to express our profound gratitude and regards to teaching and non-teaching staff, Dept. of Aerospace Engineering, ACSCE, Bangalore for their valuable support and guidance extended to us throughout the course of our project work

Finally, I thank our friends and all those who have assisted us directly or indirectly at various stages of the project.

## **ABSTRACT**

A satellite is an object that has been intentionally placed into orbit. These objects are called artificial satellites to distinguish them from natural satellites such as Earth's Moon. Cost of putting mass in space is about 14000 dollars per pound of weight. Therefore, reducing the weight while not giving up on functionality is a primary requirement of satellites. In recent years, miniaturization and cost reduction in the field of electronics has facilitated manufacturing and operating satellites which are much smaller than conventional satellites for certain applications such as earth observation, amateur radio and are also used to demonstrate technologies intended for use on larger more expensive conventional satellites. Smaller satellites which weigh less than 10kg are called CubeSats. Conventional chemical propulsion systems require plumbing, storage tanks, flow control mechanisms which cannot be accommodated on to a CubeSat due to its lack of available space on board. This limits their life cycle and operability even though they have a large potential in terms of technology. However, few of the electric propulsion units can be used to provide the CubeSats with the thrust which allows it to maintain orbit, have attitude control and for other requirements. This project presents the conceptual design of a micro-Pulsed Plasma Thruster (micro-PPT) an electric propulsion unit and a propulsion module consisting of eight micro-PPTs to be used on a CubeSat. The computer-aided mechanical design of the micro-PPT, the propulsion module and its integration in the 1U are presented.

# Table of Contents

Acknowledgement	iii
Abstract	iv
Table of Contents	v
Table of Figures	vii
Table of Tables	xiv
Table of Authorship	xv
<b>CHAPTER 1: INTRODUCTION</b>	<b>1</b>
Types of Satellites	1
1.1 Classification of Satellites Based on Function	1
1.2 Classification of Satellites Based on Size	4
1.3 Electric Propulsion Systems	5
1.3.1 Classification of Electric Propulsion Systems	5
1.3.1.1 Ion and Plasma Drives	6
1.3.1.2 Non-Ion Drives	7
1.4 Pulsed Plasma Thrusters	8
1.4.1 Working of Pulsed Plasma Thrusters (PPT)	8
1.5 Software Packages Used	10
<b>CHAPTER 2: LITERATURE SURVERY</b>	<b>11</b>
<b>CHAPTER 3: METHODOLOGY AND PROBLEM IDENTIFICATION</b>	<b>14</b>
3.1 Methodology	14
3.2 Problem Identification	15
3.3 Objectives and Scope	15
3.3.1 Objectives	15
3.3.2 Scope	15
<b>CHAPTER 4: MECHANICAL DESIGN</b>	<b>16</b>
4.1 Mechanical Design Requirements	16
4.2 Conceptual Designs	17
4.2.1 First Conceptual Design	18
v	
4.2.1.1 Limitation of First Conceptual Design	19
4.2.2 Second Conceptual Design	19

4.3 Material Selection	20
<b>CHAPTER 5: ANALYSIS, RESULTS AND CONCLUSIONS</b>	<b>24</b>
5.1 Ansys Structural Analysis	24
5.1.1 Modal Analysis	25
5.1.2 Random Vibration	32
5.2 Electrical Analysis	63
5.2.1 Vacuum Arc Ignition Circuit	65
5.3 Thermal Analysis of Fuel Block	67
5.3.1 Heat Transfer in Solids	67
5.3.2 Meshing	69
5.4 STK Integration	84
5.4.1 Solar Panel Groups	85
5.4.2 Creating Ancillary Files	86
5.4.3 Implementation in STK	88
5.4.3.1 Orbit Transfer using STK Astrogator	93
5.4.3.2 Orbit Transfer using Finite Manoeuvre type	95
5.4.3.3 Manoeuvre Summary	102
5.4.4 Lifetime Analysis	106
5.4.5 SEET (Space Environment and Effect Tool)	111
5.4.6 Satellite Temperature	114
5.5 Conclusion	116
<b>REFERENCES</b>	<b>118</b>

## Table of Figures

<b>Figure No.</b>	<b>Description</b>	<b>Page No.</b>
<b>Fig 1.1</b>	Hubble telescope	1
<b>Fig 1.2</b>	Sputnik 2	2
<b>Fig 1.3</b>	ERS 2	2
<b>Fig 1.4</b>	Orion satellite	3
<b>Fig 1.5</b>	GPS Constellation	3
<b>Fig 1.6</b>	CubeSat Configurations	5
<b>Fig 1.7</b>	Hall Effect Thruster	6
<b>Fig 1.8</b>	Arcjet Schematic	7
<b>Fig 1.9</b>	Pulsed Plasma Thruster Schematic	7
<b>Fig 1.10</b>	Variants of PPTs	9
<b>Fig 4.1</b>	1U Satellite Design Specifications	17
<b>Fig 4.2</b>	1U CubeSat	18
<b>Fig 4.3</b>	First Conceptual Design	18
<b>Fig 4.4</b>	Second Conceptual Design	19
<b>Fig 5.1</b>	General Environmental Verification Standard for Random Vibration	24
<b>Fig 5.2</b>	Modal Analysis of PPT mounted on base plate	25
<b>Fig 5.3</b>	1 <sup>st</sup> Mode Shape Isometric View of single PPT mounted on baseplate	27
<b>Fig 5.4</b>	1 <sup>st</sup> Mode Shape Front View of single PPT mounted on baseplate	27
<b>Fig 5.5</b>	2 <sup>nd</sup> Mode Shape Isometric View of single PPT mounted on baseplate	28
<b>Fig 5.6</b>	2 <sup>nd</sup> Mode Shape Front View of single PPT mounted on baseplate	28
<b>Fig 5.7</b>	3 <sup>rd</sup> Mode shape Isometric View of single PPT mounted on baseplate	29
<b>Fig 5.8</b>	3 <sup>rd</sup> Mode Shape Front View of single PPT mounted on baseplate	29

<b>Fig 5.9</b>	4 <sup>th</sup> Mode Shape Isometric View of single PPT mounted on baseplate	30
<b>Fig 5.10</b>	4 <sup>th</sup> Mode Shape Front View of single PPT mounted on baseplate	30
<b>Fig 5.11</b>	5 <sup>th</sup> Mode Shape Isometric View of single PPT mounted on baseplate	31
<b>Fig 5.12</b>	5 <sup>th</sup> Mode Shape Front View of single PPT mounted on baseplate	31
<b>Fig 5.13</b>	Random Vibration Chart	32
<b>Fig 5.14</b>	Random Vibration Input Values and Graph	33
<b>Fig 5.15</b>	(X-Axis Test) X-Axis Deformation 1 Sigma	34
<b>Fig 5.16</b>	(X-Axis Test) X-Axis Deformation 2 Sigma	34
<b>Fig 5.17</b>	(X-Axis Test) X-Axis Deformation 3 Sigma	35
<b>Fig 5.18</b>	(X-Axis Test) Y-Axis Deformation 3 Sigma	35
<b>Fig 5.19</b>	(X-Axis Test) Z-Axis Deformation 3 Sigma	36
<b>Fig 5.20</b>	Equivalent Stresses for Case 1.1	36
<b>Fig 5.21</b>	(Y-Axis Test) X Axis deformation 3 Sigma	37
<b>Fig 5.22</b>	(Y-Axis Test) Y Axis deformation 3 Sigma	37
<b>Fig 5.23</b>	(Y-Axis Test) Z Axis deformation 3 Sigma	38
<b>Fig 5.24</b>	Equivalent Stresses for Case 1.2	38
<b>Fig 5.25</b>	(Z-Axis Test) X Axis deformation 3 Sigma	39
<b>Fig 5.26</b>	(Z-Axis Test) Y Axis deformation 3 Sigma	39
<b>Fig 5.27</b>	(Z-Axis Test) Z Axis deformation 3 Sigma	40
<b>Fig 5.28</b>	Equivalent Stresses for Case 1.3	40
<b>Fig 5.29</b>	4 PPTs Mounted on Base Plate	41
<b>Fig 5.30</b>	4 PPTs Mounted on Base Plate Top View	41
<b>Fig 5.31</b>	1 <sup>st</sup> Mode Shape of 4 PPT's mounted on baseplate	42
<b>Fig 5.32</b>	2 <sup>nd</sup> Mode Shape of 4 PPT's mounted on baseplate	42
<b>Fig 5.33</b>	3 <sup>rd</sup> Mode Shape of 4 PPT's mounted on baseplate	43

<b>Fig 5.34</b>	4 <sup>th</sup> Mode Shape of 4 PPT's mounted on baseplate	43
<b>Fig 5.35</b>	5 <sup>th</sup> Mode Shape of 4 PPT's mounted on baseplate	44
<b>Fig 5.36</b>	(X-Test) Random Vibration Acting on X-Axis	45
<b>Fig 5.37</b>	(X-Test) Random Vibration Acting on Y-Axis	45
<b>Fig 5.38</b>	(X-Test) Random Vibration Acting on Z-Axis	46
<b>Fig 5.39</b>	Equivalent Stresses Acting on X-Axis	46
<b>Fig 5.40</b>	(Y-Test) Random Vibration Acting on X-Axis	47
<b>Fig 5.41</b>	(Y-Test) Random Vibration Acting on Y-Axis	47
<b>Fig 5.42</b>	(Y-Test) Random Vibration Acting on Z-Axis	48
<b>Fig 5.43</b>	Equivalent Stresses Acting on Y-Axis	48
<b>Fig 5.44</b>	(Z-Test) Random Vibration Acting on X-Axis	49
<b>Fig 5.45</b>	(Z-Test) Random Vibration Acting on Y-Axis	49
<b>Fig 5.46</b>	(Z-Test) Random Vibration Acting on Z-Axis	50
<b>Fig 5.47</b>	Equivalent Stresses Acting on Z-Axis	50
<b>Fig 5.48</b>	1 <sup>st</sup> and 2 <sup>nd</sup> Mode Shapes of CubeSat frame and thruster	52
<b>Fig 5.49</b>	3 <sup>rd</sup> and 4th Mode Shapes of CubeSat frame and thruster	53
<b>Fig 5.50</b>	5 <sup>th</sup> and 6 <sup>th</sup> Mode Shapes of CubeSat frame and thruster	54
<b>Fig 5.51</b>	7 <sup>th</sup> and 8 <sup>th</sup> Mode Shapes of CubeSat frame and thruster	55
<b>Fig 5.52</b>	9 <sup>th</sup> and 10 <sup>th</sup> Mode Shapes of CubeSat frame and thruster	56
<b>Fig 5.53</b>	(X-Axis Test) Random Vibration Acting on X-Axis and Y-Axis	57
<b>Fig 5.54</b>	(X-Axis Test) Random Vibration Acting on Z-Axis and Equivalent Stresses for case 3.1	58
<b>Fig 5.55</b>	(Y-Axis Test) Random Vibration Acting on X-Axis and Y-Axis	59
<b>Fig 5.56</b>	(Y-Axis Test) Random Vibration Acting on Z-Axis and Equivalent Stresses for case 3.2	60
<b>Fig 5.57</b>	(Z-Axis Test) Random Vibration Acting on X-Axis and Y-Axis	61
<b>Fig 5.58</b>	(Z-Axis Test) Random Vibration Acting on Z-Axis and Equivalent Stresses for case 3.3	62

<b>Fig 5.59</b>	Vacuum Ignition Circuit	65
<b>Fig 5.60</b>	Input Pulse Signal	66
<b>Fig 5.61</b>	Marx Circuit Output	66
<b>Fig 5.62</b>	COMSOL Interface	68
<b>Fig 5.63</b>	COMSOL Mesh Settings	69
<b>Fig 5.64</b>	Time = 0 Seconds	70
<b>Fig 5.65</b>	Time = 1 Second	70
<b>Fig 5.66</b>	Time = 2 Seconds	70
<b>Fig 5.67</b>	Time = 4 Seconds	71
<b>Fig 5.68</b>	Time = 6 Seconds	71
<b>Fig 5.69</b>	Time = 10 Seconds	71
<b>Fig 5.70</b>	Time = 20 Seconds	72
<b>Fig 5.71</b>	Time = 80 Seconds	72
<b>Fig 5.72</b>	Time = 200 Seconds	72
<b>Fig 5.73</b>	Time = 1200 Seconds	73
<b>Fig 5.74</b>	Time = 1560 Seconds	73
<b>Fig 5.75</b>	(Iso) Time = 0 Seconds	74
<b>Fig 5.76</b>	(Iso) Time = 1 Second	74
<b>Fig 5.77</b>	(Iso) Time = 2 Seconds	75
<b>Fig 5.78</b>	(Iso) Time = 4 Seconds	75
<b>Fig 5.79</b>	(Iso) Time = 6 Seconds	75
<b>Fig 5.80</b>	(Iso) Time = 10 Seconds	76
<b>Fig 5.81</b>	(Iso) Time = 20 Seconds	76
<b>Fig 5.82</b>	(Iso) Time = 80 Seconds	76
<b>Fig 5.83</b>	(Iso) Time = 200 Seconds	77

<b>Fig 5.84</b>	(Iso) Time = 1200 Seconds	77
<b>Fig 5.85</b>	(Iso) Time = 1560 Seconds	77
<b>Fig 5.86</b>	Meshing of Prototype and Base Plate	78
<b>Fig 5.87</b>	(1 Prototype) Time = 0 Seconds	78
<b>Fig 5.88</b>	(1 Prototype) Time = 200 Seconds	79
<b>Fig 5.89</b>	(1 Prototype) Time = 1200 Seconds	79
<b>Fig 5.90</b>	(1 Prototype) Time = 2000 Seconds	79
<b>Fig 5.91</b>	Meshing of 4 Prototypes on Base Plate	80
<b>Fig 5.92</b>	(4 Prototype) Time = 0 Seconds	80
<b>Fig 5.93</b>	(4 Prototype) Time = 20 Seconds	81
<b>Fig 5.94</b>	(4 Prototype) Time = 80 Seconds	81
<b>Fig 5.95</b>	(4 Prototype) Time = 200 Seconds	82
<b>Fig 5.96</b>	(4 Prototype) Time = 800 Seconds	82
<b>Fig 5.97</b>	(4 Prototype) Time = 1200 Seconds	83
<b>Fig 5.98</b>	(4 Prototype) Time = 2000 Seconds	83
<b>Fig 5.99</b>	Final Rendered CAD Model of CubeSat with Prototypes in Blender	84
<b>Fig 5.100</b>	Solar Cells Grouping in Blender	85
<b>Fig 5.101</b>	Collada file Opened in Notepad++	86
<b>Fig 5.102</b>	Solar Panels Group and Assigned Nodes	87
<b>Fig 5.103</b>	CubeSat Model Implementation in STK	88
<b>Fig 5.104</b>	Solar Panel Tool in STK	89
<b>Fig 5.105</b>	Solar Panel Power Profile	89
<b>Fig 5.106</b>	CubeSat Model with its body Axes and a Vector Pointing the Sun	91
<b>Fig 5.107</b>	Power Profile at 20° Inclination	92
<b>Fig 5.108</b>	Power Profile at 0° Inclination	92

<b>Fig 5.109</b>	Initial Orbit	93
<b>Fig 5.110</b>	Transfer Orbit	94
<b>Fig 5.111</b>	Final Orbit	94
<b>Fig 5.112</b>	Hohmann Transfer	95
<b>Fig 5.113</b>	Engine Model: Pulsed Plasma Thruster	96
<b>Fig 5.114</b>	Spacecraft Parameters and Fuel Tank	96
<b>Fig 5.115</b>	Thruster Attitude, Engine and Propagator	97
<b>Fig 5.116</b>	Stopping Sequence	98
<b>Fig 5.117</b>	Initial State of CubeSat	99
<b>Fig 5.118</b>	Apogee Raise Propagate Segment options	100
<b>Fig 5.119</b>	Perigee Raise Propagate Segment options	100
<b>Fig 5.120</b>	Apogee Raise Propagate Segment	101
<b>Fig 5.121</b>	Perigee Raise Propagate Segment	101
<b>Fig 5.122</b>	CubeSat Iterations Around Earth	101
<b>Fig 5.123</b>	Apogee V/S Perigee Radius Increment Over Time	105
<b>Fig 5.124</b>	Low Drag V/S High Drag Configuration	106
<b>Fig 5.125</b>	Lifetime Analysis Tool in STK	107
<b>Fig 5.126</b>	Lifetime of CubeSat at 400 km	108
<b>Fig 5.127</b>	Lifetime Graph of CubeSat at 400 km	108
<b>Fig 5.128</b>	Lifetime of CubeSat at 450 km	109
<b>Fig 5.129</b>	Lifetime Graph of CubeSat at 450 km	109
<b>Fig 5.130</b>	CubeSat After Orbital Transfer	110
<b>Fig 5.131</b>	Lifetime Graph of CubeSat After Orbit Transfer	110
<b>Fig 5.132</b>	SEET Conditions	111
<b>Fig 5.133</b>	SEET Thermal Model	111

<b>Fig 5.134</b>	Magnetic Field Model	111
<b>Fig 5.135</b>	Galactic Cosmic Ray	112
<b>Fig 5.136</b>	Particle Flux Model	112
<b>Fig 5.137</b>	Magnetic Field (B Field vs Total Intensity F)	113
<b>Fig 5.138</b>	CubeSat Temperature	114

## Table of Tables

<b>Table No.</b>	<b>Description</b>	<b>Page No.</b>
<b>Table 2.1</b>	Literature review	11
<b>Table 4.1</b>	Values for initial CES selection stage.	21
<b>Table 4.2</b>	Erosion characteristics of electrode materials.	21
<b>Table 4.3</b>	Torlon 4203 Data Sheet (All-state Industries)	23
<b>Table 5.1</b>	Material Properties and Mesh Statistics	26
<b>Table 5.2</b>	Case 1 Mode and Frequency	26
<b>Table 5.3</b>	PSD Acceleration Values for Random Vibration Test	33
<b>Table 5.4</b>	Case 2 Mode and Frequency	44
<b>Table 5.5</b>	Case 3 Mode and Frequency	51
<b>Table 5.6</b>	Methods for Vacuum Arc Ignition	64
<b>Table 5.7</b>	All Solar Panel Group Power Generated in Watts	90
<b>Table 5.8</b>	Apogee Raise Manoeuvre Summary	102
<b>Table 5.9</b>	Perigee Raise Manoeuvre Summary	103
<b>Table 5.10</b>	Apogee Raise Statistics	104
<b>Table 5.11</b>	Perigee Raise Statistics	104
<b>Table 5.12</b>	Typical Values of Solar cell Used in Thermal Mode	113
<b>Table 5.13</b>	Operating Temperature and Survival Temperature	114
<b>Table 5.14</b>	Satellite Temperature	115

## **Table of Authorship**

Introduction	Both
Background and Literature Survey	Both
Mechanical Model design	Both
Structural Analysis	Sarvesh. J (1AH17AS029)
Electric Analysis	Ruthvik Vijaykumar Joshi (1AH17AS026)
Thermal Analysis	Sarvesh. J (1AH17AS029)
STK Integration	Sarvesh. J (1AH17AS029)
Conclusion	Both

# **CHAPTER 1**

## **INTRODUCTION**

The history of artificial satellites began when Soviet Union put Sputnik into orbit on 4<sup>th</sup> October 1957. Since then, multiple nations have launched multiple satellites amounting to about 6000 satellites orbiting our planet, of which according to The Union of Concerned Scientists (UCS) 2666 satellites are operational while the rest are space junk.

### **Types of Satellites**

Satellites are classified based on their function and size.

#### **1.1 Classification of Satellites Based on Function**

Satellites are classified as Astronomical Satellites, Biosatellites, Earth-Observation satellites, Communication satellites and Navigational satellites based on their function.

- **Astronomical satellites**

Astronomical satellites also called as space telescopes are used to observe distant objects in space. Example: Hubble Space Telescope.



Fig 1.1: Hubble Telescope

- **Biosatellites**

Biosatellites carry biological matter such as plants and animals into space for research purposes. Primary research conducted in Biosatellites are related to the effect of space environment on biomatter. Example: Sputnik 2



Fig 1.2: Sputnik 2

- **Earth-Observation Satellites**

Earth-Observation satellites or Earth Remote Sensing satellites are used for multiple functions including spying, environment monitoring, meteorology, etc. Example: European Remote Sensing (ERS) Satellite series.



Fig 1.3: ERS 2

- **Communication Satellites**

A communication satellite uses a transponder to relay and amplify telecommunication signals. These satellites are usually placed in Geo-synchronous orbit (35,785 km above the equator). Example: Orion.



Fig 1.4: Orion Satellite

- **Navigation Satellites**

Navigation satellites are satellites which use radio time signals transmitted to enable mobile receivers on the ground to determine their exact location. These satellites operate in constellations to accomplish their purpose. Example: Global Positioning System



Fig 1.5: GPS Constellation

## 1.2 Classification of Satellites Based on Size

Satellites are classified as Large satellites, Medium satellites, and Small satellites.

- **Large Satellites**

Large satellites have their mass greater than 1000kg.

- **Medium Satellites**

Medium satellites have their mass between 500kg and 1000kg.

- **Small Satellites**

Small Satellites consist of further classifications based on their masses, minisatellites:

100kg-500kg, microsatellite: 10kg-100kg, nanosatellite: 1kg-10kg, picosatellites:  
<1kg.

The Small satellites which have a mass less than 10kg are called as CubeSats and they are all based on the standard CubeSat unit, namely **a cube-shaped structure measuring 10x10x10 centimeters** with a mass of 1kg-1.33kg. This unit is called 1U. After the first few years, this modular unit was multiplied and larger nanosatellites are now common (**1.5U, 2U, 3U, 6U, 12U**). Today, new configurations are under development.

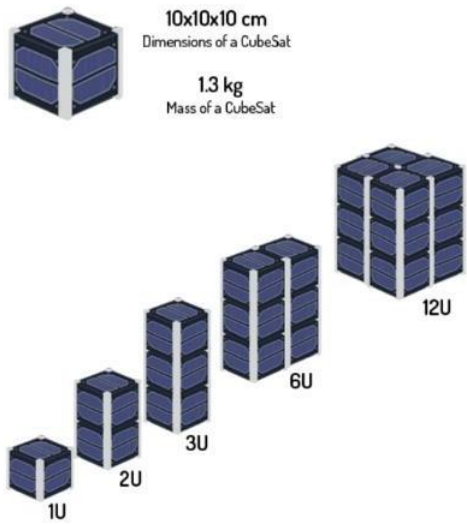


Fig 1.6: CubeSat Configurations

The CubeSats that are deployed today do not have any propulsion system which limits their functionality. Few of the electric propulsion systems which are explained in detail below can be used to overcome this limitation.

## 1.3 Electric Propulsion Systems

The idea of using electric propulsion for spacecrafts was proposed in 1911 by Konstantin Tsiolkovsky. Electrically powered propulsion systems use electrical and possibly also magnetic fields to provide thrust to the spacecraft. They typically expel propellants (reaction mass) electrically at very high speed to generate thrust. The higher exhaust velocity (higher specific impulse) than chemical rockets means that the system uses much less propellant compared to chemical rockets.

Due to limited electrical power available, the thrust produced by electric propulsion systems is very low, however, they can provide the thrust for a longer time which in due time translates to the space craft having very high velocities.

### 1.3.1 Classification of Electric Propulsion Systems

The Electric Propulsion Systems are broadly classified into Ion and Plasma Drives and Non-Ion Drives.

### **1.3.1.1 Ion and Plasma Drives**

These types of Electric Propulsion Systems are reaction engines similar to rockets and produce thrust by using the propellant carried with the spacecraft. Ion and Plasma drives are classified into three types based on the working principle, Electrostatic, Electrothermal and Electromagnetic.

- **Electrostatic**

If Coulombs force is the main cause for the acceleration in the spacecraft, then the system is said to be Electrostatic. Examples: Grid ion thruster, Hall-effect thruster, Colloid ion thruster, Field Emission Electric Propulsion, Nano-Particle Field Extraction thruster.

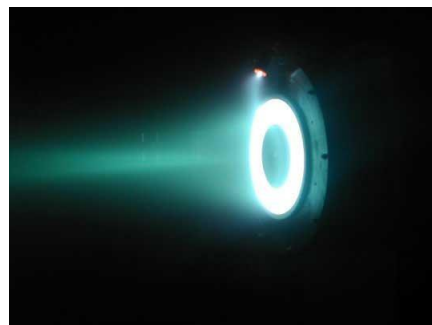


Fig 1.7: Hall-Effect thruster

- **Electrothermal**

In an Electrothermal thruster, electric fields are used to generate plasma to increase the temperature of the bulk propellant. The thermal energy imparted to the propellant is now converted to kinetic energy by either using nozzles or by magnetic fields. Examples: Arcjet, Microwave Arcjet, Resistojet, Variable Specific Impulse Magnetoplasma Rocket (VASIMR).

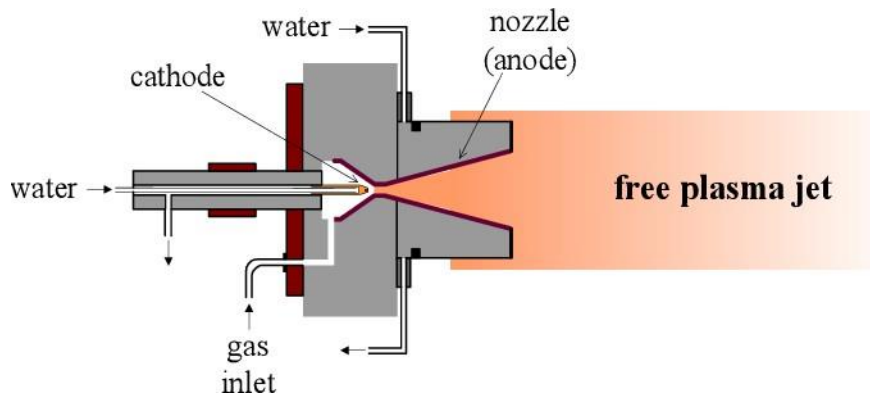


Fig 1.8: Arcjet Schematic

- **Electromagnetic**

In Electromagnetic thrusters, ions are accelerated by Lorentz force or by electromagnetic field where the electric fields are not in the direction of acceleration. Examples: Electrodeless plasma thruster, magnetoplasmadynamic thruster, Pulsed inductive thruster, Pulsed plasma thruster, Helicon double layer thruster.

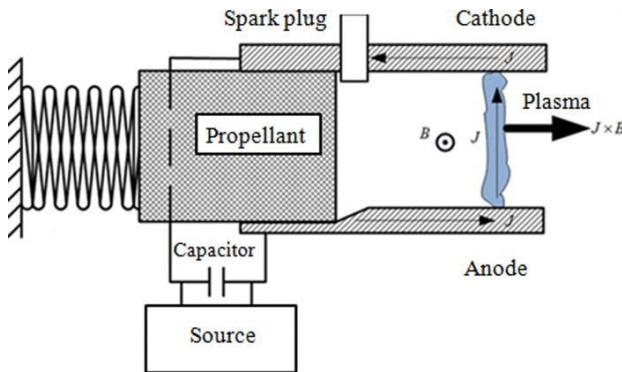


Fig 1.9: Pulsed Plasma Thruster Schematic

### 1.3.1.2 Non-Ion Drives

Non-Ion Drives have two technologies under development and study, Photon Drivers and Electromagnetic Tethers.

- **Photonic Drivers**

In photonic drivers, the acceleration is generated by expelling photons. Examples: Laser Propulsion, Photonic Laser Thruster, Photonic Rocket.

- **Electromagnetic Tethers**

Electrodynamic tethers are long conducting wires, such as one deployed from a tether satellite, which can operate on electromagnetic principles as generators, by converting their kinetic energy to electrical energy, or as motors, converting electric energy to kinetic energy. Electric potential is generated across a conductive tether by its motion through the Earth's magnetic field.

## 1.4 Pulsed Plasma Thrusters

On November 30, 1964, the Zond 2 spacecraft was launched toward Mars from Baikonur in the Soviet Union. Several months later, radio communication was lost, and with it control of the electric propulsion system designed to provide three axis attitude control. The Zond 2 pulsed plasma thrusters (PPTs) were the first application of electric propulsion on any spacecraft. Since then, during the past several decades, the research and development of electric propulsion has embraced a great variety of candidate systems of pulsed plasma thrusters.

### 1.4.1 Working of Pulsed Plasma Thrusters (PPT)

Most PPTs use a solid material (normally PTFE, more commonly known as Teflon) for propellant, although very few use liquid or gaseous propellants. The first stage in PPT operation involves an arc of electricity passing through the fuel, causing ablation and sublimation of the fuel. The heat generated by this arc causes the resultant gas to turn into plasma, thereby creating a charged gas cloud. Due to the force of the ablation, the plasma is propelled at low speed between two charged plates (an anode and cathode). Since the plasma is charged, the fuel effectively completes the circuit between the two plates, allowing a current to flow through the plasma. This flow of electrons generates a strong electromagnetic field which then exerts a Lorentz force on the plasma, accelerating the plasma out of the PPT exhaust at high velocity.

The pulsing occurs due to the time needed to recharge the plates following each burst of fuel, and the time between each arc. The energy used in each pulse is stored in a capacitor. By varying the time between each capacitor discharge, the thrust and power draw

of the PPT can be varied allowing versatile use of the system. The frequency of pulsing is normally very high and so it generates an almost continuous and smooth thrust. While the thrust is very low, a PPT can operate continuously for extended periods of time, yielding a large final speed.

Variants of the PPT include the so-called “side-fed” system, which can be used in rectangular or coaxial geometry, uses two propellant bars, advanced from opposite sides. Coaxial PPT arrangement was originally developed in the form of magnetoplasmadynamic devices and is now part of the PPT family.

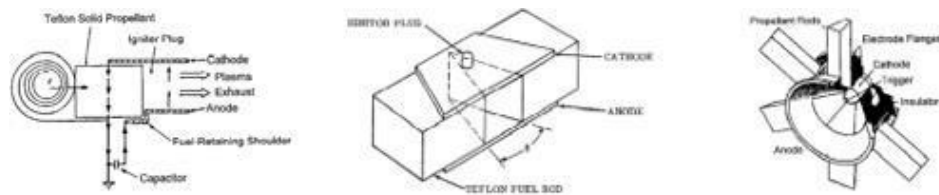


Fig 1.10: Variations of PPTs

## **1.5 Software Packages Used**

- Solidworks
- Catia V5
- Ansys 2019 R3
  - Modal
  - Random Vibrations
- COMSOL
  - Heat transfer in Solids
- AGI: STK
  - Solar panels power profile
  - Orbital analysis
  - Propulsion model integration
  - Lifetime
  - SEET (Space Environment and Effect Tool)
  - Satellite temperature
- Blender 3D

## CHAPTER 2

### LITERATURE SURVEY

This chapter outlines some work and report available in the past related to pulsed plasma thrusters and talks about few properties related to optimization of PPTs and the development of PPT's for Nanosatellites

Table 2.1: Literature Survey

SL.NO	AUTHORS	TITLE	JOURNAL NAME & PUBLISHED YEAR	CONCLUSION
1.	W. A. Hoskins and R. J. Cassady	APPLICATIONS FOR PULSED PLASMA THRUSTERS AND THE DEVELOPMENT OF SMALL PPTs FOR MICRO SPACECRAFT	AIAA-2000-3434 36th AIAA/ASME/S AE/ASEE Joint Propulsion Conference and Exhibit	<p>There is a wide and evolving set of missions for which the PPT is well suited.</p> <p>Station keeping for Little LEO and Government LEO Constellations represent one of the strongest potentials for PPT application. MEO missions such as GPS Station keeping and ACS (Advanced Camera for Surveys) are also well within the capability of present systems.</p> <p>In addition to these conventional missions, PPTs represent the strongest propulsion option for micro spacecraft. To meet this need, it is imperative that a new 10 W class of PPT be developed.</p>

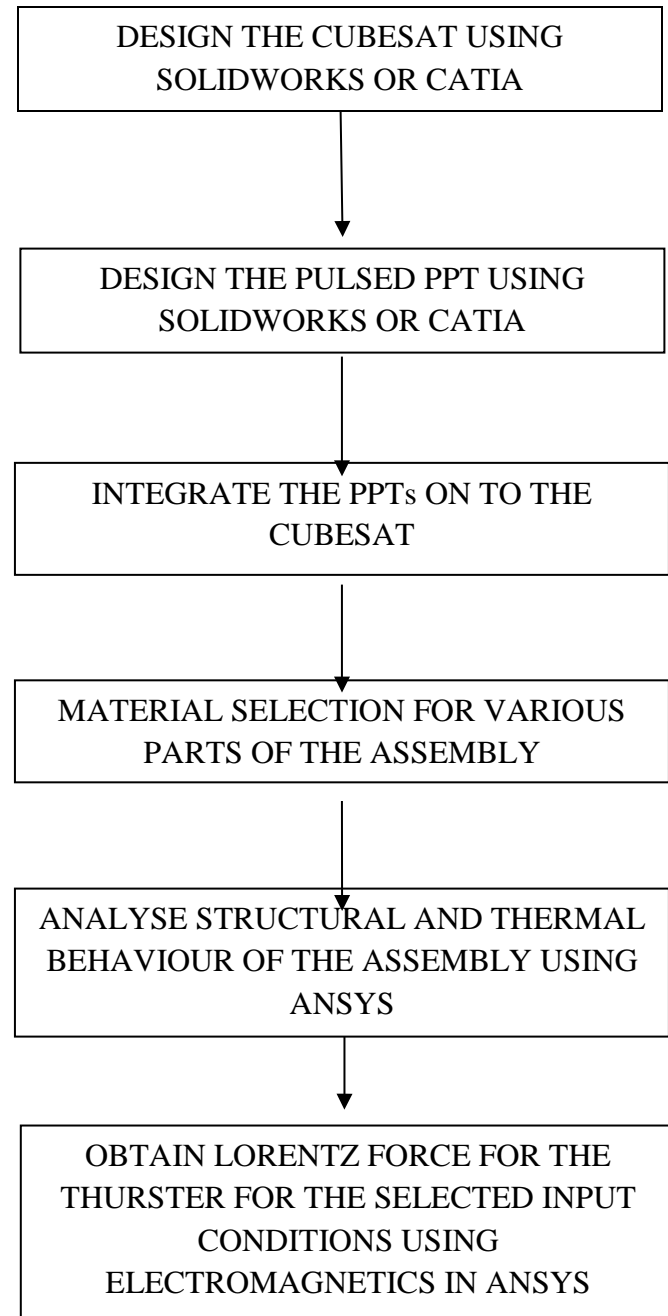
<b>SLNO.</b>	<b>AUTHORS</b>	<b>TITLE</b>	<b>JOURNAL NAME &amp; PUBLISHED YEAR</b>	<b>CONCLUSION</b>
2.	Zhiwen Wu, Guorui Sun, Tiankun Huang, Xiangyang Liu, Kan Xie, and Ningfei Wang	Optimization of the Energy Distribution in Ablative Pulsed Plasma Thrusters (APPT <sub>s</sub> )”	AIAA JOURNAL 2018	<p>APPTs which were the earliest electric propulsion systems, have low thrust efficiencies. In our study, a double-discharge ablative pulsed plasma thruster (DD-APPTs) that allocates the same total energy to two capacitors and discharges at different locations was designed.</p> <p>The DD-APPT performance was significantly improved compared to that of a regular APPT in which all the energy is stored in a capacitor.</p> <p>For a constant total energy, as the energy allocated to the secondary capacitor increased, both the thrust efficiency and specific impulse increased significantly</p>
3.	Linghan Zeng Zhiwen Wu, Guorui Sun, Tiankun Huang, Xiangyang Liu, Kan Xie, and Ningfei Wang	A new ablation model for ablative pulsed plasma thrusters	Acta Astronautica 160 (2019) 317-322 2019	<p>The model has been found to be a very useful tool for the evaluation of the ablated mass bit of APPTs. The model is based on the random degradation of molecular chains in PTFE and statistical methods. The obtained theoretical results for the ablated mass bit show good agreement with the results from experimental studies. The average relative error ranges from approximately -15.7% to 12.4%. The model has the following additional applications:</p> <ul style="list-style-type: none"> <li>(1) Conducting a preliminary performance evaluation of a new version of an APPT.</li> <li>(2) Permitting the incorporation of more developed sub models.</li> </ul>

SLNO.	AUTHORS	TITLE	JOURNAL NAME & PUBLISHED YEAR	CONCLUSION
4.	Ephraim Chen	Gas-Fed Pulsed Plasma Thrusters: From Spark Plugs to Laser Initiation (GFPPT)"	Electric Propulsion and Plasma Dynamics Laboratory (EPPDyL) 2006	After wrestling with the various electronic components for a spark plug-initiated GFPPT, one must conclude that it is very difficult to use spark plugs for precisely-timed, consistent firing of sparks. The uniqueness of each plug presents different impedances for the mutually coupled secondary transformer windings. Over time, spark plugs become unpredictable. This alone can be a strong impetus for development of laser-initiation. Furthermore, the use of semiconductors for repeated high voltage use is unsustainable; other methods of high-speed switching for pulsed thrusters like GFPPTs should be looked into.
5.	Sebastian Eslava, Jordan Marchetto, and Erik Scougal	Design of a Micro-Pulsed Plasma Thruster for 3U CubeSat	AIAA JOURNAL 2014	A $\mu$ -PPT is an even more attractive option because of its small size which makes integration into a 3U CubeSat possible. Although PPTs are limited by their low efficiencies they prove to be structurally integrate able with 3U CubeSat architecture. Present day CubeSats have never flown with a propulsion subsystem and as a result are typically operational for only up to 1 year. Successful integration of 8 $\mu$ PPTs on board a 3U CubeSat would extend mission life through 3-axis yaw, pitch, and roll control.

## CHAPTER 3

# METHODOLOGY AND PROBLEM IDENTIFICATION

### 3.1 Methodology



## **3.2 Problem Identification**

CubeSats are not equipped with any propulsion units which limit their life cycle and operability. As we know conventional small propulsion units such as inert gas thrusters require a lot of plumbing and the system occupies a lot of space. In a small satellite such as CubeSats a system that occupies a lot of space does not allow room for payloads, hence cannot be used. A perfect solution to this would be to use small electric propulsion units.

## **3.3 Objectives and Scope**

### **3.3.1 Objectives**

- To integrate CubeSats with Pulsed Plasma Thrusters.
- To keep the satellite weight to a minimum even after the integration.
- To obtain Structural behaviour of the assembly.
- To obtain the Lorentz force of the thrusters.

### **3.3.2 Scope**

Addition of a propulsion system to a CubeSat allows the lifecycle of the satellite to be increased. The micro-PPT design process is driven by CubeSat and mission requirements that dictate size and performance specifications. A mission's impulse budget determines how many total pulses a micro-PPT needed. The design of the micro-PPT needs performance, geometric, electrical and material considerations. A PPT performance model (Laperriere et al., 2005) is used in conjunction with a PPT ablation model (Gatsonis et al. 2007; Stechmann 2007) to provide the basic operational requirements for the design.

## **CHAPTER 4**

# **MECHANICAL DESIGN**

### **4.1 Mechanical Design Requirements**

This part talks about the methodology and procedure embraced for the mechanical design furthermore, primary investigation of the micro-PPT and the micro-PPT assembly. The section presents the plan boundaries including material choice, design updates, CAD models as well as ANSYS analysis.

#### Mechanical Design Requirements

1. The micro-PPT must fit within 1U of a CubeSat (10x10x10 cm).
2. The micro-PPT assembly needed for attitude control must fit within 1U.
3. Material selection must meet necessary parameters for each part of PPT.
4. Electrode must have high conductivity to generate arcing.
5. Electrodes must be resistant to sputtering.
6. Housing material must resist Teflon ablation temperatures.
7. Materials must have appropriate resistive, capacitive, and inductive properties so ringing and late time ablation effects are mitigated.
8. The micro-PPT must be able to withstand vibrational loads as outlined in the NASA GEVS document (NASA Goddard Space Flight Center 2013) for spaceflight validation.

### Mechanical Design and Structural Analysis Approach and Methods:

1. Use SolidWorks to perform mechanical design of a single micro-PPT unit.
2. Use SolidWorks to perform integration of the micro-PPTs assembly into the 1U assembly.
3. Use SolidWorks and previous CAD model for a 3U to integrate the micro-PPT assembly into the 3U CubeSat.
4. Perform material selection for electrodes and housing.
5. Perform vibration analysis using ANSYS on a single micro-PPT to meet load required in NASA GEVS document.

## 4.2 Conceptual Designs

The Standard 1U satellite was designed based on the following reference.

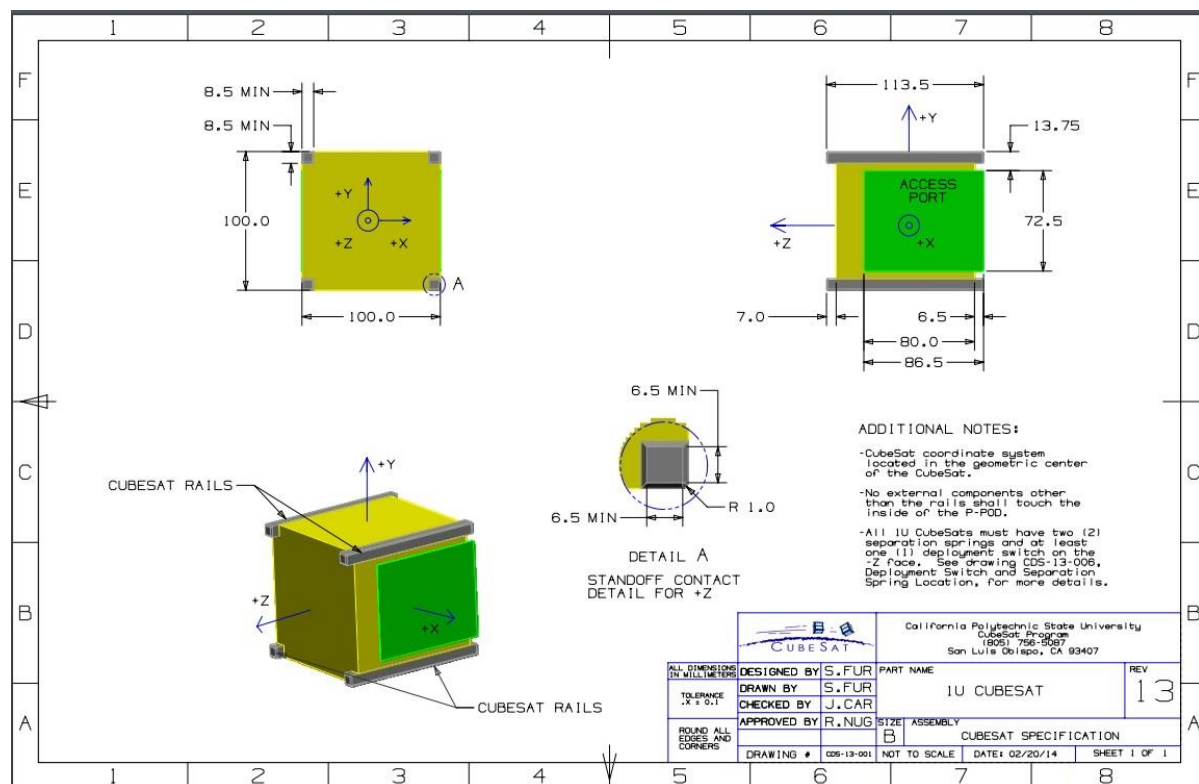


Fig 4.1: 1U satellite design specifications

The 1U satellite is as shown below:

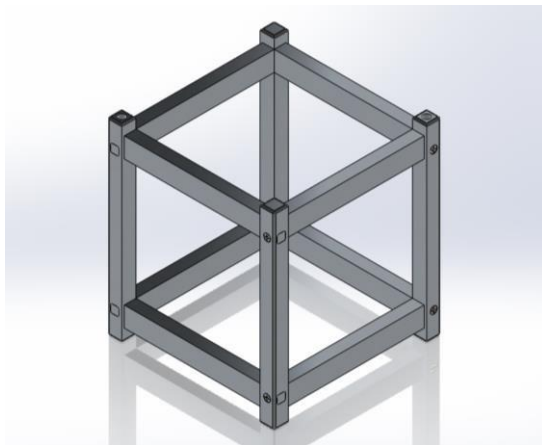


Fig 4.2: 1U CubeSat

#### 4.2.1 First Conceptual Design

The first conceptual design of the CubeSat unit containing the propulsion system consists of four thrusters placed along the longitudinal axis therefore acting as the main propulsion unit for the satellite. This concept allows us to maintain orbit by firing all four thrusters in case of de-orbit caused by aerodynamic drag (especially in LEO where most CubeSats are injected). Using differential thrust, attitude control is also possible using this particular conceptual design.

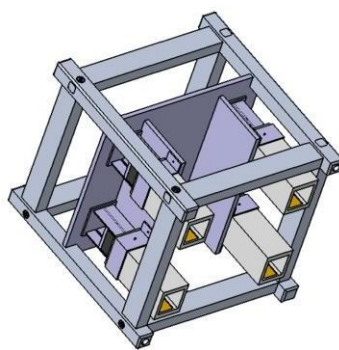


Fig 4.3: First Conceptual Design

#### **4.2.1.1 Limitation of First Conceptual Design**

Even though attitude control is possible it is limited as control about the longitudinal axis is not possible. This is due to the fact that four thrusters needed for control about the longitudinal axis cannot be placed such that control is possible in both clockwise and anti-clockwise directions. Way the thrusters occupy the volume inside the cube sat unit does not allow space for other systems such as batteries and electronics to be placed easily. The second conceptual design solves this issue allowing attitude control about all three axes and orbit maintenance is also possible in a simpler way.

#### **4.2.2 Second Conceptual Design**

The second conceptual design allows for 3-axis attitude control, has enough volume inside the CubeSat to incorporate batteries and electronics and orbit maintenance is possible. The Conceptual design incorporates 8 thrusters arranged as shown in Fig 4.4 which helps to negate the limitations of first conceptual design.

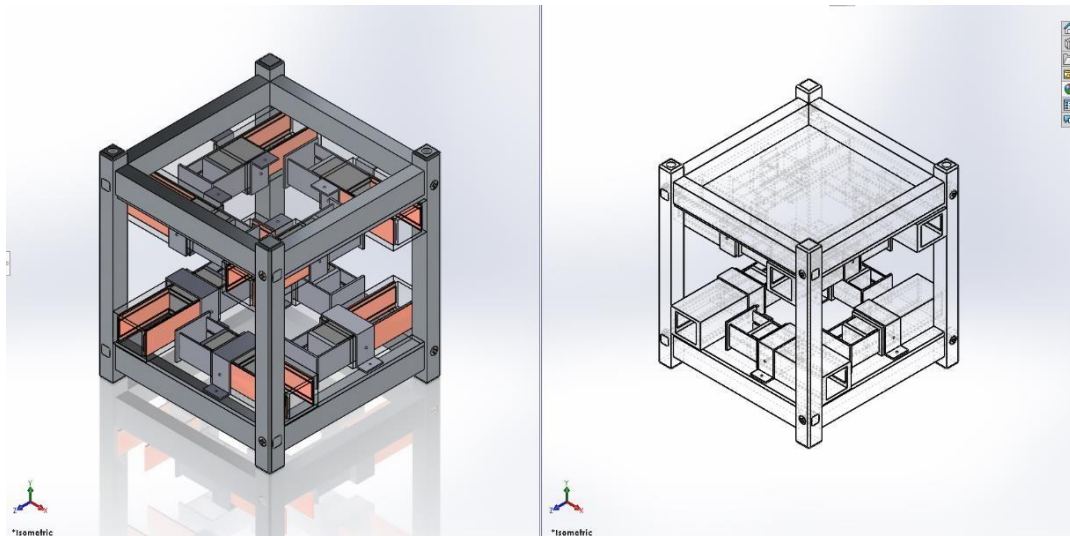


Fig 4.4: Second Conceptual Design

## 4.3 MATERIAL SELECTION

Electrode materials were investigated first. The electrode plates needed to have the following properties; low electrical resistance; high melting point; low thermal expansion; and erosion resistance. The low electrical resistance is related directly to the principle of PPT operation that requires an arc across the two highly conductive plates. Secondly, due to electrical arcing and ablation of the solid Teflon, the temperatures of the PPT will become very high and therefore the electrodes need to be able to withstand the expected temperatures. Lastly, the ablation of the Teflon material causes ions to be accelerated out of the PPT creating thrust. That being said, these ions have the chance to impact the electrodes and impinge on them causing damage thus a material that has the ability to resist this affect would be highly desired. From these parameters previously designed PPT's were looked at for their electrode materials. From this search copper and copper alloys appeared to be the most commonly used electrode materials. From this the Granta CES Edu Pack software was utilized to explore material properties.

The review of previous PPTs include the Dawgstar (Cassady, et al),  $\mu$ Lab-SatII (Kumagai, et al., 2003), and Clyde Space (Coletti et al., 2011). The electrodes on the Dawgstar PPT were copper (Cassady, et al. 2000). The  $\mu$ Lab-SatII PPT investigated the use of molybdenum in place of their original material, brass. They found that molybdenum had similar performance properties to brass, but had significantly better erosion characteristics (Kumagai, et al., 2003). Lastly, the Clyde Space team used a 70% W 30% Cu alloy for its electrodes. The Tungsten-Copper alloy was “chosen for its low electrical resistivity and its good mechanical and thermal properties and reduced erosion rates” (Coletti et al., 2011).

The thermal properties of the materials are relevant properties since the electrodes will be exposed to the hot plasma and their own resistive heat generation and must not melt, must expand as little as possible, and should have a low a thermal conductivity to stop heat conduction through the electrodes and into the surrounding material. The low thermal expansion will serve to prevent the thruster geometry, a characteristic important to the thruster performance (Pottinger and Scharlemann, 2007), from changing significantly. The low thermal

conductivity will alleviate possible impact due to heat conduction to the CubeSat bus and components. Lastly density was considered. Due to the mass requirements set by CubeSat specifications, the PPT materials should not be exceedingly dense so as to keep the thruster mass low. Applying these key characteristics to the materials used by other teams, a set of minimum requirements for the electrode materials was created. CES EduPack (Granta, 2013) was used to find the values for all the materials. Using that information, the following values for the first selection stage were compiled as shown in Table below:

Table 4.1: Values for initial CES selection stage.

Minimum Melting Point	1000 °C
Max. Thermal Expansion	1.68 e-5 strain/°C
Max. Elec. Resistance	6 e-8 Ohm.m
Max Thermal Conductivity	398 W/m°C

Later the electrode materials selection was revisited, this time with a focus on the erosion properties of the materials. The erosion characteristics were obtained from a PPT design study by Peter Vallis Shaw in which he references a study by Fairchild Industries. The results of this study is shown below in table

Table 4.2:Erosion characteristics of electrode materials. (Shaw, 2011).

Anode Material	Anode Erosion per discharge µg	Cathode Erosion per discharge µg
Copper	11.99	4.36
Graphite	4.59	3.17
Thoriated Tungsten	40.25	4.10
Tantalum	27.72	1.76
Tungsten coated copper	15.16	1.55
Molybdenum	16.93	3.48
25% Copper 75% Tungsten	27.81	3.86
Platinum	22.79	1.18

Next the material for the casing needed to be explored. The main parameters required for the casing are the following: good dielectric, high melting temperature, heat and electrical insulator. It is important for the casing material to be a good dielectric material to increase the charge felt across the two electrode plates creating arcing as efficiently as possible, Second the arcing and ablation of Teflon creates very high temperatures within the PPT so the casing must be able to withstand these temperatures and not fail. Additionally, part of the thrust generated by a PPT is developed by the gas dynamics formed by thermal expansion. Therefore, if the casing can act as a heat insulator and trap and increase the heat within the chamber it will increase efficiency of the PPT slightly. Lastly with electrical arcing taking place between the electrodes we do not want the casing material to be electrically conductive and charge the outside spacecraft bus. Once again previous PPT designs were taken into account for a starting point.

Several PPT's used a thermoplastic material called Torlon. From this Torlon alternatives were looked at. Alternatives examined were; Tecator, PEEK, Vespel, and Techtron. PEEK is an alternative that did not have electrical properties as good as that of Torlon. Vespel had similar properties but all values were not on par however it was a very cheap alternative making it a great option for scaled testing. Techtron did not quite have the thermal properties compared to Torlon. Lastly Tecator had nearly identical properties to that of Torlon and was similar in price. However, since Torlon has been a proven material to work with PPT's we decided to choose this as the casing material. Torlon 4203 properties can be seen in the Table below.

Table 4.3: Torlon 4203 Data Sheet (All-state Industries)

<b>Physical Properties</b>	<b>Metric</b>	<b>English</b>	<b>Methods</b>
Specific Gravity	1.41 g/cc	.051 lb/in <sup>3</sup>	ASTM D792
Water Absorption	0.4%	0.4 %	Immersion, 24hr; ASTM D570(2)
Water Absorption at Saturation	1.7%	1.7 %	Immersion; ASTM D570(2)
<b>Mechanical Properties*</b>			
Hardness, Rockwell M		M120	ASTM D785
Hardness, Rockwell		E80	ASTM D785
Hardness, Shore D		90	ASTM D2240
Tensile Strength, Ultimate	138 MPa	20,000 psi	ASTM D638
Elongation at Break	15 %	15 %	ASTM D638
Tensile Modulus	4136 MPa	600,000 psi	ASTM D638
Flexural Modulus	4136 MPa	600,000 psi	ASTM D790
Flexural Yield Strength	165 MPa	24,000 psi	ASTM D790
Compressive Strength	165 MPa	24,000 psi	10% Def.; ASTM D695
Compressive Modulus	3,296 MPa	478,000 psi	ASTM D695
Izod Impact (notched)	105 J/M	2.0	ASTM D256 Type A
<b>Thermal Properties</b>			
Melt Point/T <sub>g</sub>	275 °C	527°F	ASTM D3418
Heat Deflection Temp (264 psi)	278°C	532°F	ASTM TMA
Coefficient of Linear Thermal Expansion	$3.1 \times 10^{-5}$ C <sup>-1</sup>	$1.7 \times 10^{-5}$ F <sup>-1</sup>	E831 TMA

## CHAPTER 5

### Analysis, Results and Conclusion

#### 5.1 ANSYS Structural Analysis

After the design was complete, it had to be evaluated for vibrational loads using the ANSYS 2019 R3 software. During launch the satellite bus, and therein the micro PPT will feel a range of vibrational loads in many frequencies. In order to be deemed space qualified, NASA created a document called the GEVS or General Environmental Verification Standard, which lays out the conditions for being regarded space qualified. This document provides a vibration profile requirement than can be seen in Figure

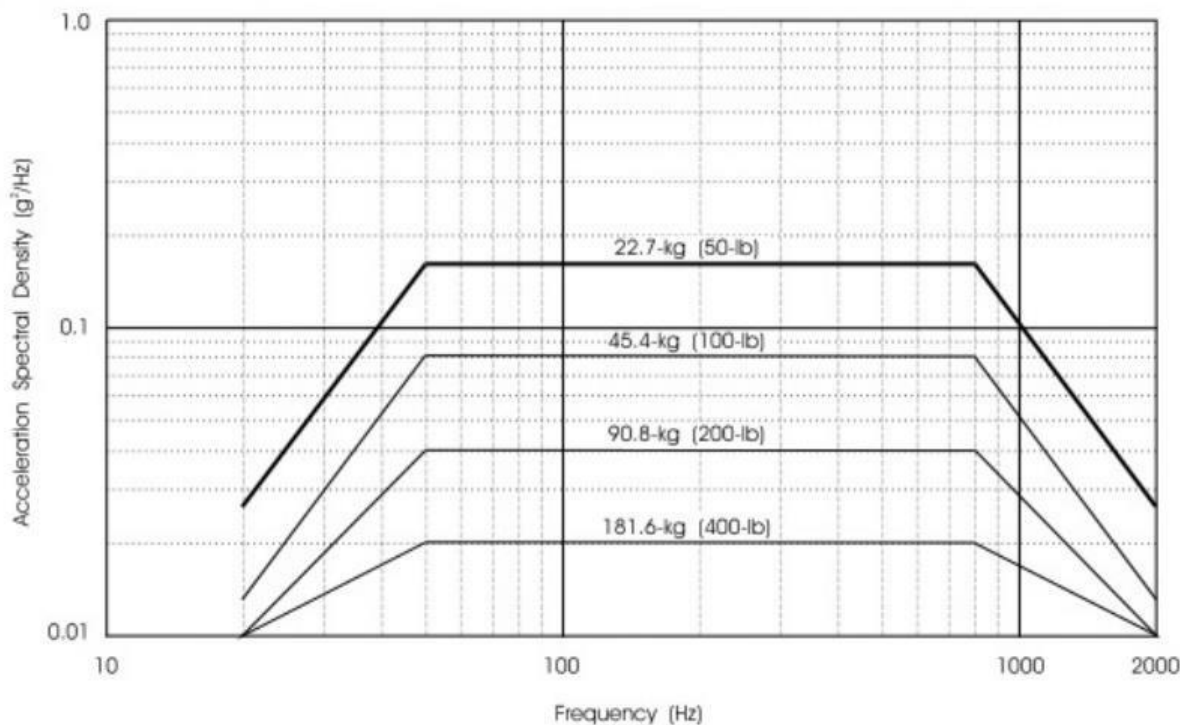
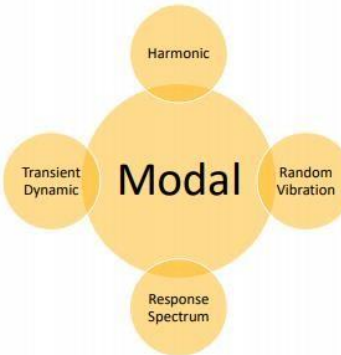


Fig 5.1: General Environmental Verification Standard for random vibration.

Modal analysis must be performed before performing the required Random vibrations test, as it is a prerequisite.

### 5.1.1 MODAL ANALYSIS:

Modal analysis is used to determine the vibration characteristics of linear elastic structures. It is also the typical common dynamic simulation for many other dynamic simulations. Modal analysis looks for natural frequencies and normal modes of a structure. Natural frequencies and modes are some of the most important properties of a structure; they determine how the



structure will respond.

Modal analysis was done using ANSYS 2019 R3 Software.

Case 1: Modal analysis of PPT mounted on base plate

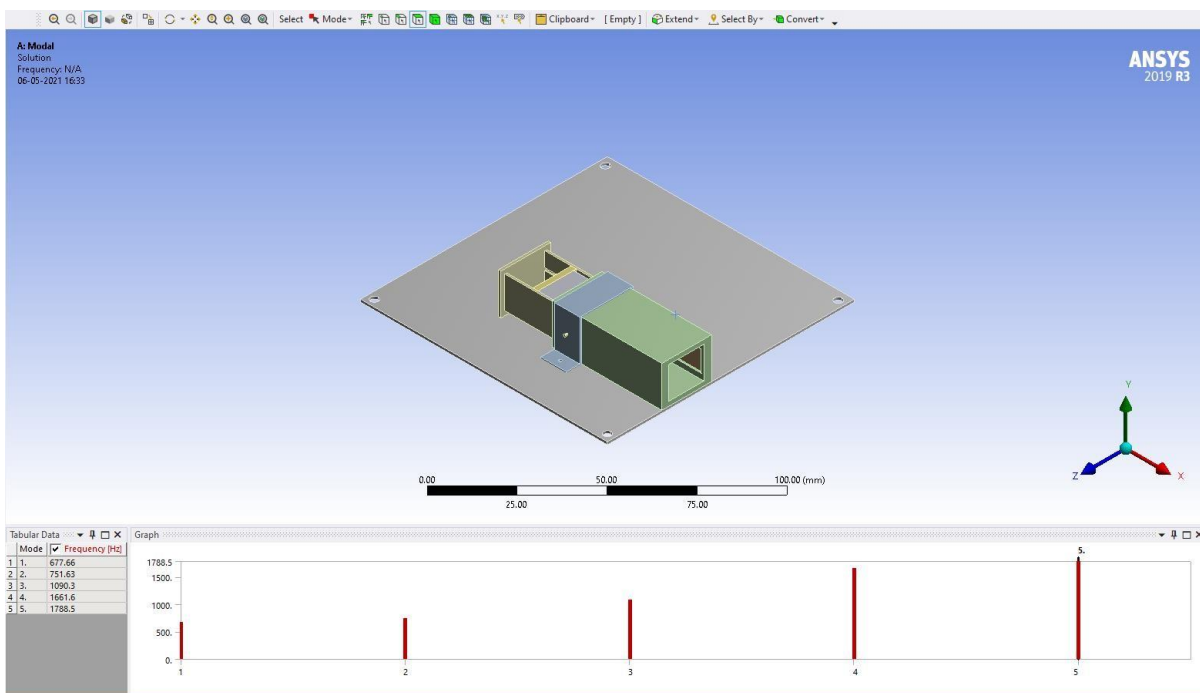


Fig 1: Modal analysis of PPT mounted on baseplate

- The Mesh consisted of 127855 Nodes and 31654 Elements.
- The mesh statistics and material properties were as follows

Table 5.1: Material properties and Mesh Statistics

Geometry > Parts							
Object Name	Solid	Solid	Solid	Solid	Solid	Solid	Solid
State							
					Meshed		
Graphics Properties							
Visible					Yes		
Transparency					1		
Definition							
Suppressed					No		
Stiffness Behaviour					Flexible		
Coordinate System					Default Coordinate System		
Reference Temperature					By Environment		
Treatment					None		
Material							
Assignment	Aluminum alloy, wrought, 7075, T6	Structural Steel	Aluminum alloy, wrought, 7075, T6 2	Copper Alloy	Aluminum alloy, wrought, 7075, T6 4	PTFE (Teflon)	Aluminum alloy, wrought, 7075, T6 3
Nonlinear Effects				Yes			
Thermal Strain Effects				Yes			
Bounding Box							
Length X	97. mm	10. mm	43. mm	32. mm	2. mm	20. mm	31. mm
Length Y	1. mm	16.69 mm	15.936 mm	12.5 mm			15.94 mm
Length Z	97. mm	32.25 mm	19.491 mm	0.75 mm	16. mm	13.9 mm	22.5 mm
Properties							
Volume	9380.7 mm <sup>3</sup>	479.8 mm <sup>3</sup>	4746.6 mm <sup>3</sup>	300. mm <sup>3</sup>	375.77 mm <sup>3</sup>	3475. mm <sup>3</sup>	847.88 mm <sup>3</sup>
Mass	2.6266e-002 kg	3.7664e-003 kg	1.3291e-002 kg	2.49e-003 kg	1.0521e-003 kg	7.5407e-003 kg	2.3741e-003 kg
Centroid X	6.1669 mm	18.167 mm	33.241 mm	37.667 mm	2.9704 mm	13.97 mm	1.051 mm
Centroid Y	24.63 mm	34.146 mm			33.098 mm		
Centroid Z	32.997 mm	50.161 mm	49.998 mm	42.662 mm	58.412 mm	50.537 mm	51.087 mm
Moment of Inertia Ip1	20.497 kg·mm <sup>2</sup>	0.51156 kg·mm <sup>2</sup>	1.1398 kg·mm <sup>2</sup>	3.2539e-002 kg·mm <sup>2</sup>	3.3488e-002 kg·mm <sup>2</sup>	0.2196 kg·mm <sup>2</sup>	0.16042 kg·mm <sup>2</sup>
Moment of Inertia Ip2	40.986 kg·mm <sup>2</sup>	0.38724 kg·mm <sup>2</sup>	2.7148 kg·mm <sup>2</sup>	0.2126 kg·mm <sup>2</sup>	2.0166e-002 kg·mm <sup>2</sup>	0.37277 kg·mm <sup>2</sup>	0.36925 kg·mm <sup>2</sup>
Moment of Inertia Ip3	20.494 kg·mm <sup>2</sup>	0.18724 kg·mm <sup>2</sup>	2.5486 kg·mm <sup>2</sup>	0.2449 kg·mm <sup>2</sup>	1.4022e-002 kg·mm <sup>2</sup>	0.34955 kg·mm <sup>2</sup>	0.28667 kg·mm <sup>2</sup>
Statistics							
Nodes	70438	4211	20761	3140		1495	16821
Elements	9921	1877	10968	416		738	3640
Mesh Metric				None			3678

The result is a set of eigen frequencies with their corresponding mode shapes.

Table 5.2 Case 1 Modes and Frequency (Hz)

Mode	Frequency [Hz]
1.	677.66
2.	751.63
3.	1090.3
4.	1661.6
5.	1788.5

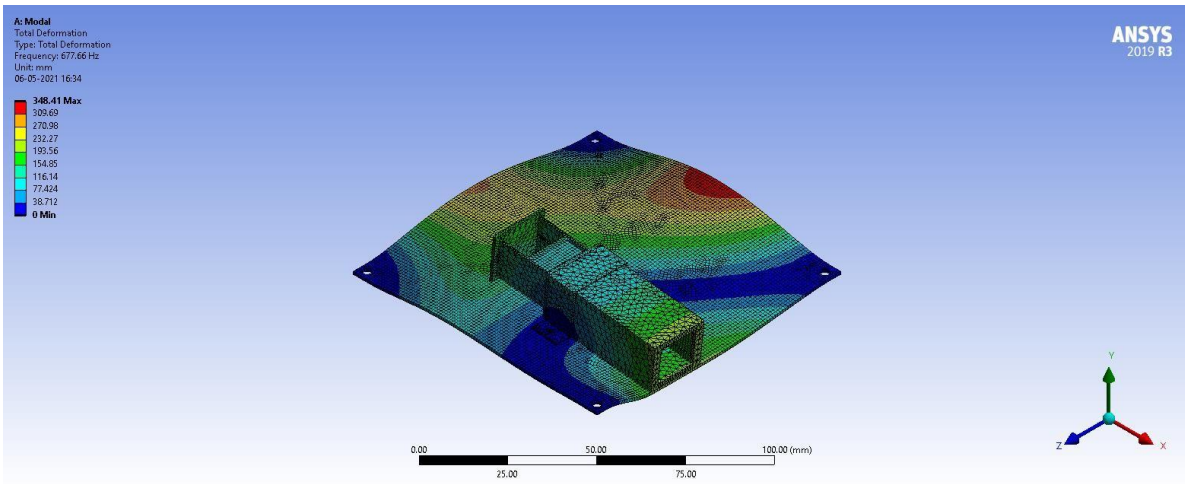


Fig 5.3: 1<sup>st</sup> Mode Shape Isometric view of single PPT mounted on baseplate

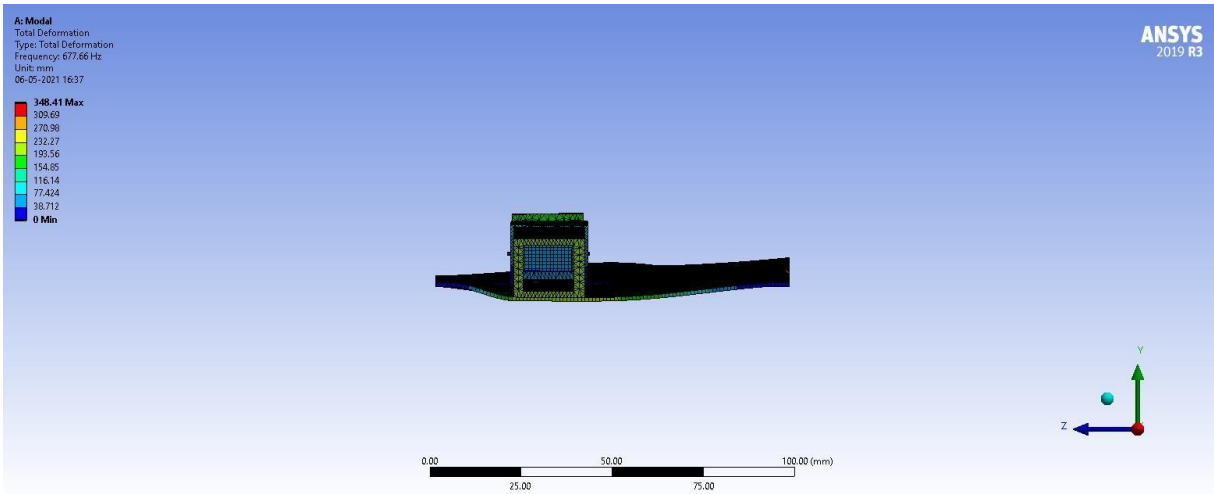


Fig 5.4: 1<sup>st</sup> Mode Shape front view of single PPT mounted on baseplate

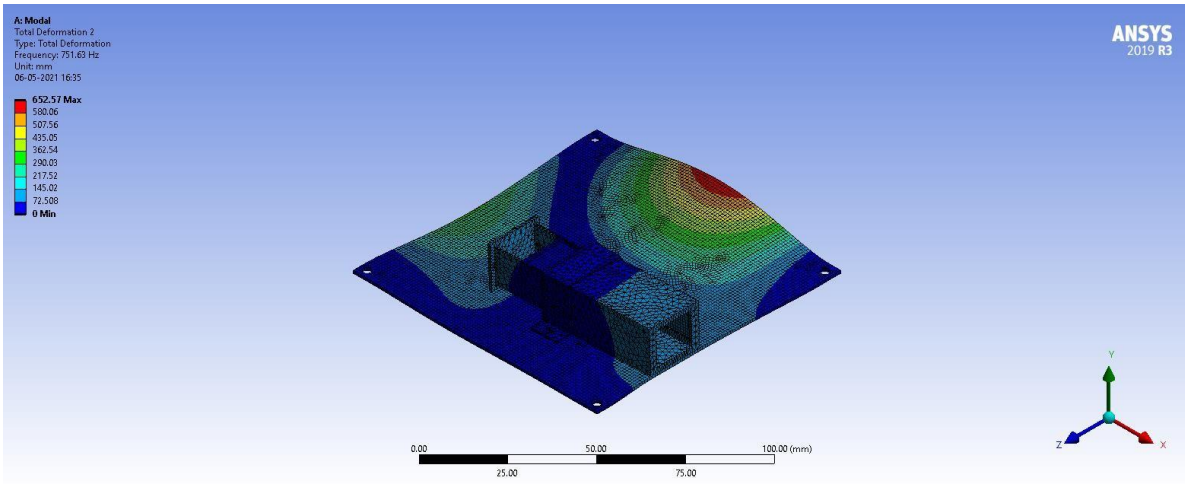


Fig 5.5: 2<sup>nd</sup> Mode Shape Isometric view of single PPT mounted on baseplate

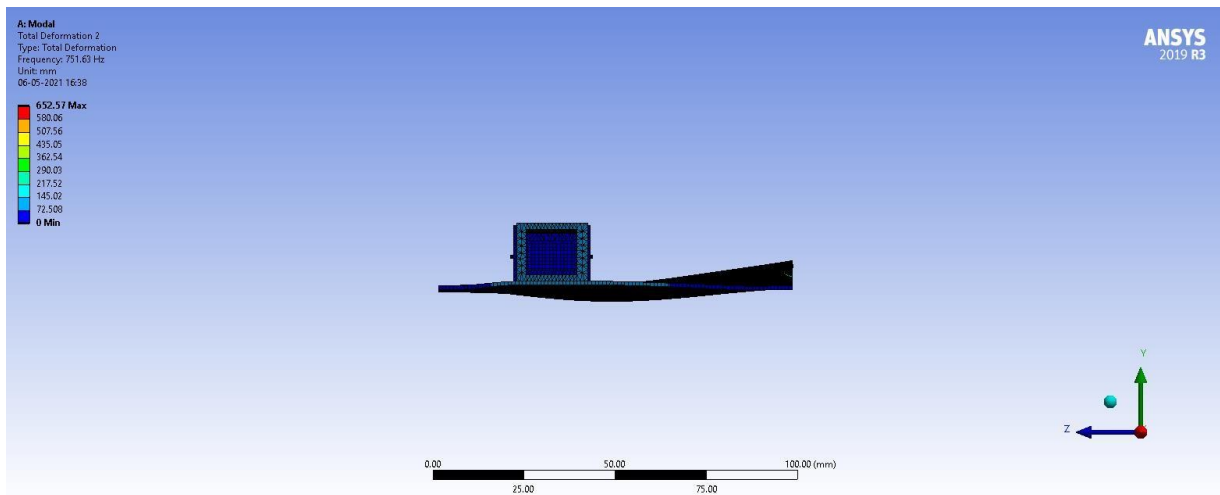


Fig 5.6: 2<sup>nd</sup> Mode Shape front view of single PPT mounted on baseplate

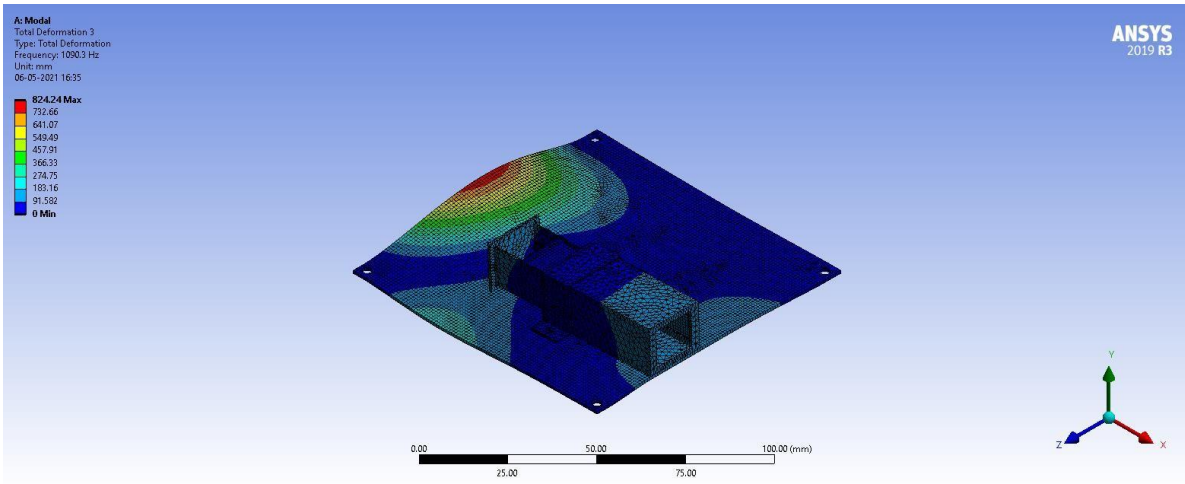


Fig 5.7 3<sup>rd</sup> Mode Shape Isometric view of single PPT mounted on baseplate

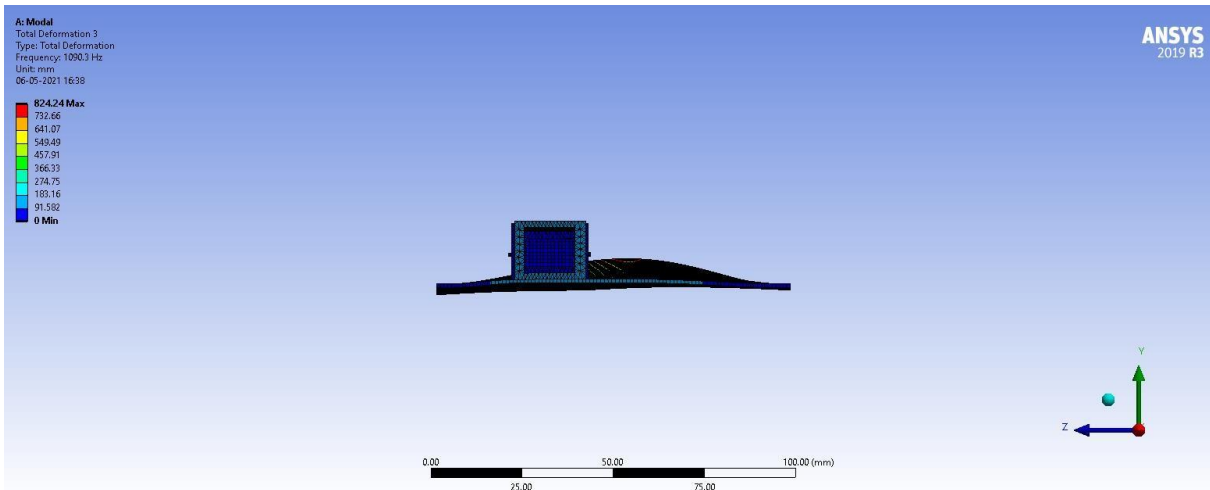


Fig 5.8 3<sup>rd</sup> Mode Shape front view of single PPT mounted on baseplate

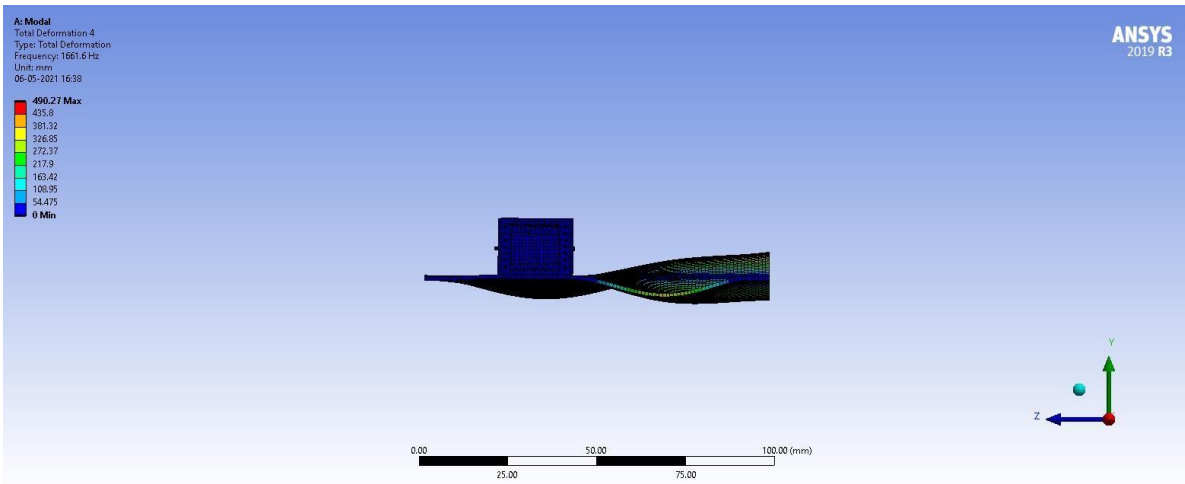


Fig 5.9 4<sup>th</sup> Mode Shape Isometric view of single PPT mounted on baseplate

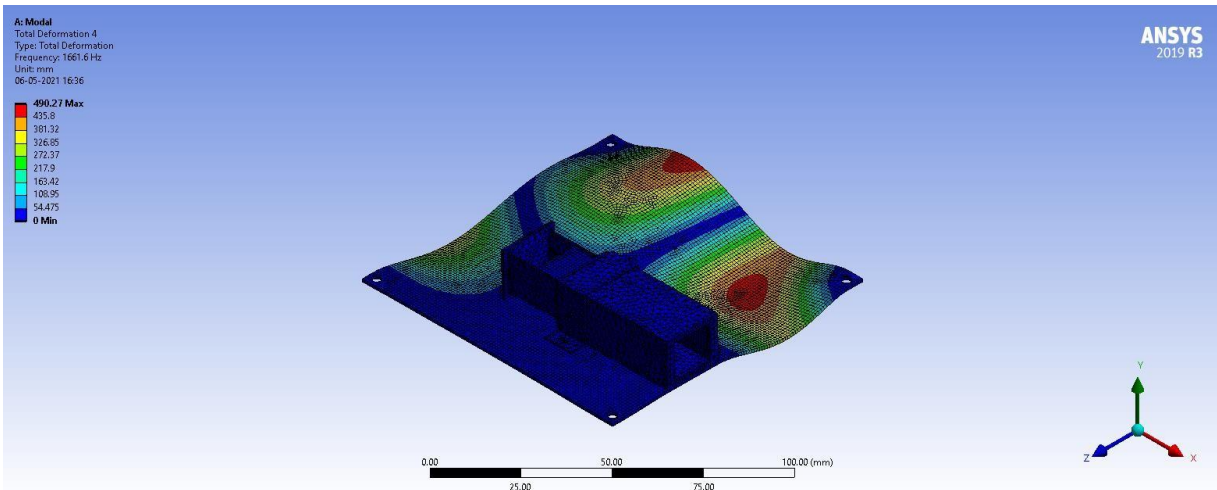


Fig 5.10: 4<sup>th</sup> Mode Shape front view of single PPT mounted on baseplate

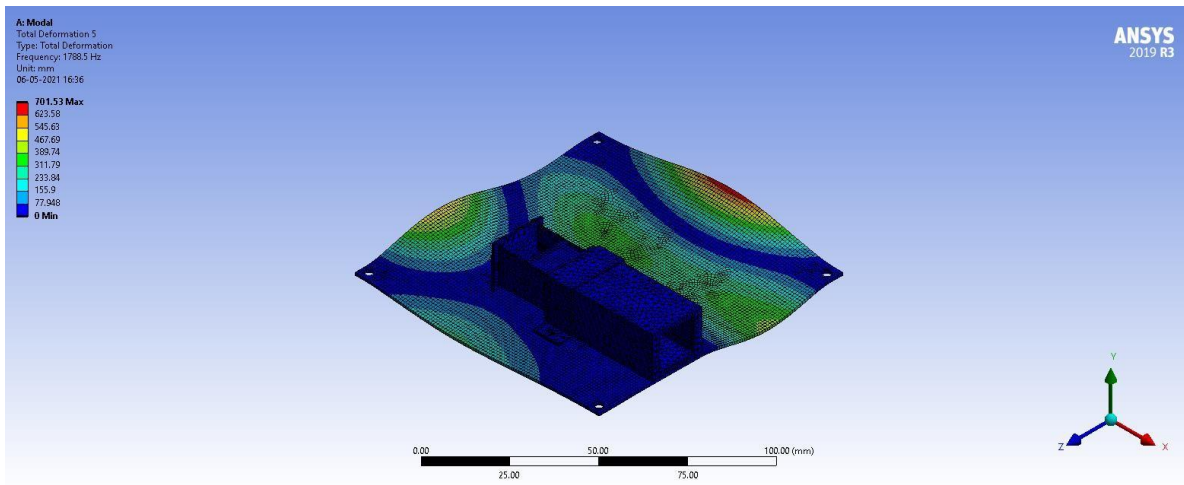


Fig 5.11: 5<sup>th</sup> Mode Shape Isometric view of single PPT mounted on baseplate

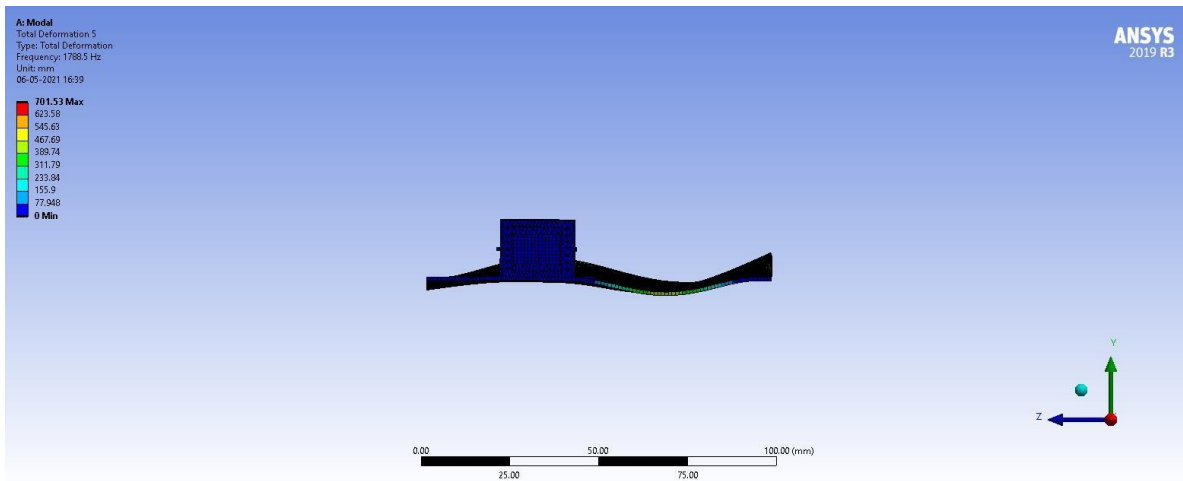


Fig 5.12: 5<sup>th</sup> Mode Shape front view of single PPT mounted on baseplate

### 5.1.2 Random Vibration:

This analysis investigates the structural response to acoustic noise due to engine vibration and noise, air friction at the beginning of the launch phase. The instantaneous magnitude of the response is not constant over time due to several possible frequencies exert on the structure at the same time. Therefore, the problem should consider in a statistical and probability distribution approach before transforming to frequency domain. The Acceleration Spectral Density (ASD) also known as Power Spectral Density (PSD) is a statistical measure of the structure response to random dynamic loads. It is a graph of the PSD versus frequencies in which PSD can be displacement, velocity, acceleration, or force. In case of acceleration the unit can be presented in  $((g^2/\text{Hz})/\text{Hz})$

Once the Modal analysis was performed then the Random Vibration test was performed using the Modal analysis values.

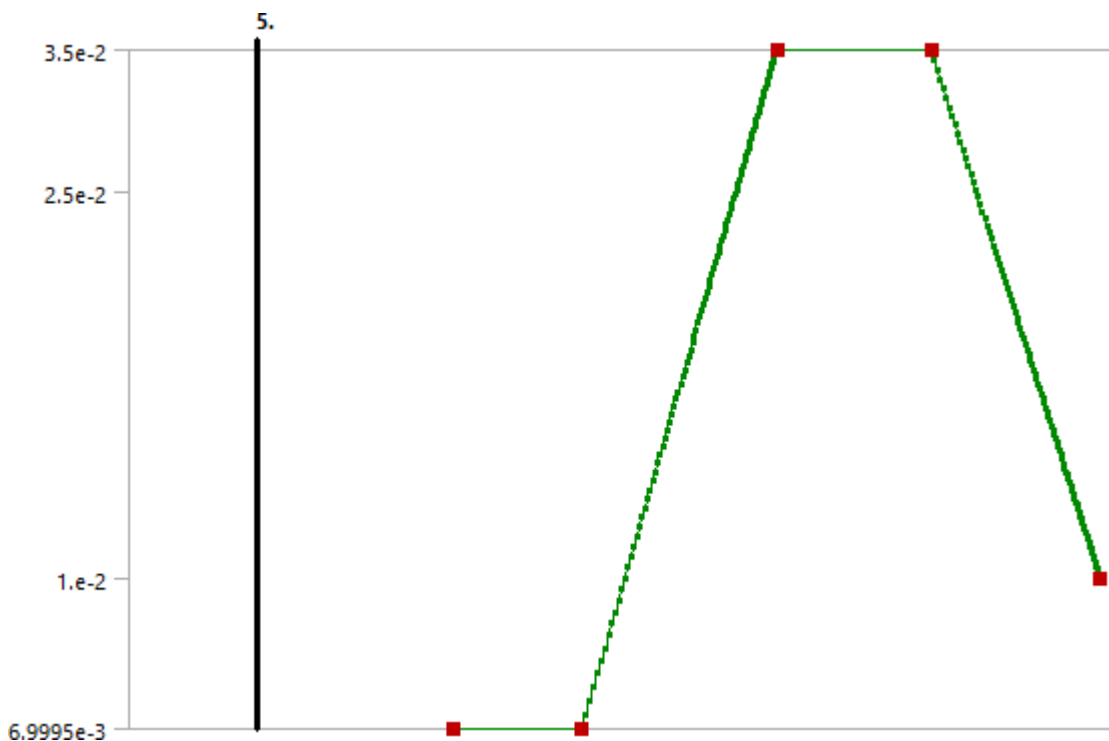


Fig 5.13 Random vibration chart Amplitude ( $\text{g}^2/\text{Hz}$ ) v/s Frequencies (Hz)

Table 5.3:PSD Acceleration values for random vibration test

Frequency [Hz]	G Acceleration [G <sup>2</sup> /Hz]
20.	7.e-003
50.	7.e-003
200.	3.5e-002
600.	3.5e-002
2000.	1.e-002

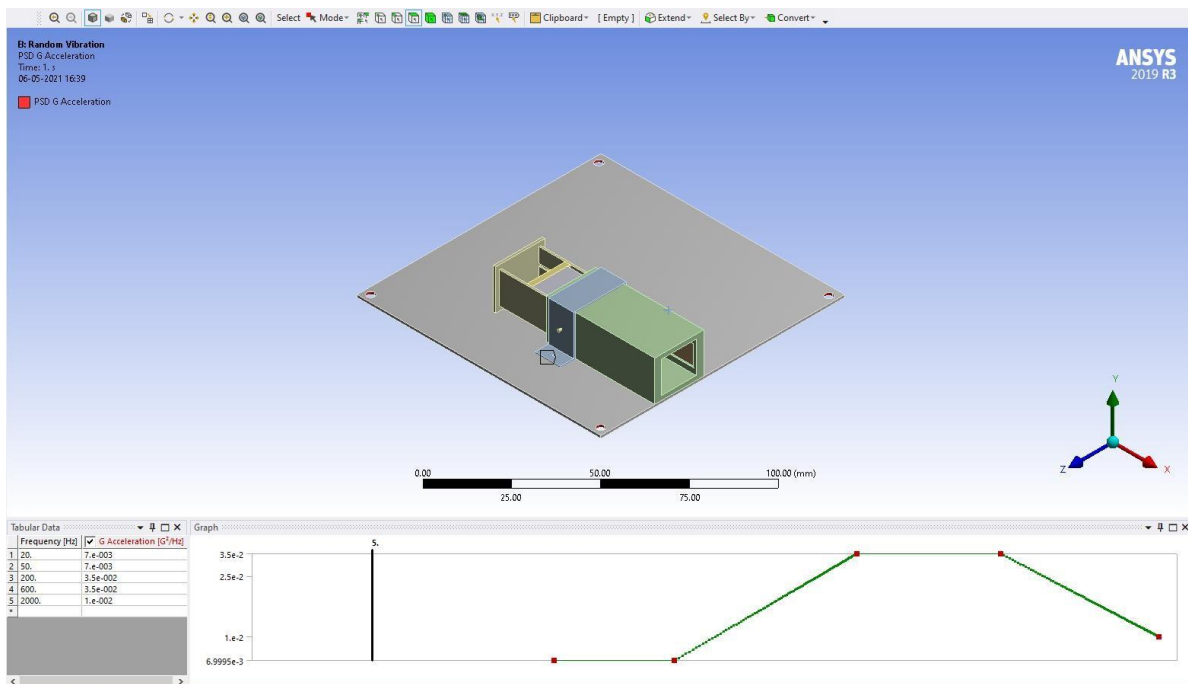


Fig 5.14: Random Vibration input values and graph

Random vibration test for case 1 was performed along all 3 axes and the directional deformation scale factors were set from 1 Sigma to 3 Sigma levels.

### Case 1.1: Random Vibration test along X axis

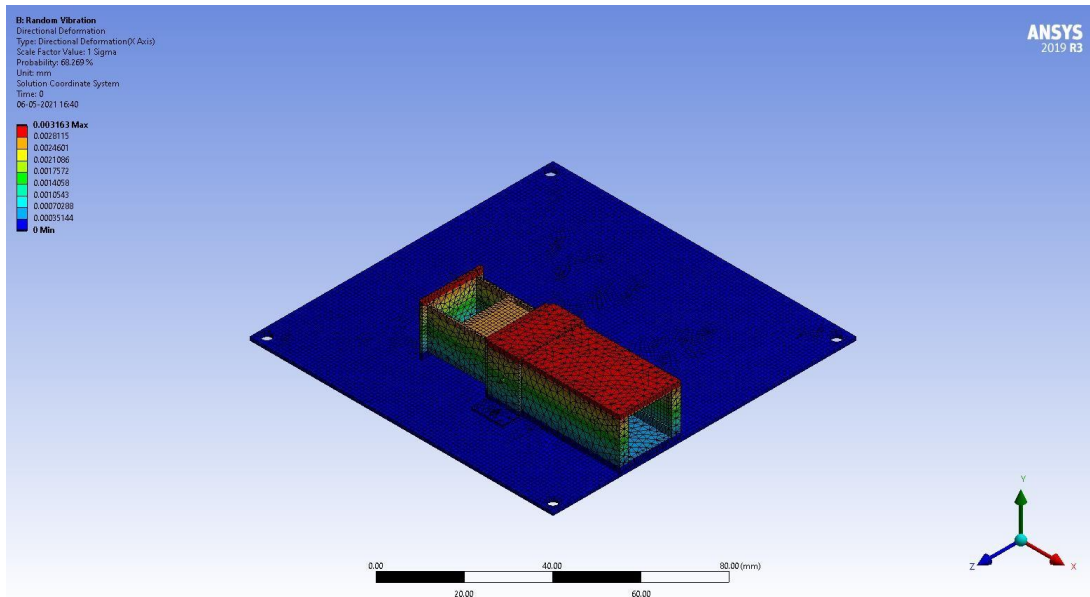


Fig 5.15 (X-Axis Test) X-Axis Deformation 1 Sigma

- X- Axis
- 1 Sigma= 66.269%
- Max Deformation = 0.003163 mm

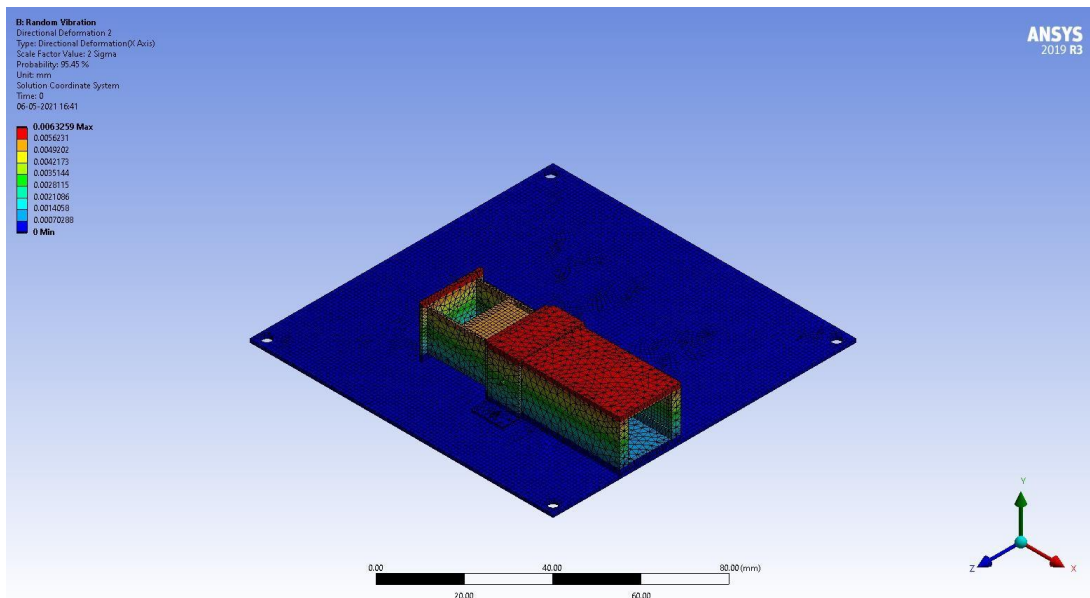


Fig 5.16 (X-Axis Test) X-Axis Deformation 2 Sigma

- X- Axis
- 2 Sigma= 95.45%
- Max Deformation = 0.0063259 mm

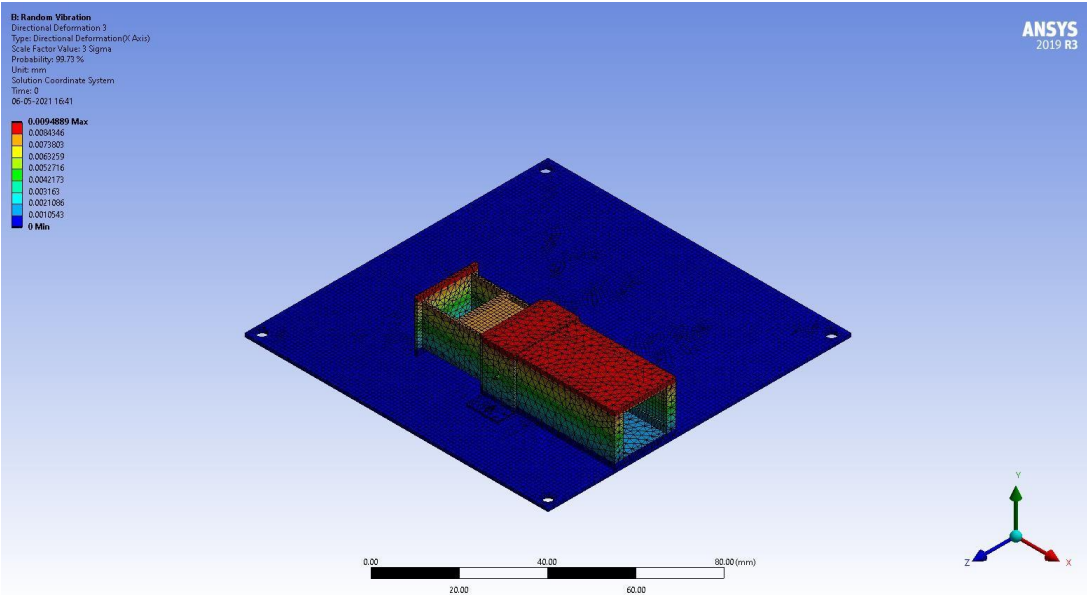


Fig 5.17 (X-Axis Test) X-Axis Deformation 3 Sigma

- X- Axis
- 3 Sigma= 99.73 %
- Max Deformation = 0.0094889 mm

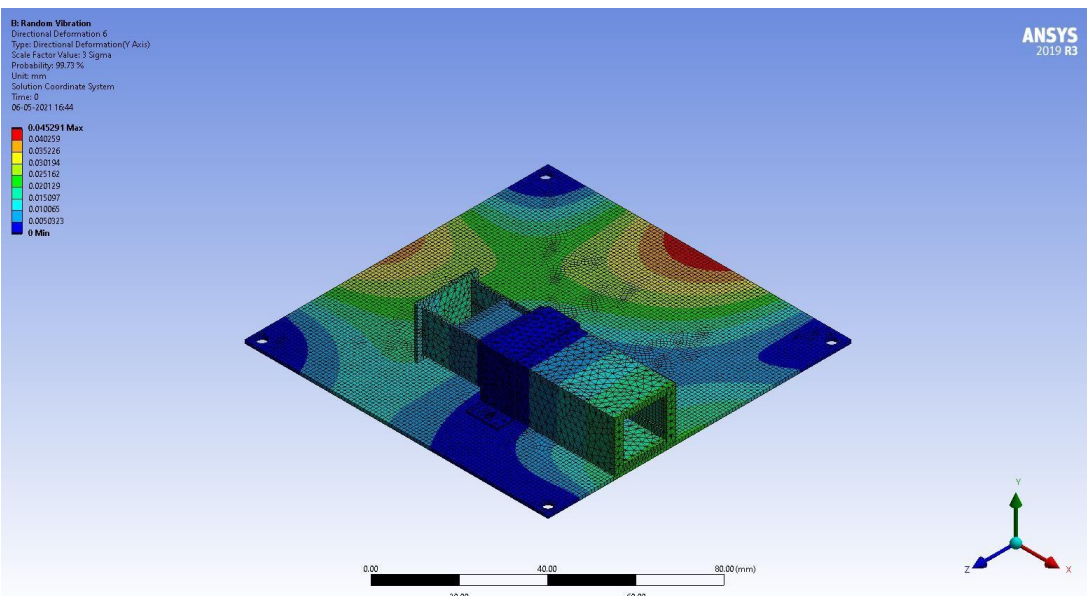


Fig 5.18 (X-Axis Test) Y-Axis Deformation 3 Sigma

- Y- Axis
- 3 Sigma= 99.73 %
- Max Deformation = 0.045291 mm

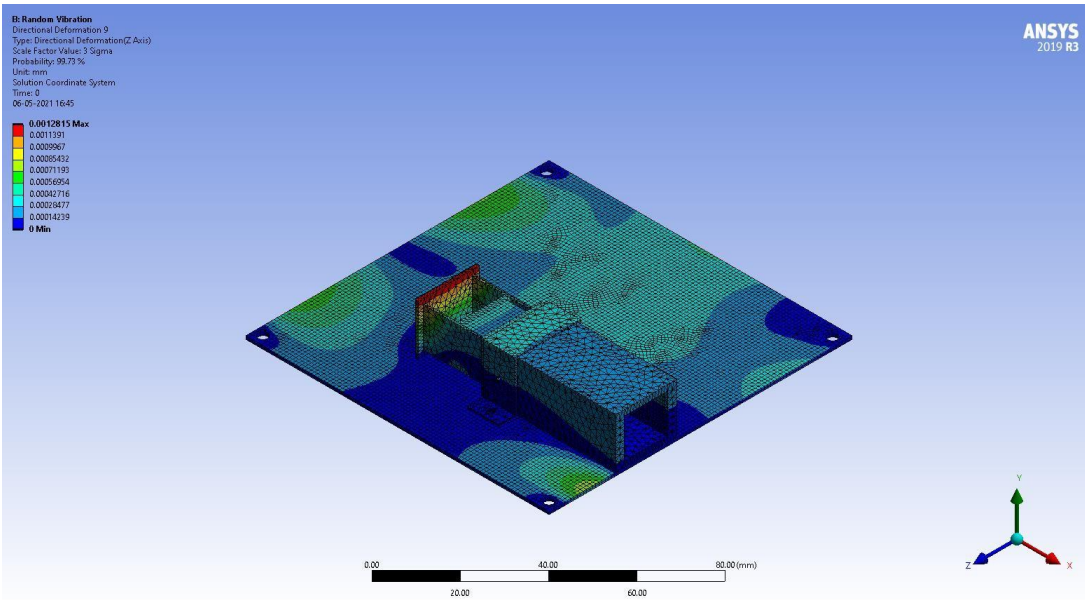


Fig 5.19: (X-Axis Test) Z-Axis Deformation 3 Sigma

- Z- Axis
- 3 Sigma= 99.73 %
- Max Deformation = 0.0012815 mm

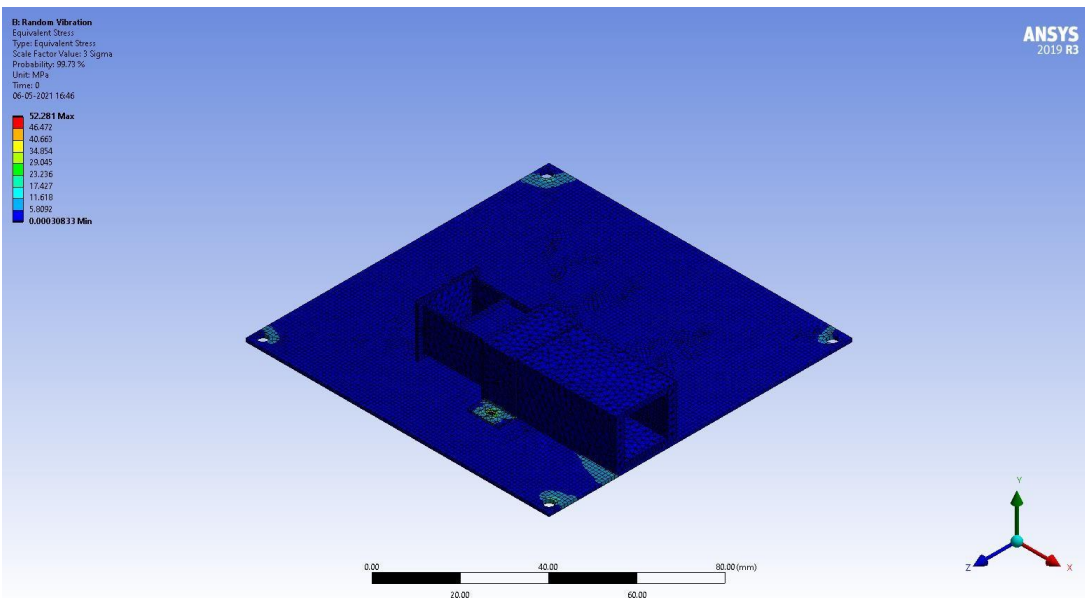


Fig 5.20: Equivalent Stresses for case 1.1

- Equivalent Stresses = 52.281 MPa

## Case 1.2 : Random Vibration acting on Y Axis

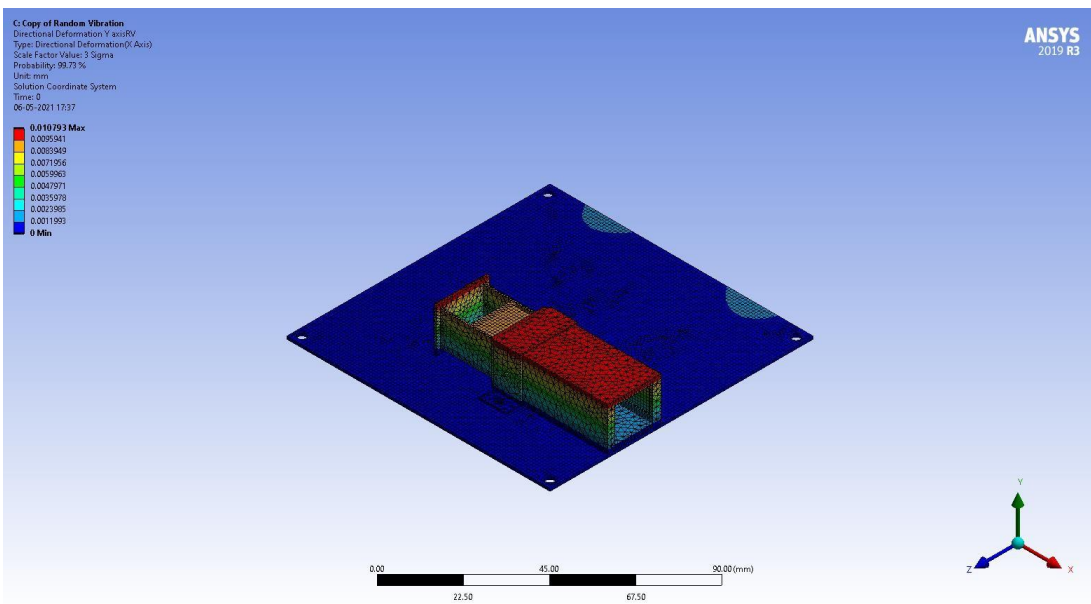


Fig 5.21: (Y-Axis Test) X Axis deformation 3 Sigma

- X- Axis
- deformation 99.73 %
- Max Deformation = 0.010793 mm

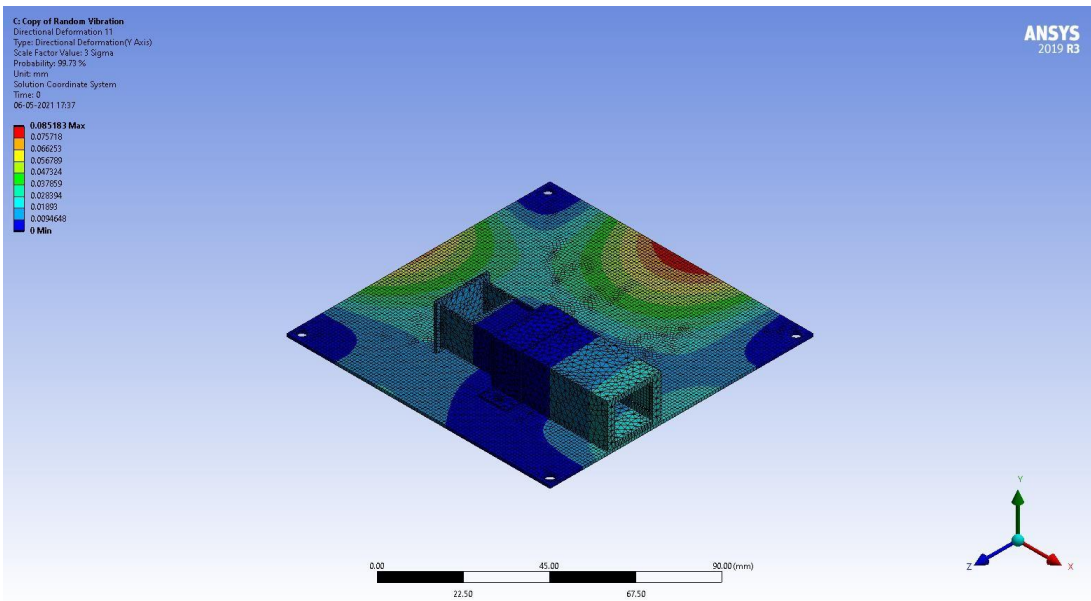


Fig 5.22: (Y-Axis Test) Y Axis deformation 3 Sigma

- Y- Axis
- deformation = 99.73 %
- Max Deformation = 0.085183 mm

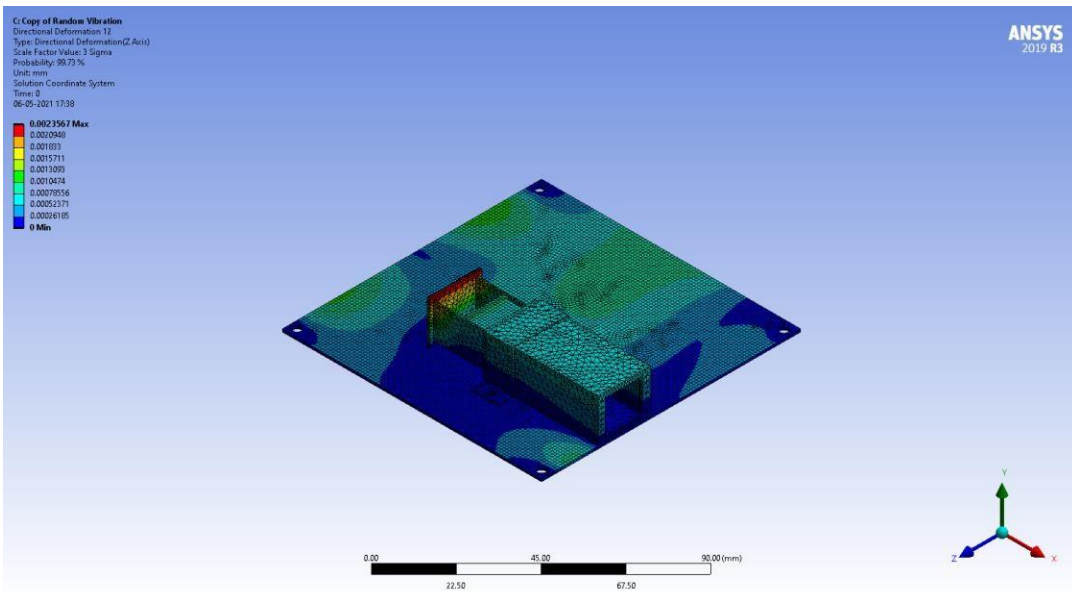


Fig 5.23: (Y-Axis Test) Z Axis deformation 3 Sigma

- deformation = 99.73 %
- Max Deformation = 0.0023567 mm

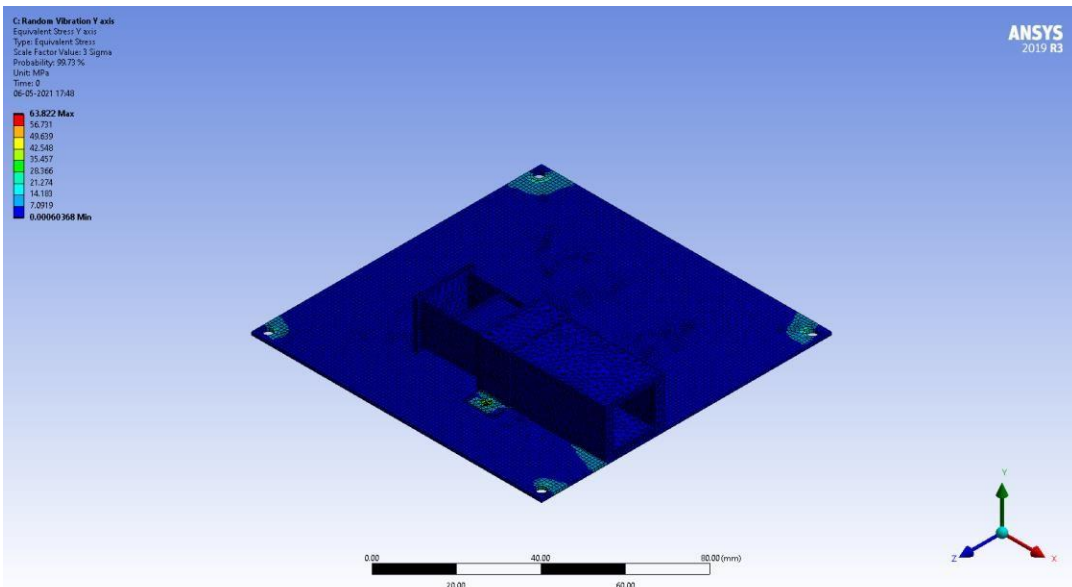


Fig 5.24 Equivalent Stresses for Case 1.2

- Equivalent Stresses = 63.822 MPa

### Case 1.3 : Random Vibration Z axis

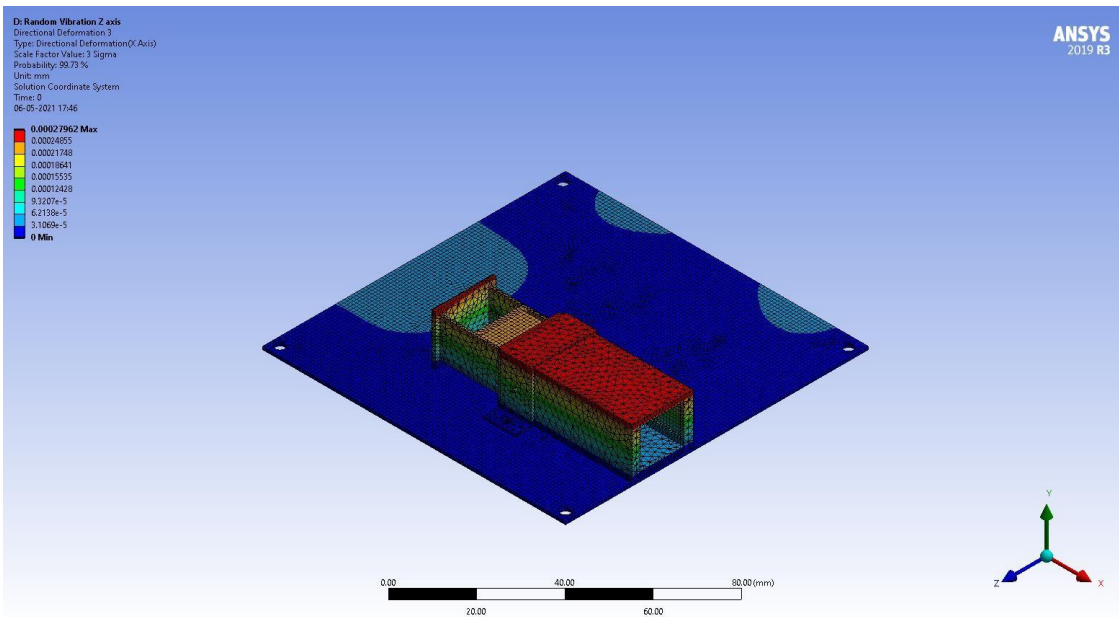


Fig 5.25 (Z-Axis Test) X Axis deformation 3 Sigma

- X- Axis
- 3 Sigma= 99.73 %
- Max Deformation = 0.00027962 mm

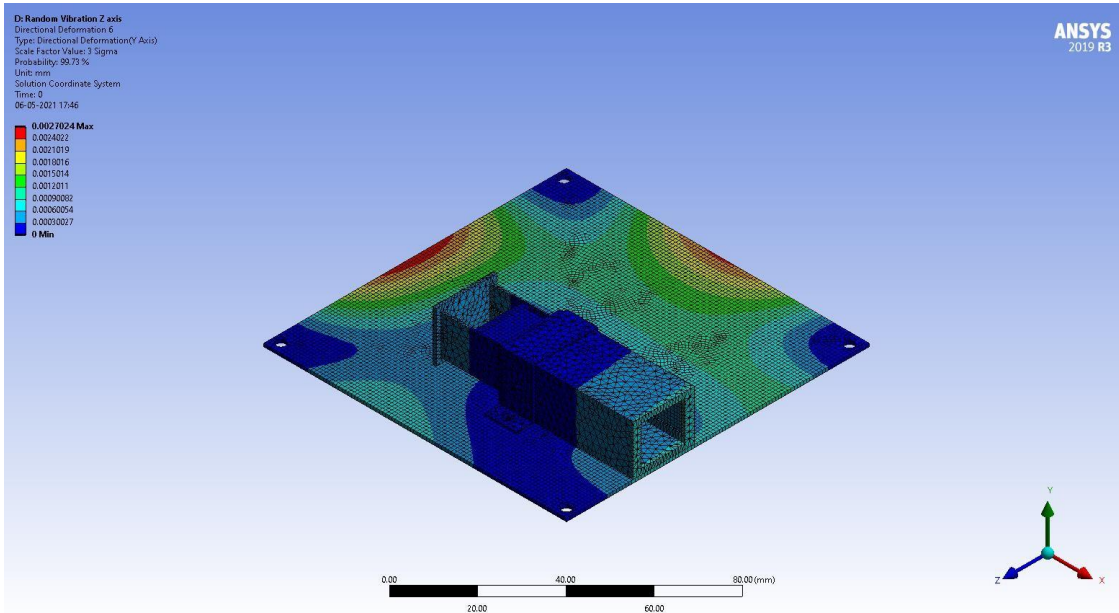


Fig 5.26 (Z-Axis Test) Y Axis deformation 3 Sigma

- Y- Axis
- 3 Sigma= 99.73 %
- Max Deformation = 0.0027024 mm

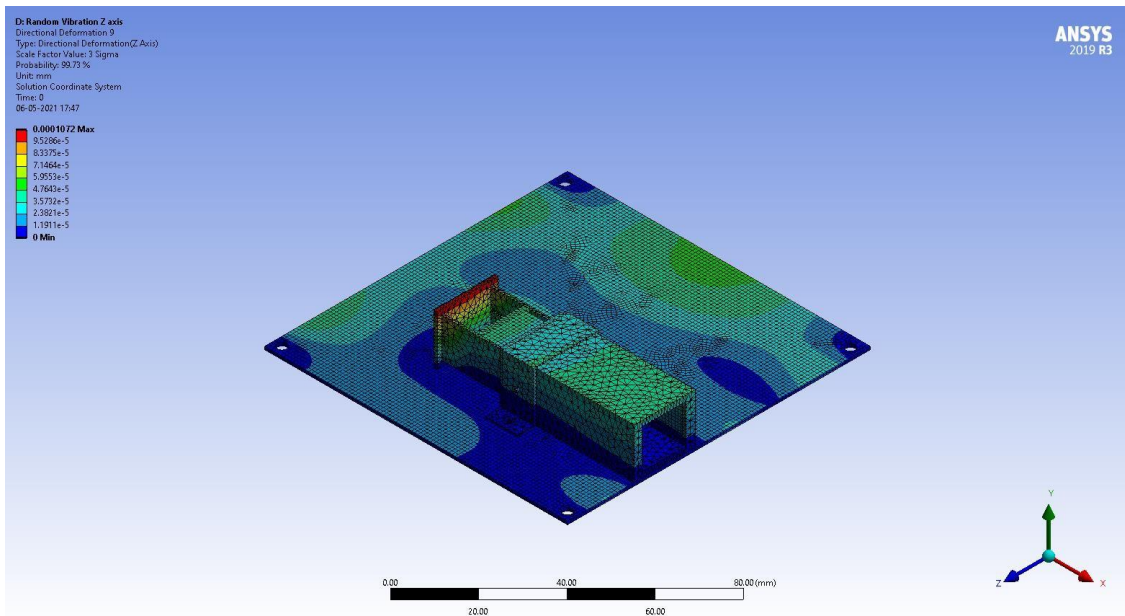


Fig 5.27: (Z-Axis Test) Z Axis deformation 3 Sigma

- Z- Axis
- 3 Sigma= 99.73 %
- Max Deformation = 0.0001072 mm

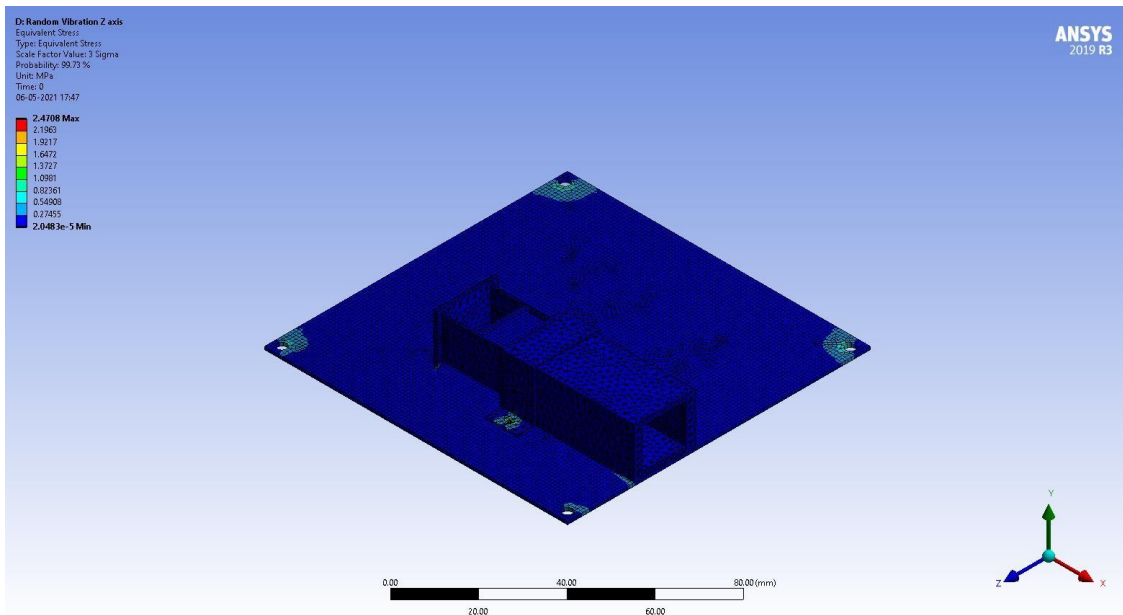


Fig 5.28: Equivalent Stresses for Case 1.3

- Equivalent Stresses = 2.4708 MPa

## Case 2: Modal Analysis of 4 PPT mounted on Baseplate

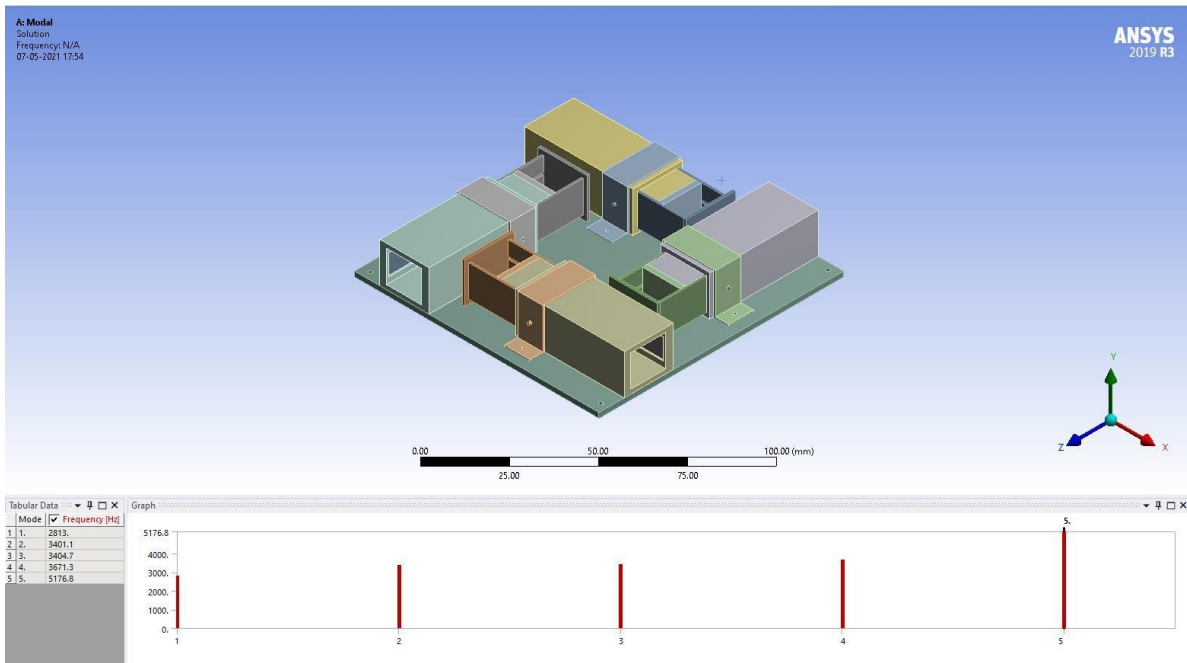


Fig 5.29: 4 PPT's mounted on baseplate



Fig 5.30: 4 PPT's mounted on baseplate top view

- The Mesh consists of 346953 Nodes and 108816 Elements

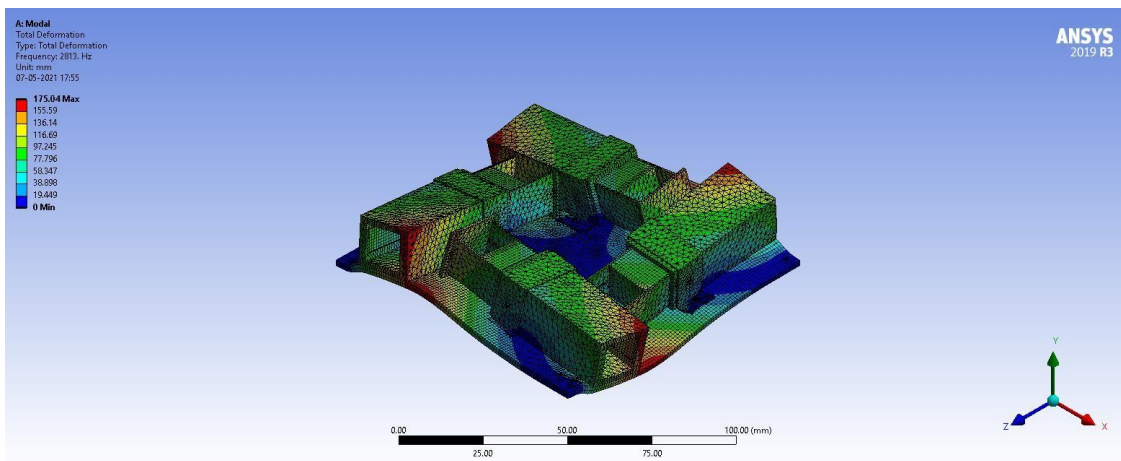


Fig 5.31: 1<sup>st</sup> Mode shape of 4 PPT's mounted on baseplate

- 1<sup>st</sup> MODE SHAPE
- Frequency : 2813 Hz

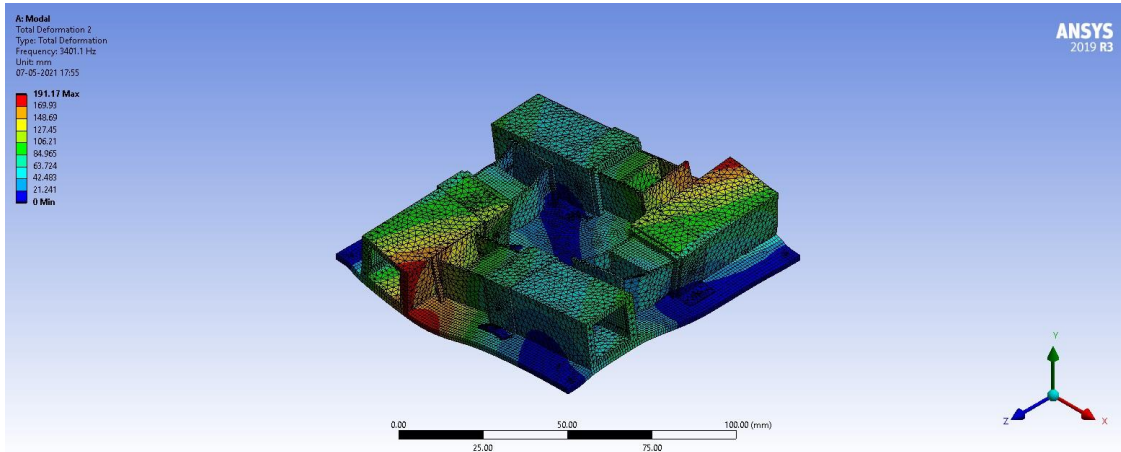


Fig 5.32: 2<sup>nd</sup> Mode shape of 4 PPT's mounted on baseplate

- 2<sup>nd</sup> MODE SHAPE
- Frequency : 3401.1 Hz

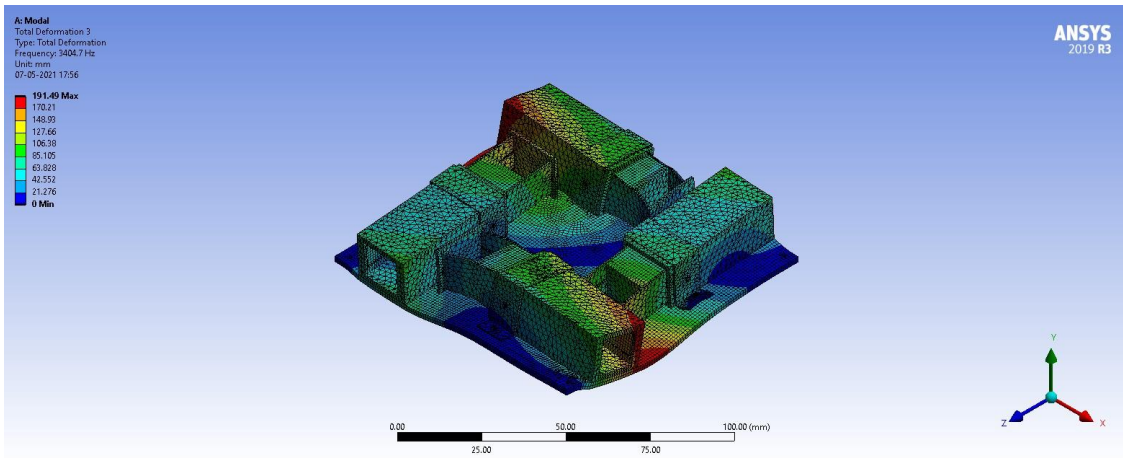


Fig 5.33: 3<sup>rd</sup> Mode shape of 4 PPT's mounted on baseplate

- 3<sup>rd</sup> MODE SHAPE
- Frequency : 3404.7 Hz

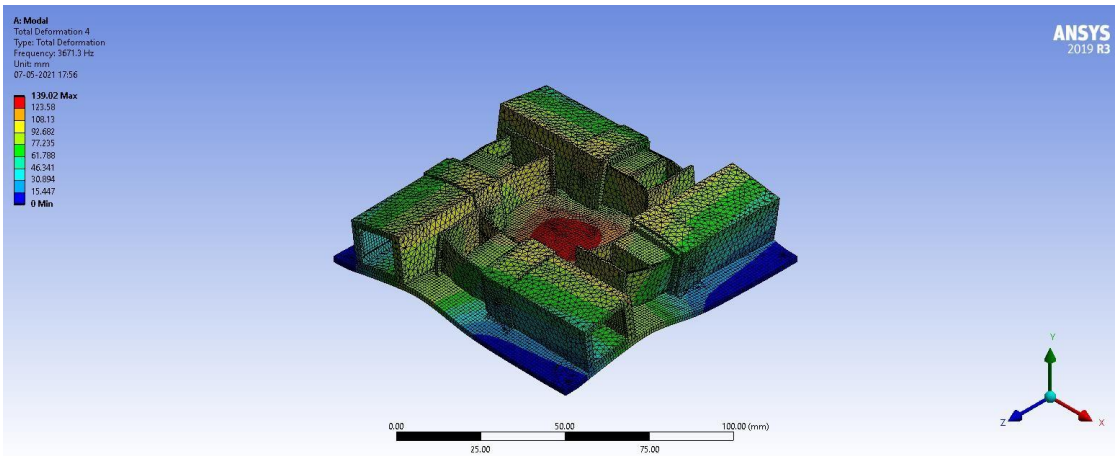


Fig 5.34 4<sup>th</sup> Mode shape of 4 PPT's mounted on baseplate

- 4<sup>th</sup> MODE SHAPE
- Frequency : 3671.3 Hz

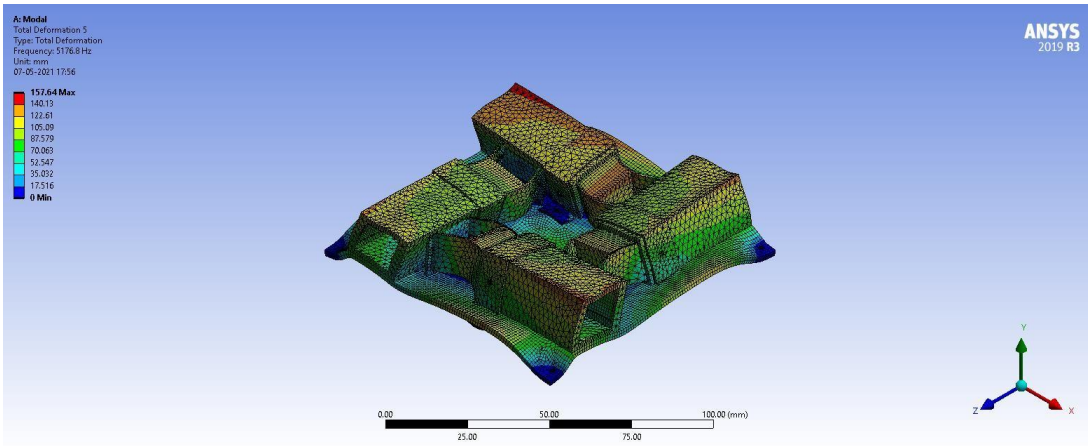


Fig 5.35: 5<sup>th</sup> Mode shape of 4 PPT's mounted on baseplate

- 5<sup>th</sup> MODE SHAPE
- Frequency : 5176.8 Hz

Table 5.4: Case2 Mode and Frequency (Hz)

Mode	Frequency [Hz]
1.	2813
2.	3401.1
3.	3404.7
4.	3671.3
5.	5176.8

## Case 2.1: Random Vibration acting on X Axis

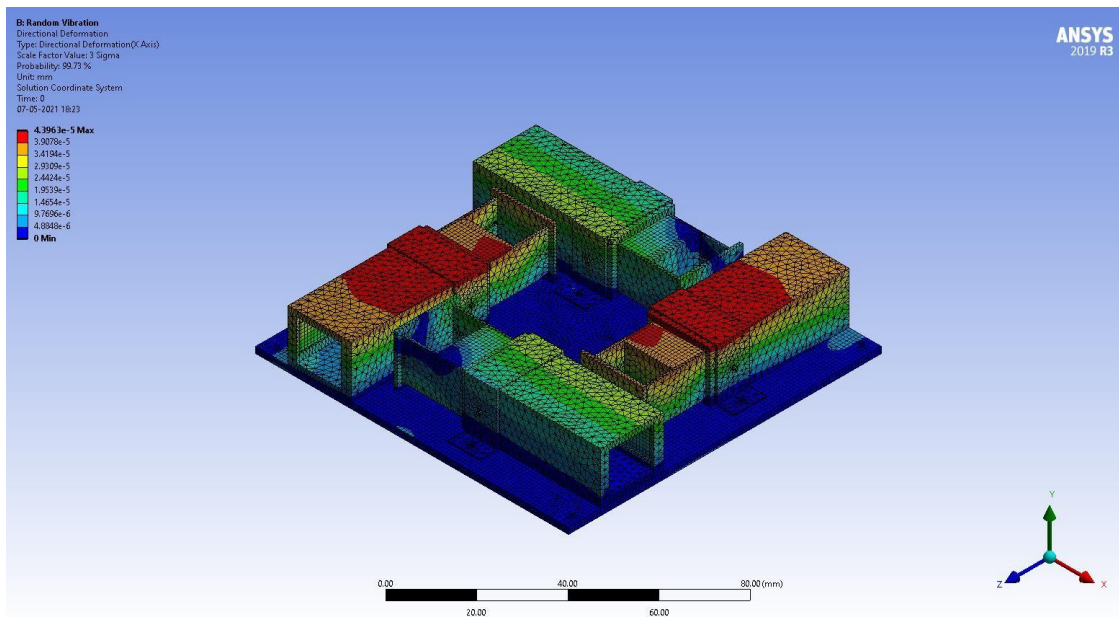


Fig 5.36: (X-Test) Random Vibration acting on X Axis

- X- Axis
- 3 Sigma— 99.73 %
- Max Deformation = 0.000043963 mm

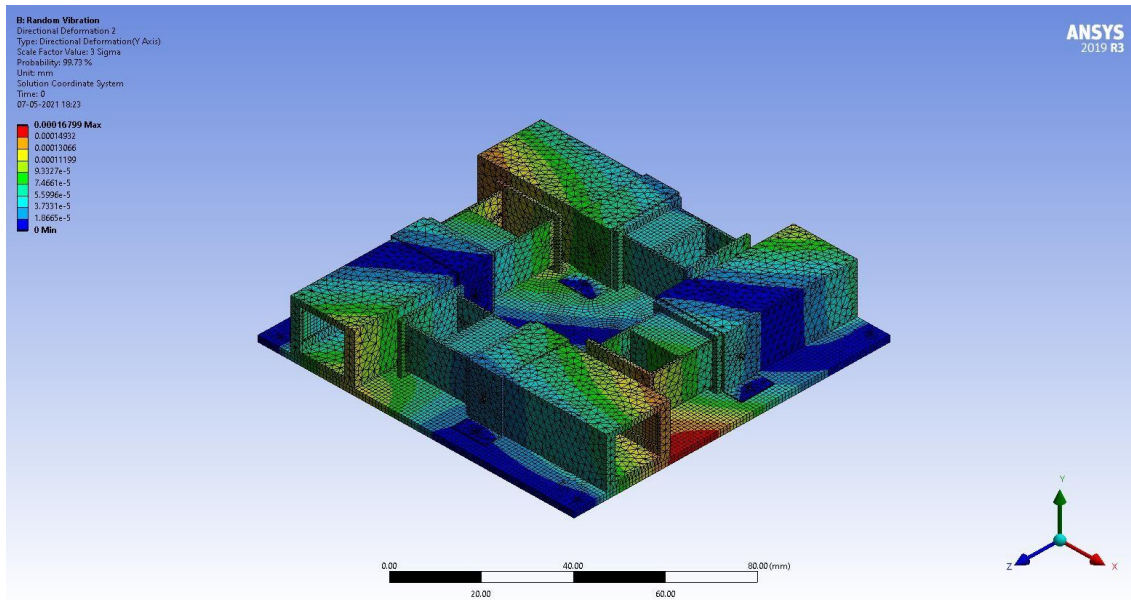


Fig 5.37: (X-Test) Random Vibration acting on Y Axis

- Y- Axis
- 3 Sigma— 99.73 %
- Max Deformation = 0.00016799 mm

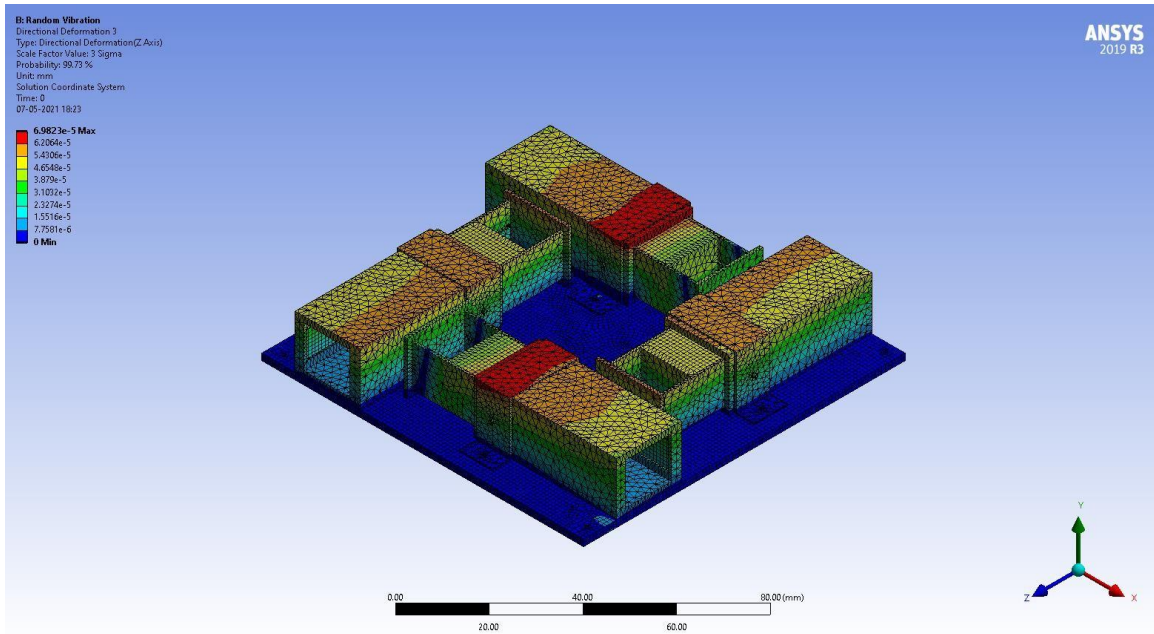


Fig 5.38: (X-Test) Random Vibration acting on Z Axis

- Z- Axis
- 3 Sigma— 99.73 %
- Max Deformation = 0.0000695 mm

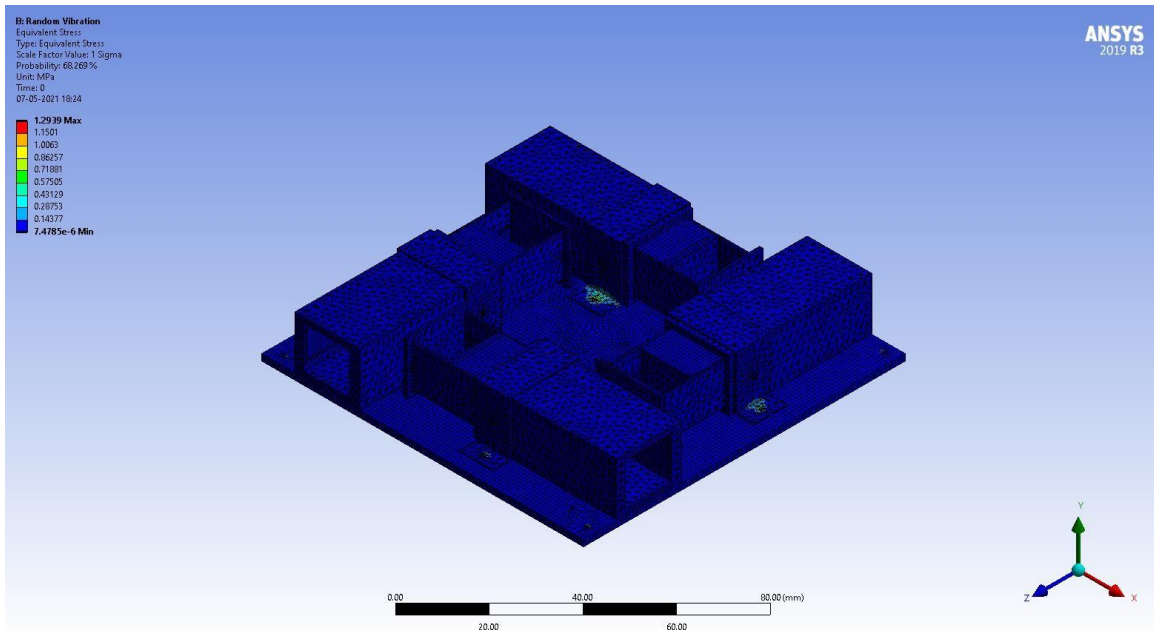


Fig 5.39: Equivalent stresses acting on X Axis

- Equivalent Stress (X - Axis) = 1.2939 MPa

## Case 2.2: Random Vibration acting on Y Axis

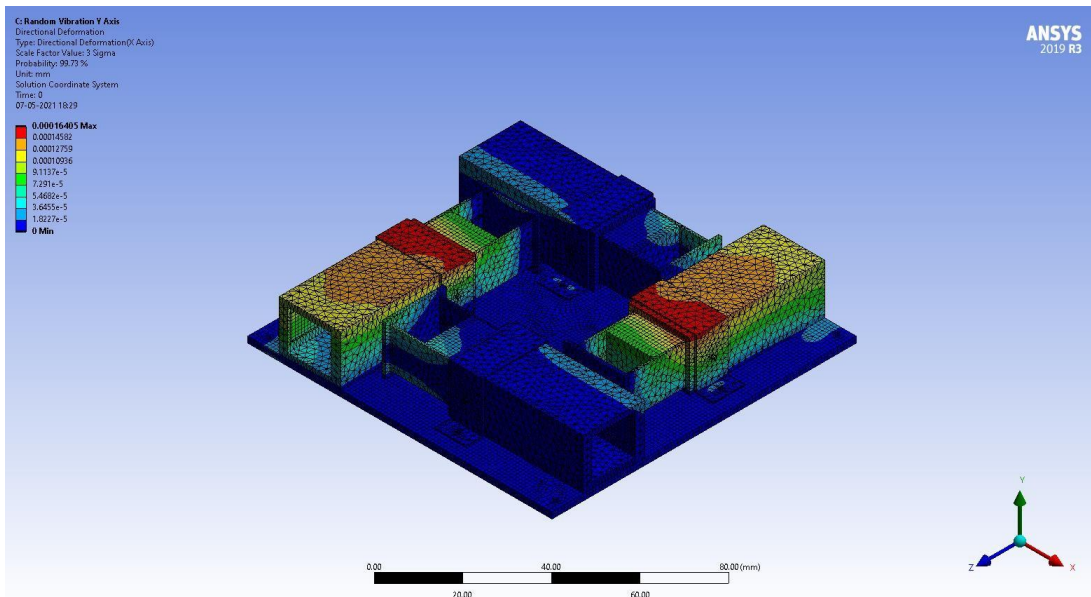


Fig 5.40: (Y-Test) Random Vibration acting on X Axis

- X - Axis
- 3 Sigma— 99.73 %
- Max Deformation = 0.00016405 mm

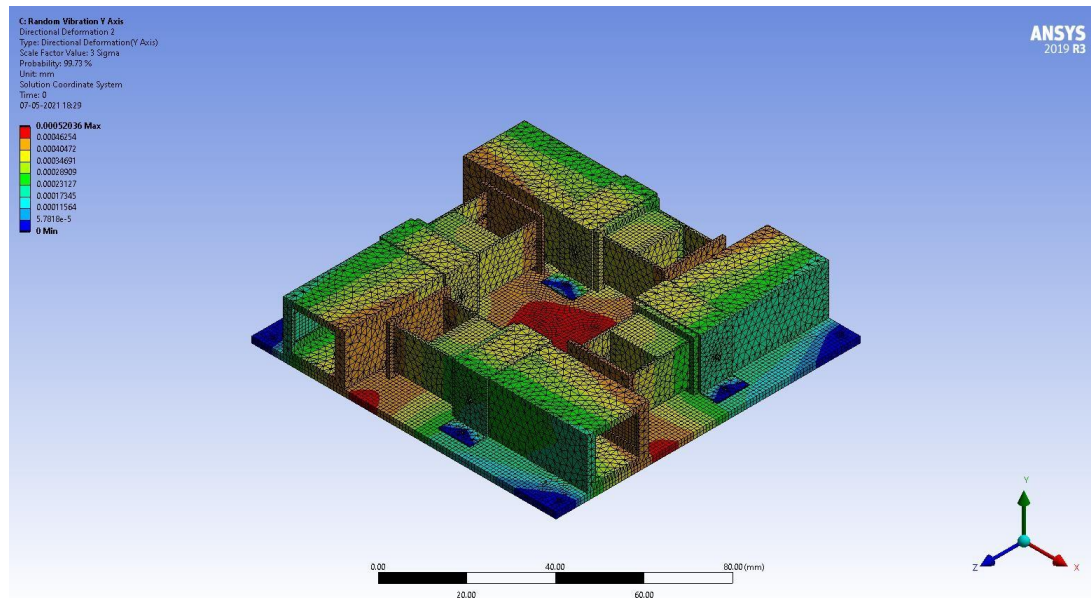


Fig 5.41: (Y-Test) Random Vibration acting on Y Axis

- Y - Axis
- 3 Sigma— 99.73 %
- Max Deformation = 0.00052036 mm

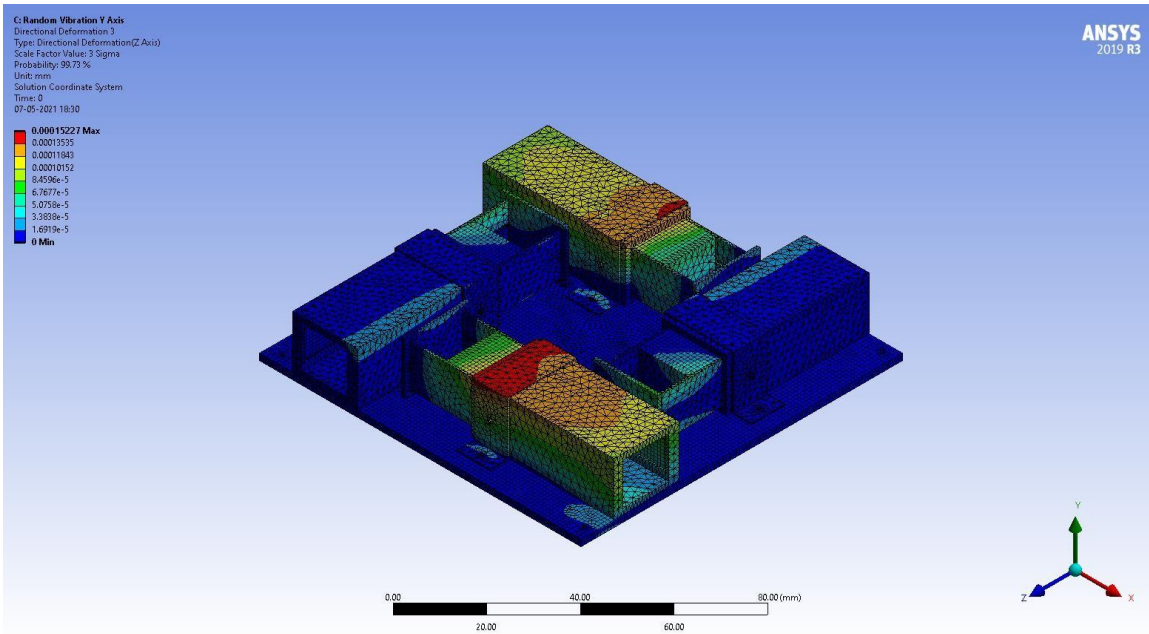


Fig 5.42: (Y-Test) Random Vibration acting on Z Axis

- Z - Axis
- 3 Sigma— 99.73 %
- Max Deformation = 0.00015227 mm

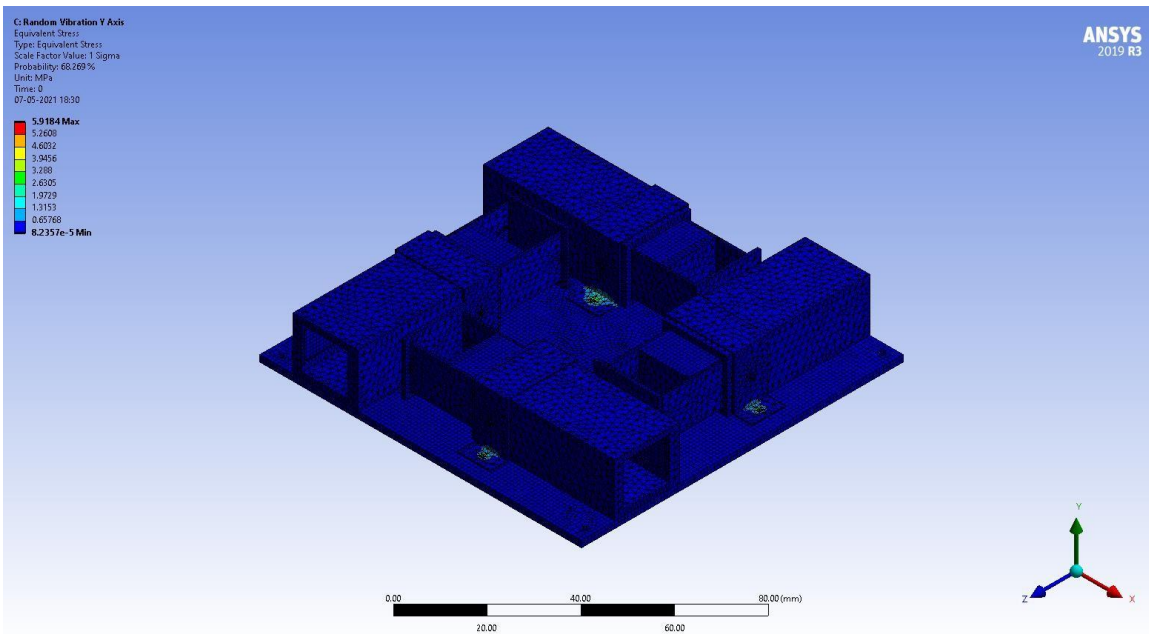


Fig 5.43: (Y-Test) Equivalent stresses acting on Y Axis

- Equivalent Stress (Y - Axis)= 5.918 MPa

### Case 2.3: Random Vibration acting on Z Axis

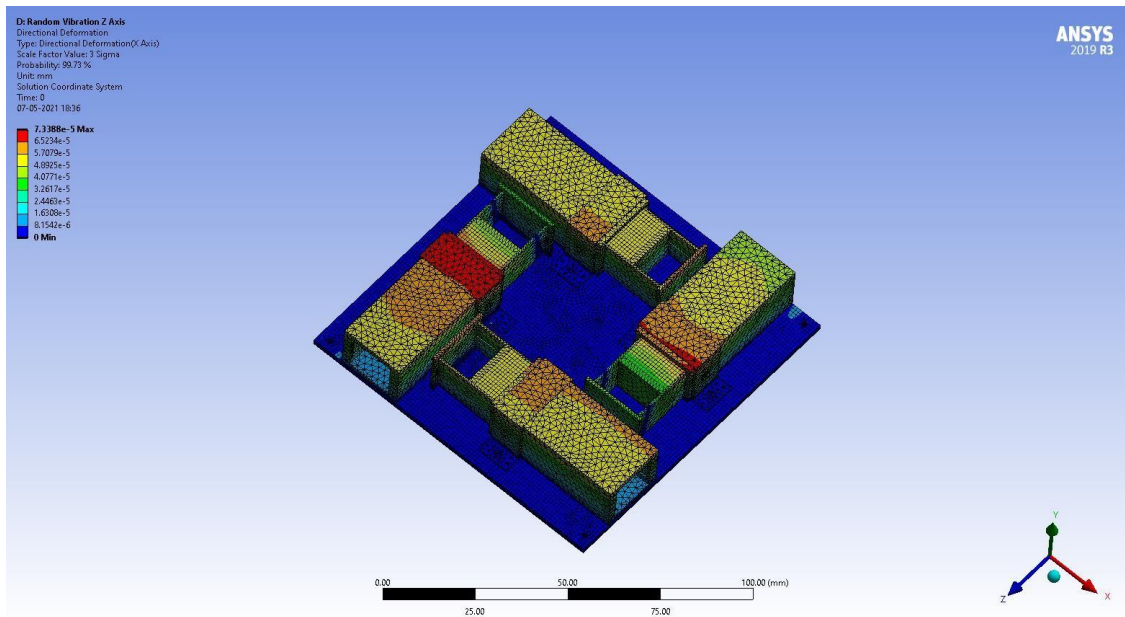


Fig 5.44: (Z-Test) Random Vibration acting on X Axis

- X - Axis
- 3 Sigma— 99.73 %
- Max Deformation = 0.000073388 mm

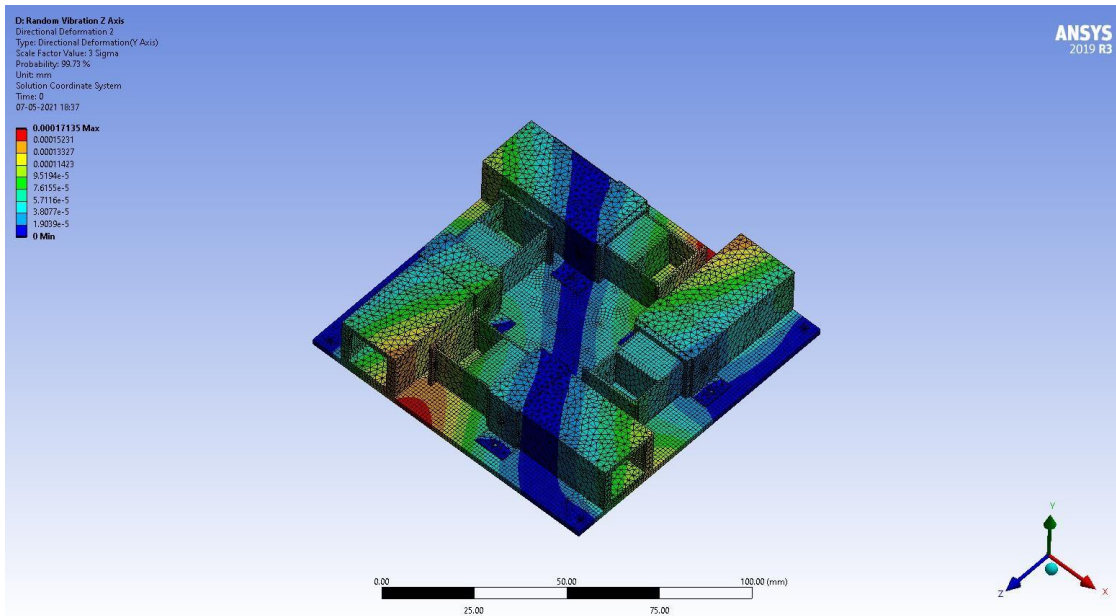


Fig 5.45: (Z-Test) Random Vibration acting on Y Axis

- Y - Axis
- 3 Sigma— 99.73 %
- Max Deformation = 0.00017835 mm

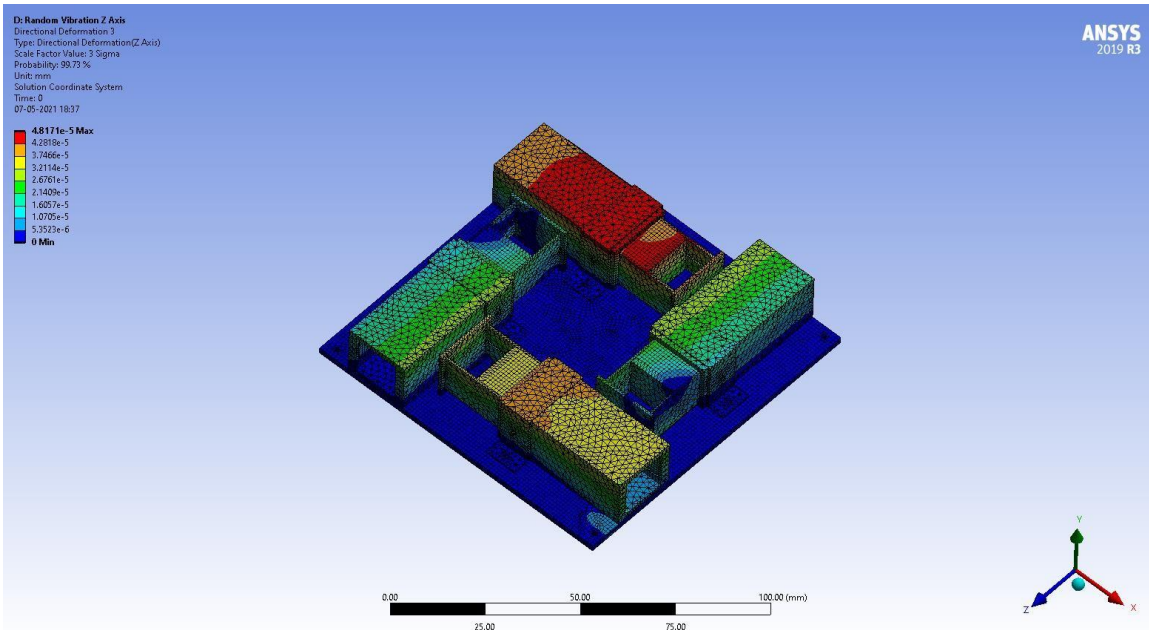


Fig 5.46: (Z-Test) Random Vibration acting on Z Axis

- Z - Axis
- 3 Sigma— 99.73 %
- Max Deformation = 0.000048171 mm

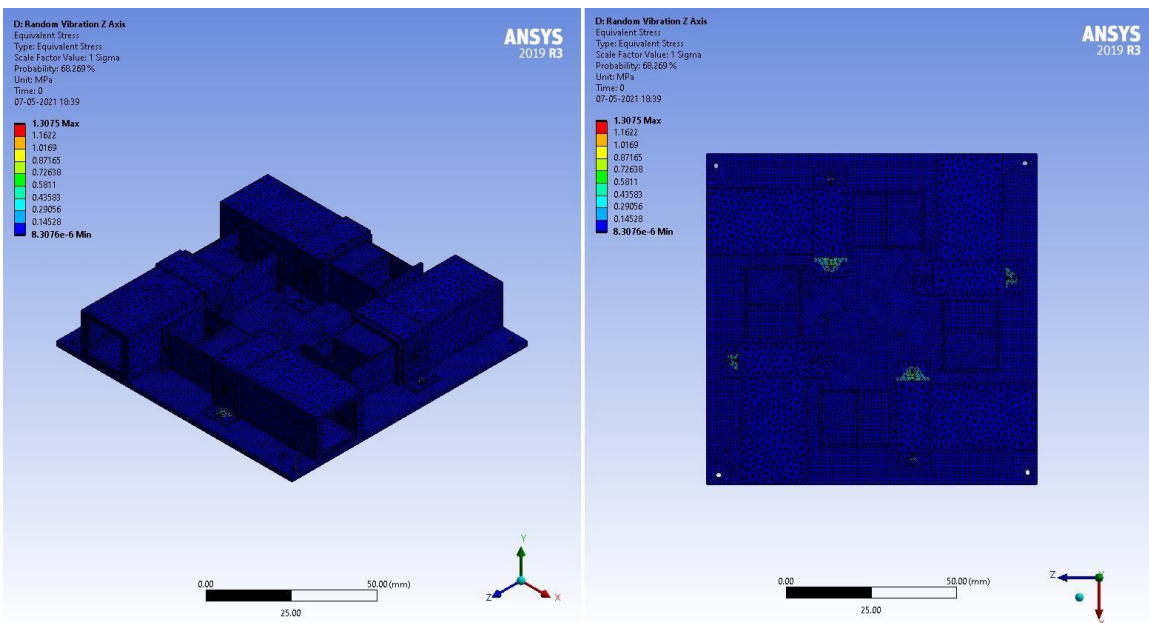


Fig 5.47: Equivalent Stresses acting on Z Axis

- Equivalent Stress (Z - Axis)= 1.3075 MPa

### **Case 3: Modal Analysis of PPT's and CubeSat frame**

The CubeSat frame was custom designed in Solidworks and followed all the design guidelines provided by California Polytechnic State University(CalPoly) CubeSat program.

In this case there were 10 mode shapes compared to only 5 for the other 2 cases.

These Mode shapes do not determine the actual deformation that occur during launch phase.

Table 5.5: Case 3 Mode and Frequency (Hz)

Mode	Frequency [Hz]
1.	277.91
2.	290.16
3.	552.27
4.	556.86
5.	567.26
6.	598.43
7.	809.3
8.	851.35
9.	1064.4
10.	1546.9

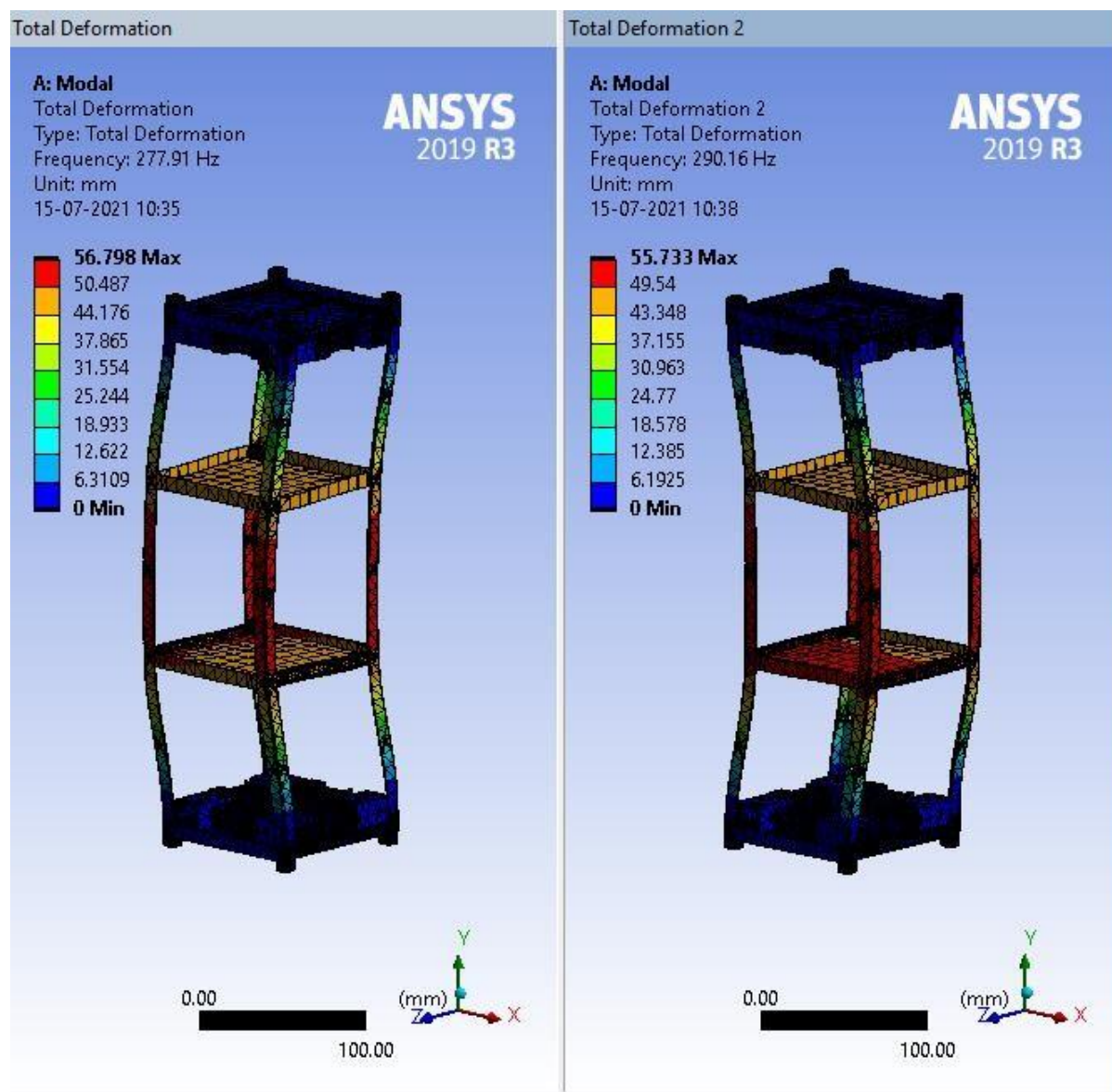


Fig 5.48: 1<sup>st</sup> and 2<sup>nd</sup> Mode Shapes of CubeSat frame and thruster

- 1<sup>st</sup> Mode Shape
- Frequency: 277.91 Hz
- 2<sup>nd</sup> Mode Shape
- Frequency: 290.16 Hz

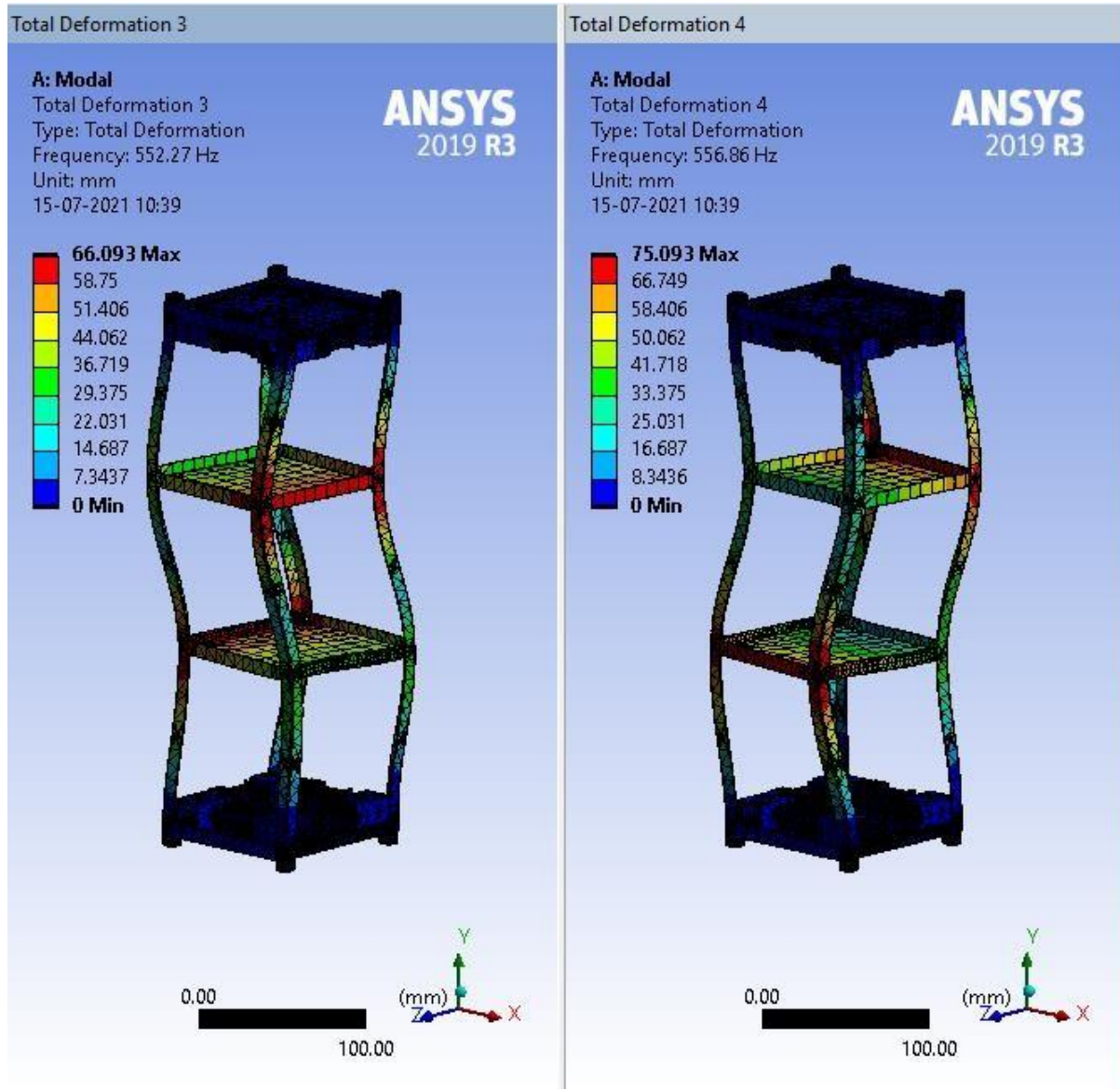


Fig 5.49: 3<sup>rd</sup> and 4<sup>th</sup> Mode Shapes of CubeSat frame and thruster

- 3<sup>rd</sup> Mode Shape
- Frequency: 552.27 Hz
- 4<sup>th</sup> Mode Shape
- Frequency: 556.86 Hz

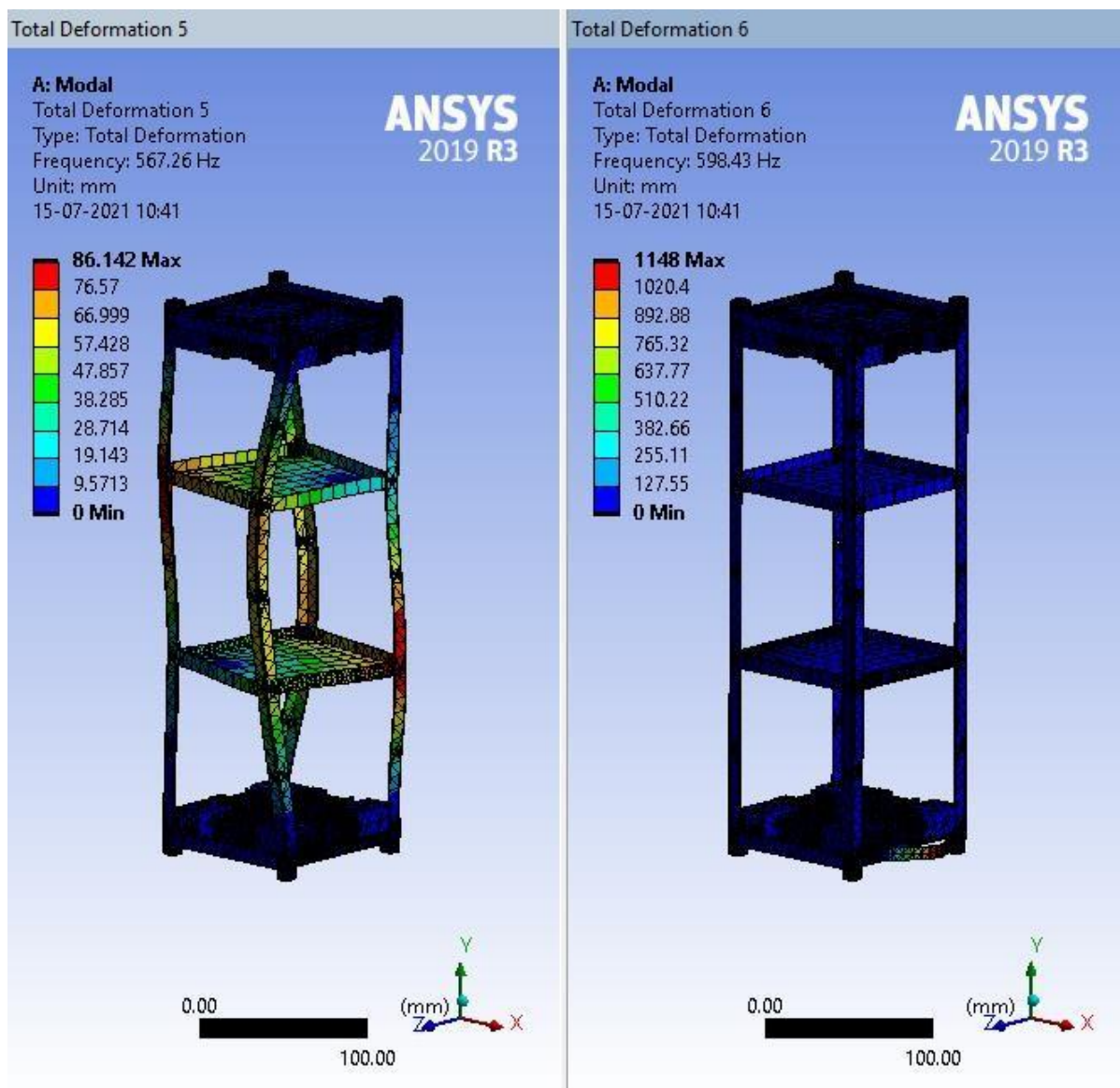


Fig 5.50: 5<sup>th</sup> and 6<sup>th</sup> Mode Shapes of CubeSat frame and thruster

- 5<sup>th</sup> Mode Shape
- Frequency: 567.26 Hz
- 6<sup>th</sup> Mode Shape
- Frequency: 598.43 Hz

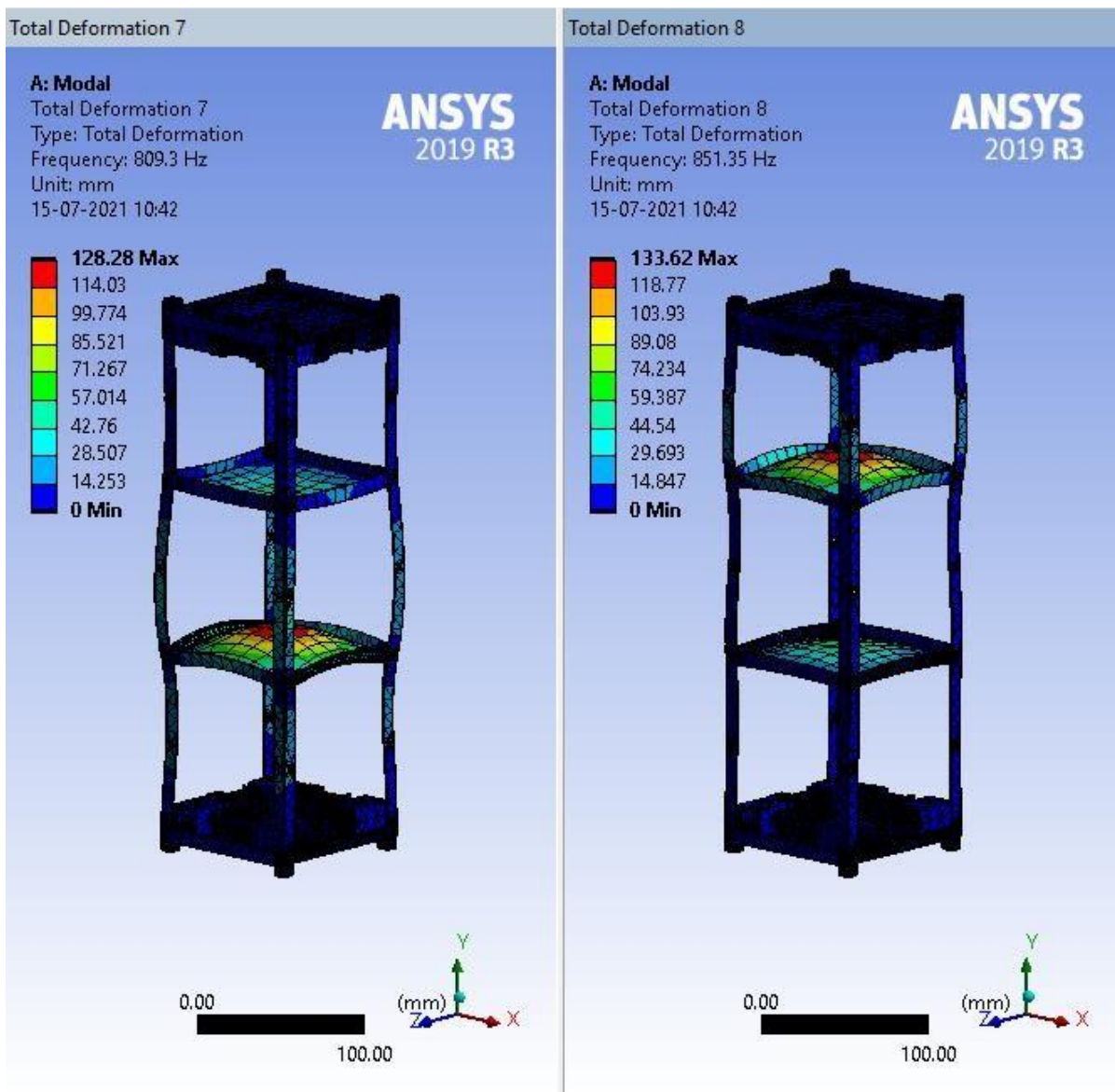


Fig 5.51: 7<sup>th</sup> and 8<sup>th</sup> Mode Shapes of CubeSat frame and thruster

- 7<sup>th</sup> Mode Shape
- Frequency: 809.3 Hz
- 8<sup>th</sup> Mode Shape
- Frequency: 851.35 Hz

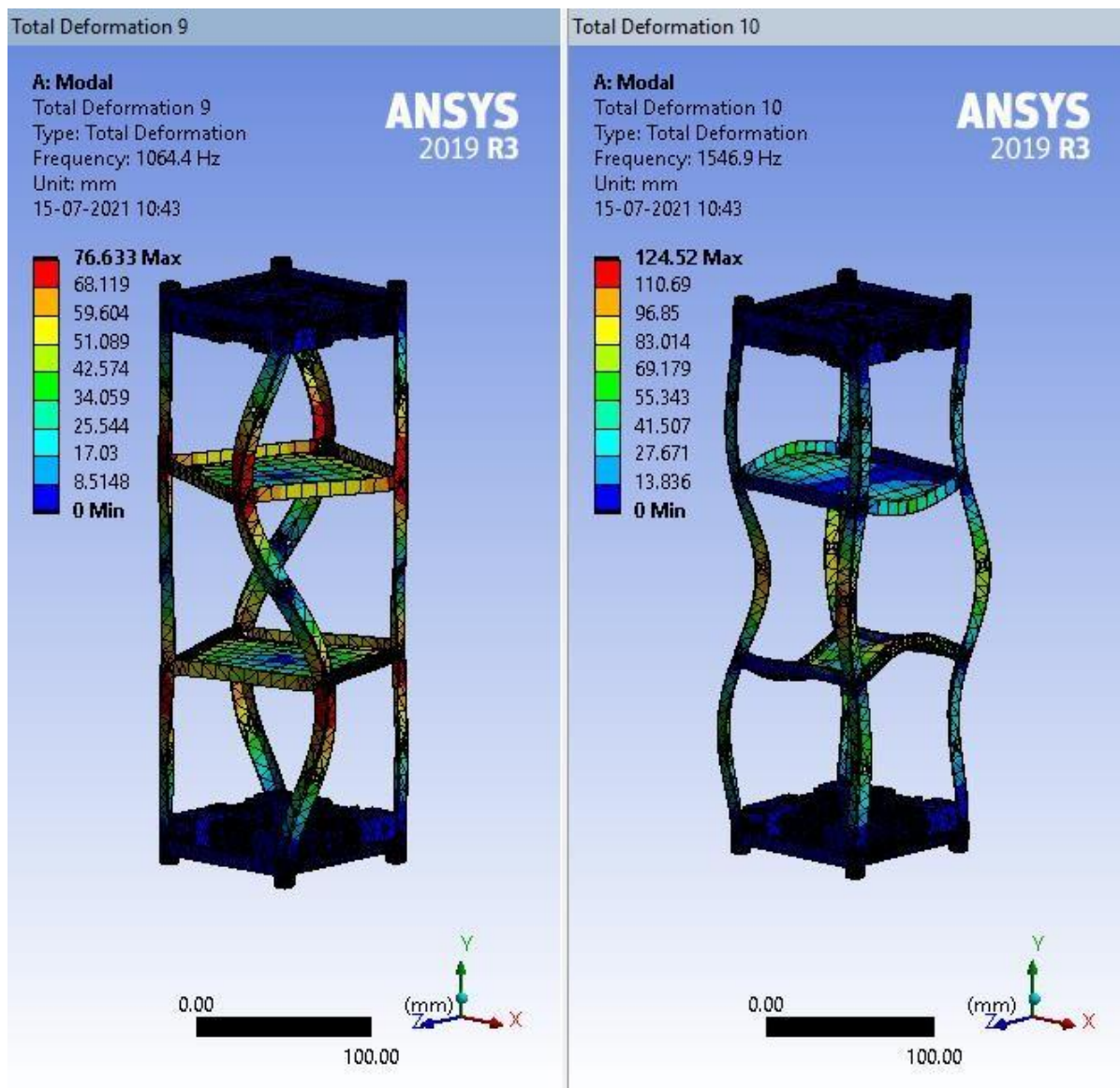


Fig 5.52: 9<sup>th</sup> and 10<sup>th</sup> Mode Shapes of CubeSat frame and thruster

- 9<sup>th</sup> Mode Shape
- Frequency: 1064.4 Hz
- 10<sup>th</sup> Mode Shape
- Frequency: 1546.9 Hz

### Case 3.1: Random Vibration acting on X Axis

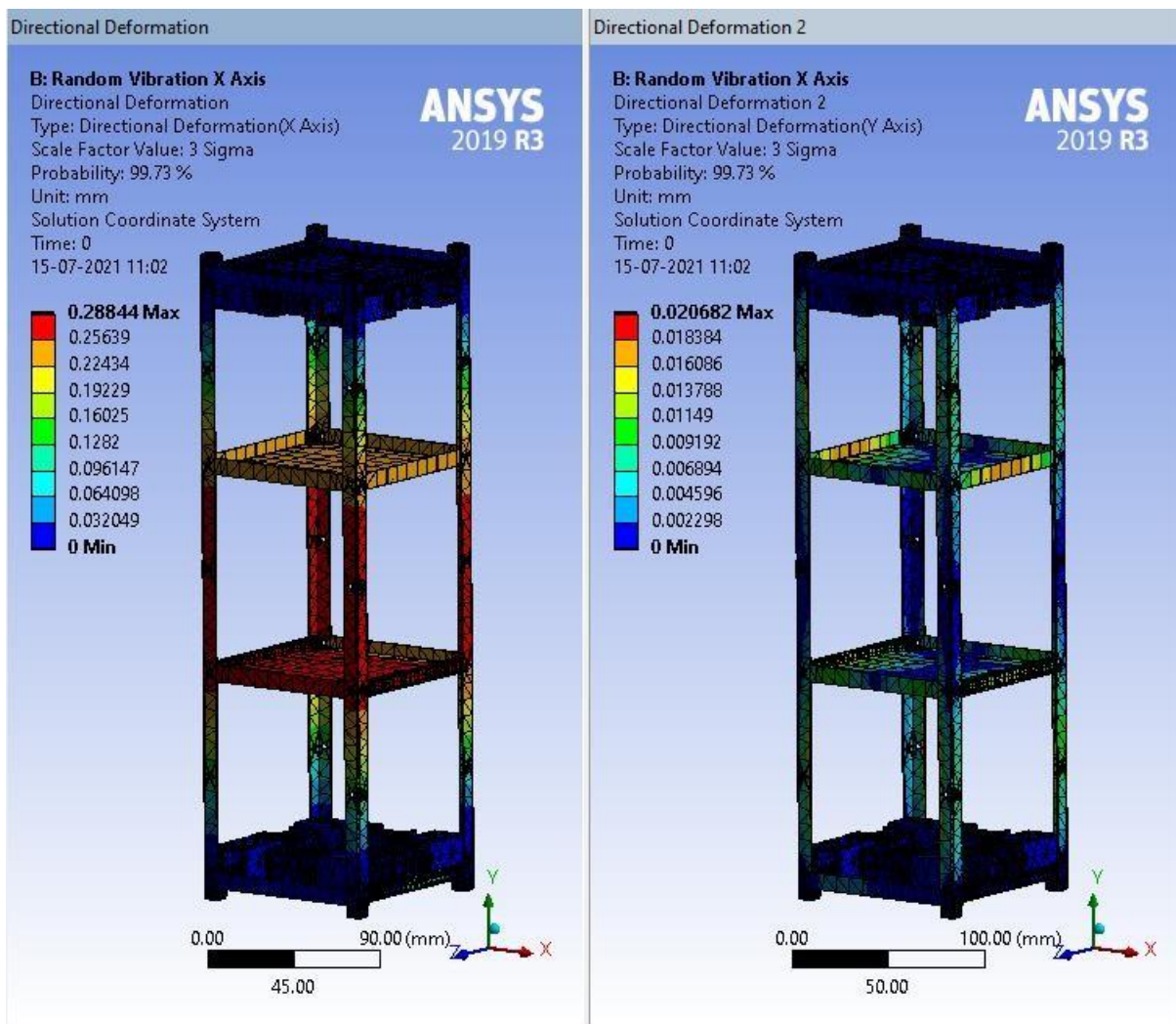


Fig 5.53: (X-Axis Test) Random Vibration acting on X Axis and Y Axis

- X - Axis
- 3 Sigma— 99.73 %
- Max Deformation = 0.28844 mm
- Y - Axis
- 3 Sigma— 99.73 %
- Max Deformation = 0.020682 mm

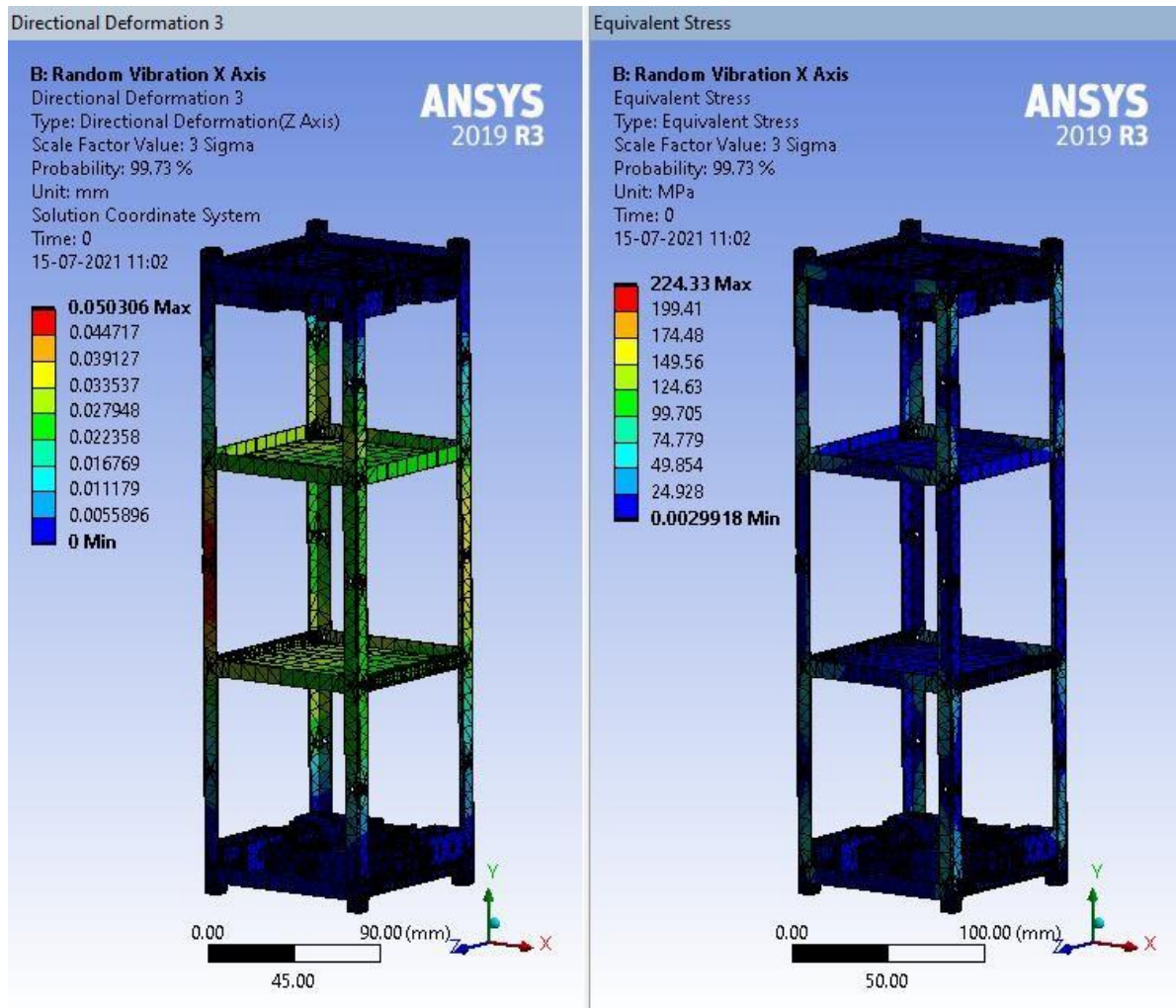


Fig 5.54: (X-Axis Test) Random Vibration acting on Z Axis and Equivalent stresses for case

3.1

- Z - Axis
- 3 Sigma— 99.73 %
- Max Deformation = 0.050306 mm
- Equivalent stresses X - Axis
- 3 Sigma— 99.73 %
- Max Stress = 22433 MPa

### Case 3.2: Random Vibration acting on Y Axis

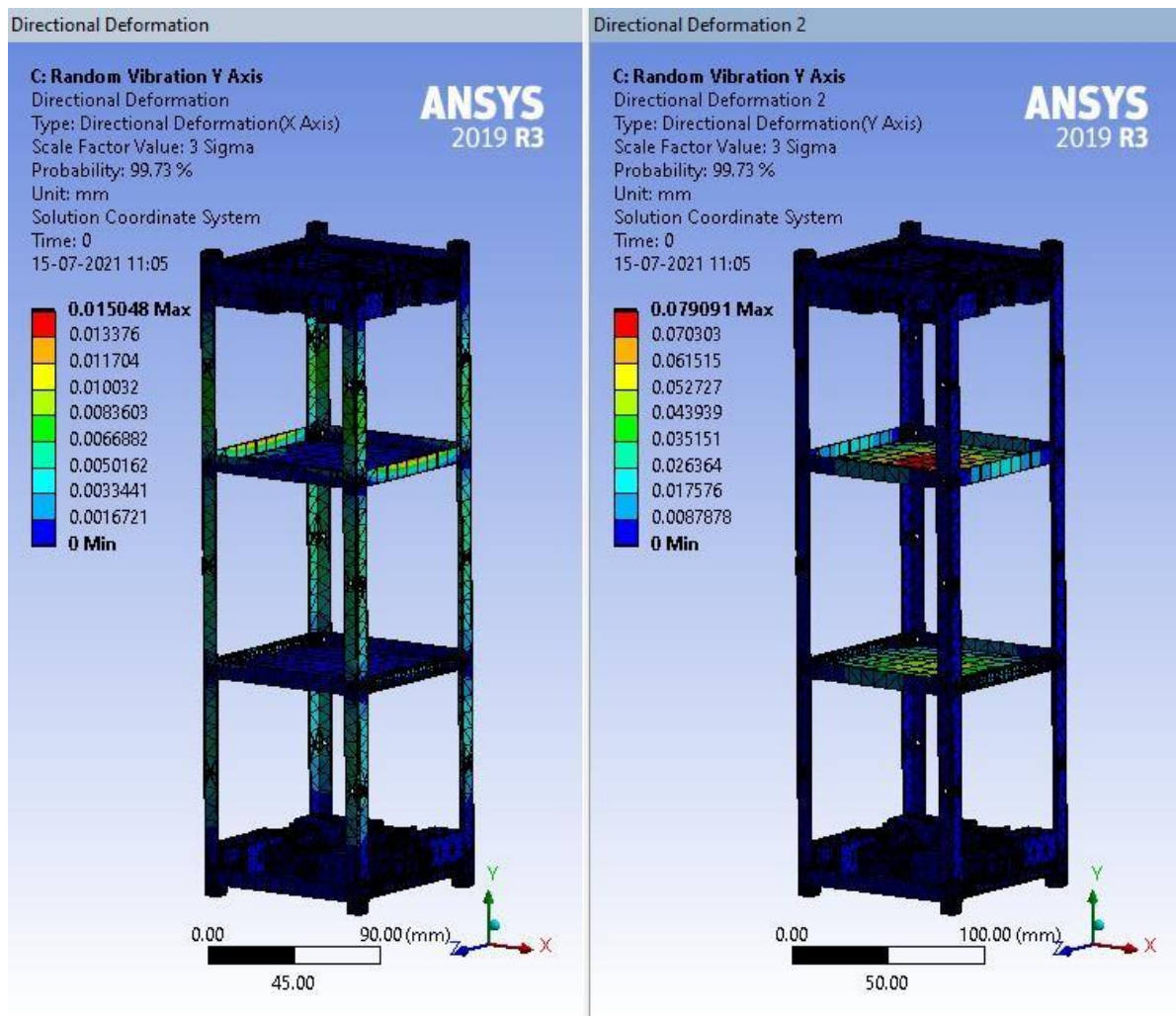


Fig 5.55: (Y-Axis Test) Random Vibration acting on X Axis and Y Axis

- X - Axis
- 3 Sigma– 99.73 %
- Max Deformation = 0.015048 mm
- Y - Axis
- 3 Sigma– 99.73 %
- Max Deformation = 0.07909 mm

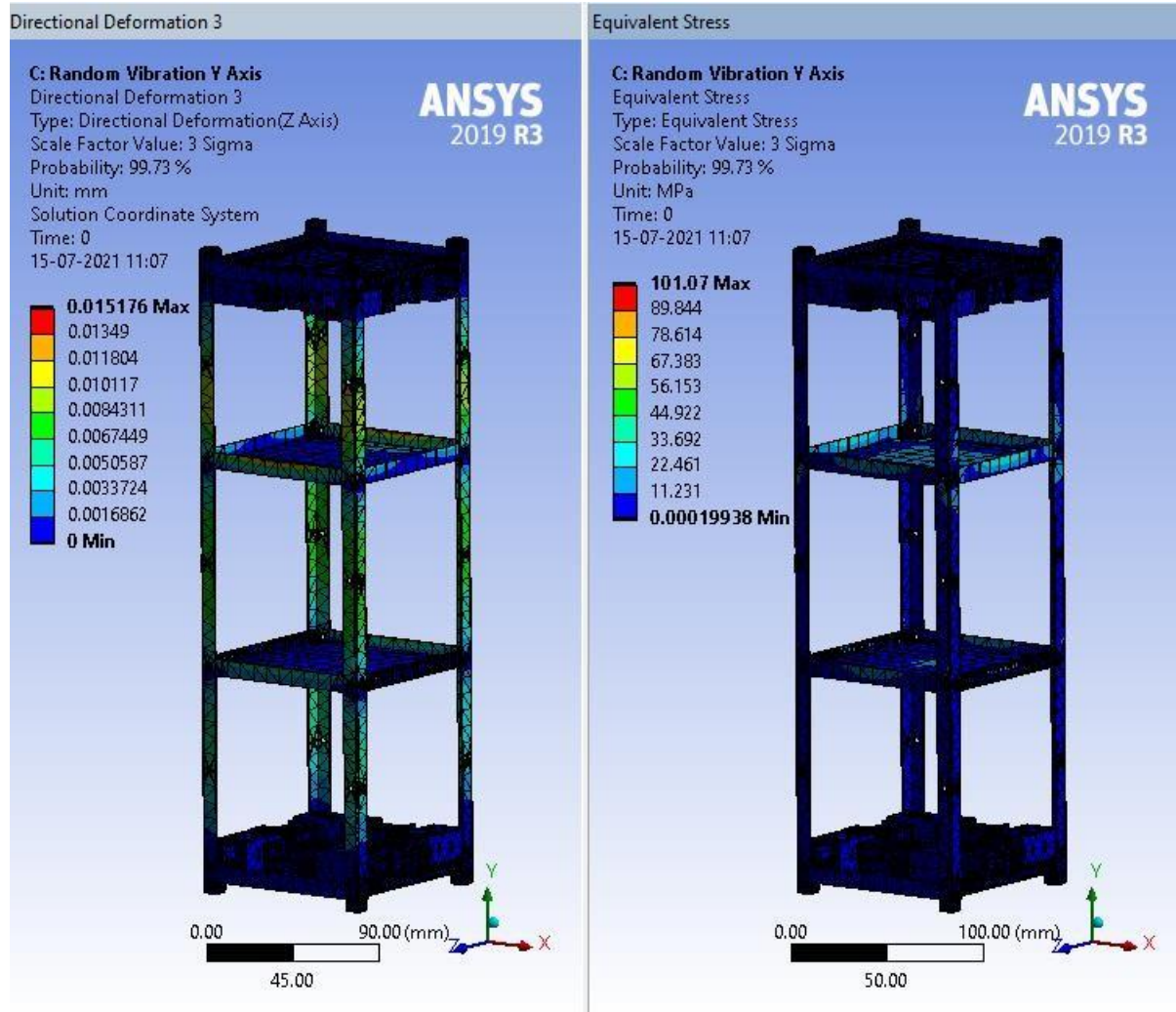


Fig 5.56: Random Vibration acting on Z Axis and Equivalent stresses for Case 3.2

- Z - Axis
- 3 Sigma— 99.73 %
- Max Deformation = 0.015176 mm
- Equivalent stresses Y - Axis
- 3 Sigma— 99.73 %
- Max Stress = 101.07 MPa

### Case 3.3: Random Vibration acting on Z Axis

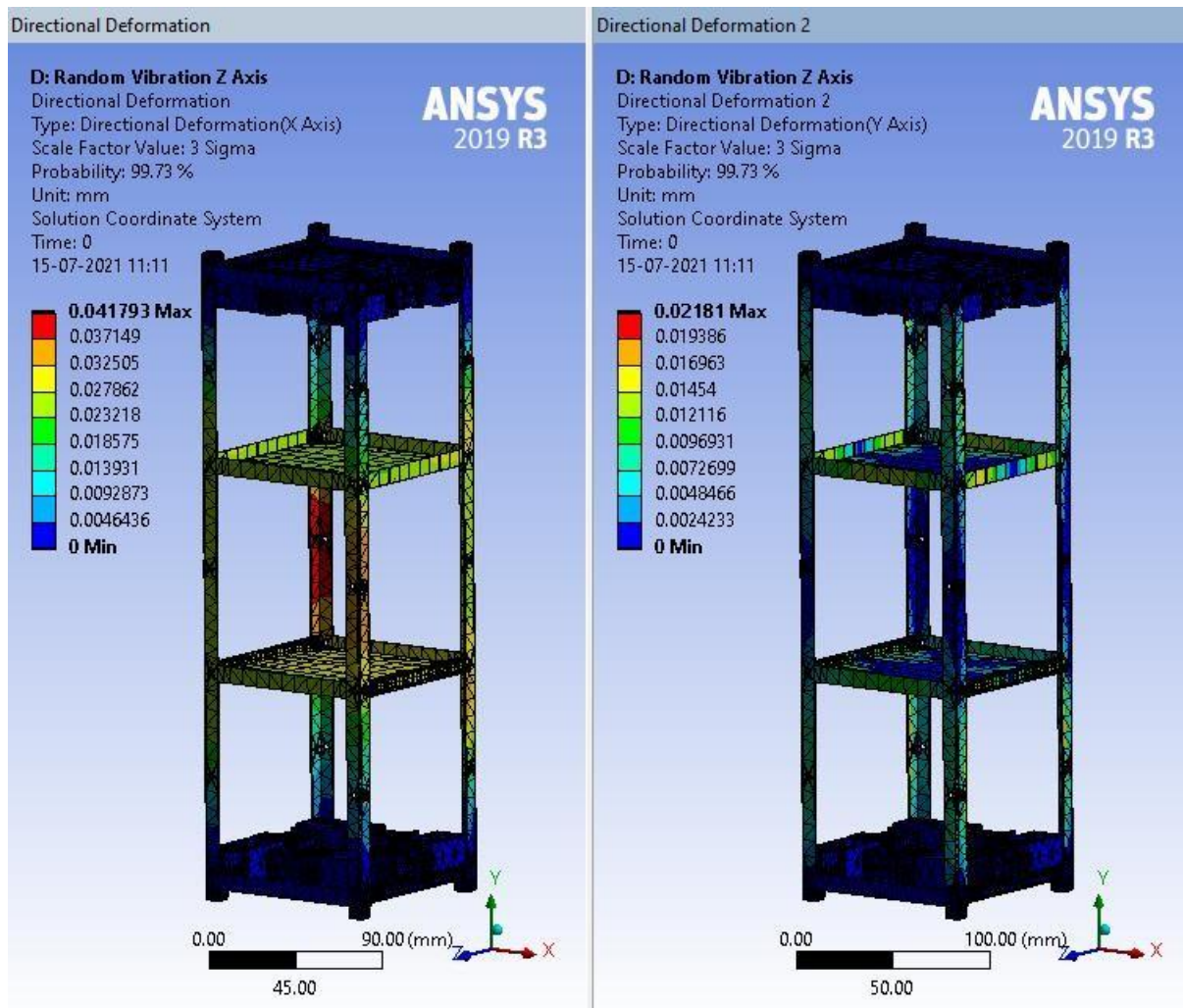


Fig 5.57: (Z-Axis Test) Random Vibration acting on X Axis and Y Axis

- X - Axis
- 3 Sigma— 99.73 %
- Max Deformation = 0.041793 mm
- Y - Axis
- 3 Sigma— 99.73 %
- Max Deformation = 0.02181 mm

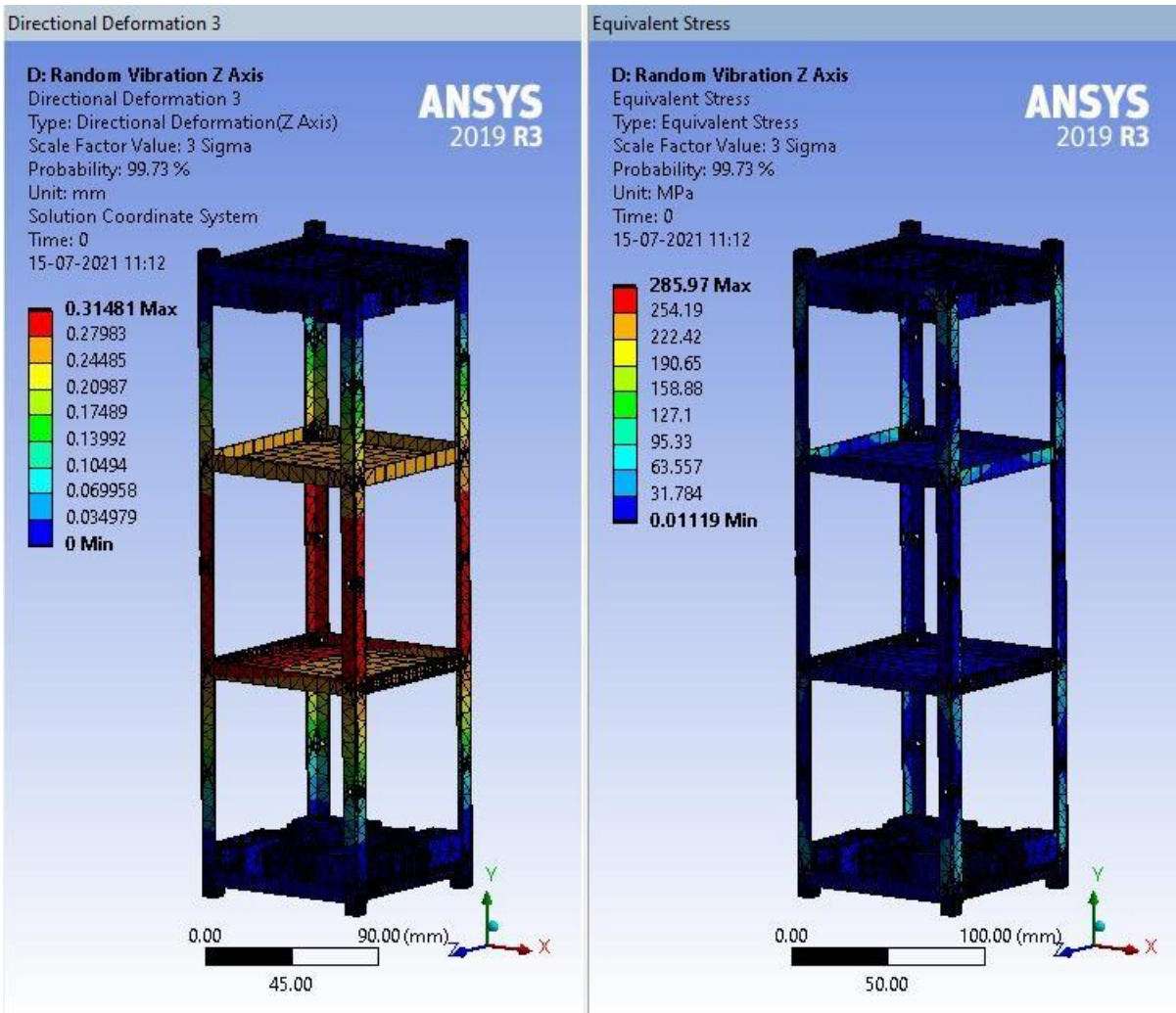


Fig 5.58: (Z-Axis Test) Random Vibration acting on Z Axis and Equivalent stresses for Case 3.3

- Z - Axis
- 3 Sigma— 99.73 %
- Max Deformation = 0.31481 mm
- Equivalent stresses Y - Axis
- 3 Sigma— 99.73 %
- Max Stress = 285.97 MPa

## 5.2 Electrical Analysis

The correct function of our micro-pulse plasma thruster will depend on the generation of an arc between two parallel electrodes. The vacuum ignition system is responsible for creating the initial conduction path for the electrons between the parallel plates of the cathode and anode. Field emission is the main electrical breakdown mechanism in vacuum. Field emission is caused by an electrostatic field, which causes electrons to be emitted from the cathode to the anode. Table 7 summarizes the vacuum ignition methods that can be used for parallel plate pulsed plasma propellants.

The ideal system should run at low voltage, be small and light to fit a 3U volume, and have a simple mechanical structure to avoid malfunctions due to the high repetition rate of spark ignition.

Because the system is simple, the non-trigger vacuum arc ignition system is more suitable for micro PPT. The system requires an arc switch and a boost circuit. The device used to create the initial driving route is a spark plug. The voltage level to achieve ignition is within the range of 700V to 2000V. The limiting factors for a trigger less vacuum arc ignition system are the size and weight of the spark plug, the size and weight of the boost circuit 38, and the maximum instantaneous power CubeSat can use to power the boost circuit.

Table 5.6: Methods for Vacuum Arc ignition

<b>Triggering Mechanisms</b>	<b>Advantages</b>	<b>Disadvantages</b>
High-Voltage Vacuum breakdown	No contamination of metal plasma	Requires a high voltage, not usable for repetitive mode operation
Fuse Wire Explosion	No Contamination of metal Plasma	Not usable for repetitive mode operation
Contact Separation	Reliable, Simple, Repeatable	Low repetition rate, Contacts may weld
Mechanical Triggering	Reliable, Relatively simple	Low repetition rate; contacts may weld and wear; limited number of triggering events (less than $10^4$ ) large jitter
High-Voltage Surface Discharge	High repetition rates, reliable typically up to $10^5$ pulses, low jitter	Needs high voltage pulser, Erosion of insulator
Plasma Injection Triggering	No trigger Supply	Needs sufficiently high Pressure in discharge vicinity, metal plasma contamination
Low-Voltage Vacuum Arc Initiation	Reliable for $10^5$ pulses, simple, high repetition rate, works without high voltage	Needs arc switch and moderate ‘booster’ voltage, May fail for low melting point and easily oxidizing cathode materials

### 5.2.1 Vacuum Arc Ignition Circuit

It is necessary to create two main circuits for each micro-PPT that we design. One circuit for the initial discharge that will create the conducting path with the help of a spark plug and a second circuit to continue the discharge after the initial circuit are used by applying a potential across the anode and cathode electrodes.

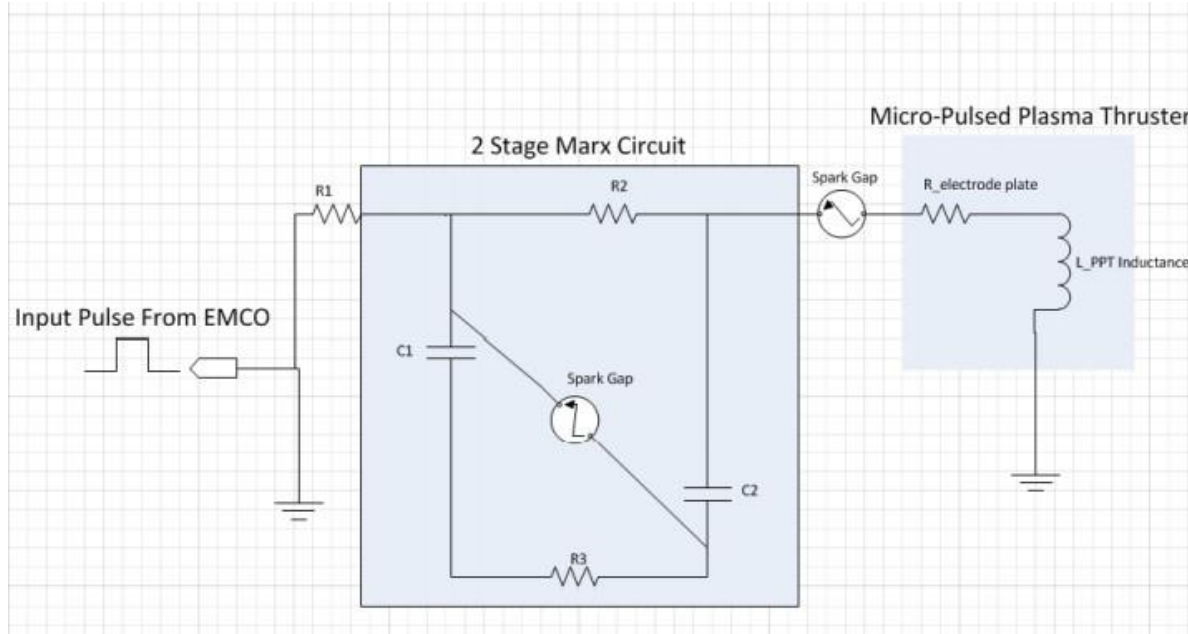


Fig 5.59: Vacuum ignition circuit

A 3V or a 5V signal is given to an EMCO Proportional Booster which gives a 750V output. The following pulse signal can be used to drive a power transistor to create the input pulse signal to the 2 Stage Marx Circuit. The PPT is represented by a resistor and a inductor depending on the material of the plates.

The Marx circuit is used to generate a high voltage pulse from a low voltage DC supply. A 1500V output signal is obtained from the Marx circuit which is applied across the electrode plates. The input signal from the power transistor and the output of the Marx circuit are shown in the figure below.



Fig 5.60: input pulse signal

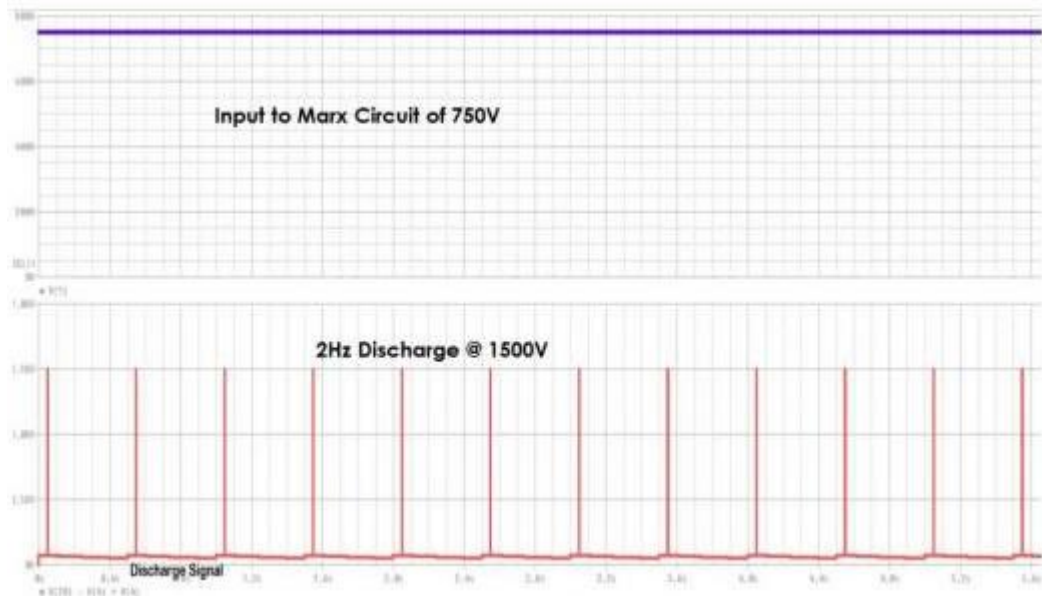


Fig 5.61: Marx circuit output

This 1.5kV of voltage being applies across the plate and to a discharge capacitor of 1uF which results in an arc which ablates the PTFE fuel and sublimates it to gas. The heat of this arc causes the gas to change to plasma thus, resulting in a charged gas cloud. This charged gas cloud gets pushed between the charged plates of anode and cathode thus effectively completing the circuit. This motion of electrons sets up an electro-magnetic field and Lorentz force propels the plasma out of the exhaust thus generating thrust.

## 5.3 Thermal Analysis of Fuel block

This section presents the thermal design and analysis of the Teflon fuel block using COMSOL.

### 5.3.1 Heat transfer in Solids

Transient thermal analysis will be conducted using Finite Element Analysis software COMSOL.

From the model wizard a 3d model was selected and under Select Physics section Heat transfer was selected, clicking on drop down icon and selecting Heat Transfer in Solids (ht) click on add and move to Study segment, under Select Study choose Time dependent study under the General studies tab.

Once the workbench is setup, under the geometry tab insert the Teflon Fuel block component and hit import.

Under Materials tab search for PTFE(Polytetrafluoroethylene) and insert in the values of Co-efficient of thermal expansion and Heat capacity at constant pressure.

Then under the Heat Transfer in Solids tab click on Solid 1 click on the equations tab, this software package solves the transient heat condition equations.

$$\rho C_p \frac{\partial T}{\partial t} + \rho C_p \mathbf{u} \cdot \nabla T + \nabla \cdot \mathbf{q} = Q + Q_{\text{ted}} \quad (5.1)$$

$$\mathbf{q} = -k \nabla T \quad (5.2)$$

Under the Heat Conduction, Solid segment insert in the values of Thermal Conductivity ( $k=0.247 \text{ w/(m-k)}$ )

Under the Thermodynamics, Solid segment insert in the values of Density ( $\rho=2200\text{kg/m}^3$ ) and Heat capacity at constant pressure ( $C_p = 1050 \text{ J/(kg-k)}$ )

Setting up the initial values, since it is dependent on the Temperature, the initial temperature was set to 296K. Thermal insulation was given to all the sides except the face where inward heat flux was acted upon.

$$-\mathbf{n} \cdot \mathbf{q} = 0 \quad (5.3)$$

Inserting a new segment called Heat flux under the main Heat Transfer in Solids section. Under the Heat Flux segment click on the General inward heat flux and  $q_0 = 20000 \text{ W/m}^2$ .

$$-\mathbf{n} \cdot \mathbf{q} = q_0 \quad (5.4)$$

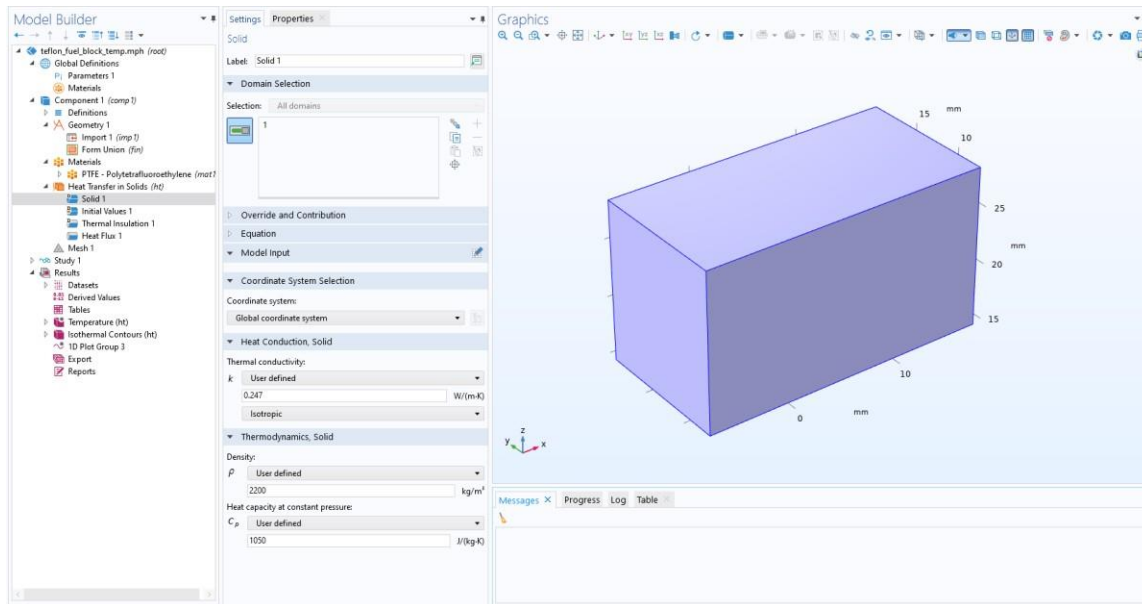


Fig 5.62: COMSOL interface

### 5.3.2 Meshing

Meshing in COMSOL is fairly easy, under the Mesh settings the sequence type chosen was Physics controlled mesh. The Element size chosen was Extra fine since the geometry was fairly a simple block.

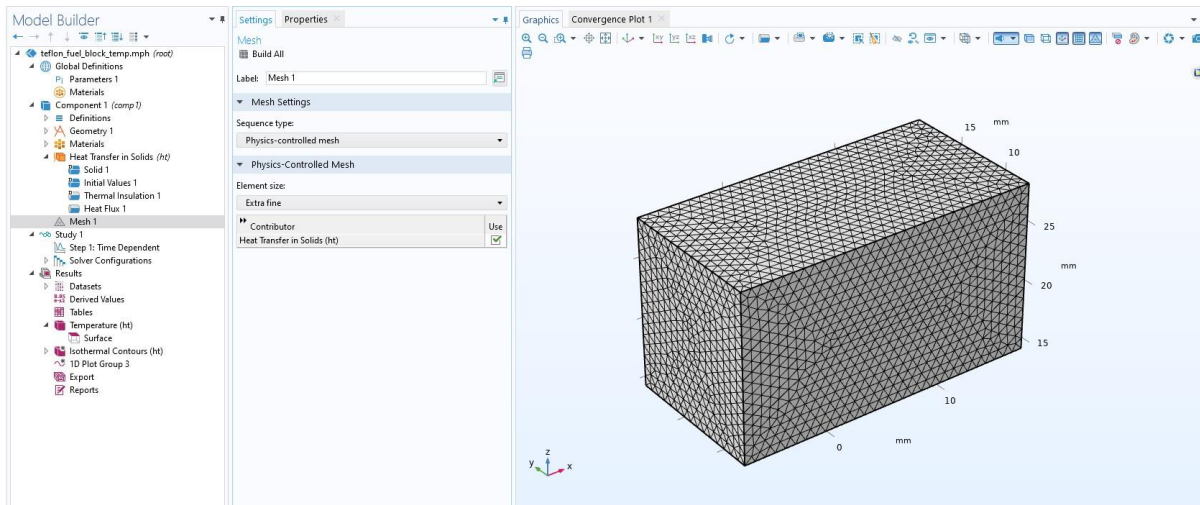


Fig 5.63: COMSOL Mesh Settings

PTFE (Teflon) propellant mesh:

Number of vertex elements: 8

Number of edge elements: 240

Number of boundary elements: 5408

Number of elements: 109386

Minimum element quality: 0.1918

Under Study segment change the time unit to seconds and add in output times and hit compute. Once the values are computed click on Plot under the Temperature contours of Results segment.

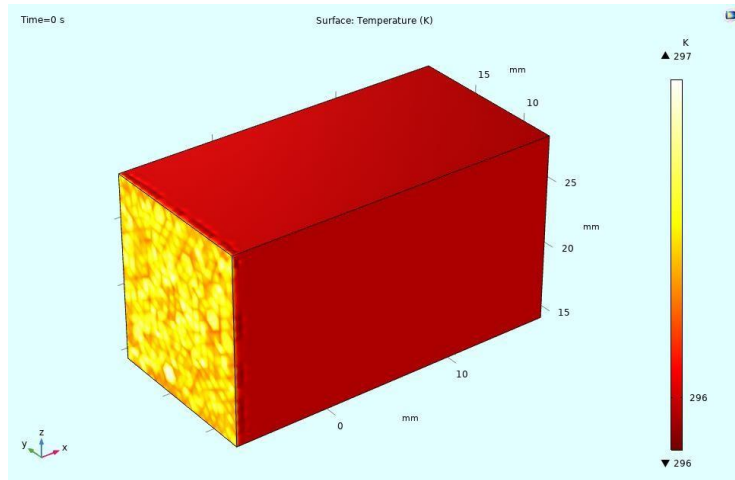


Fig 5.64: Time = 0 seconds

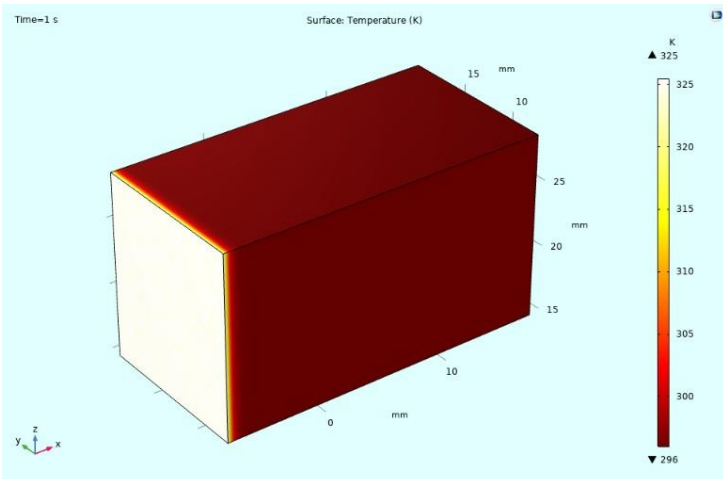


Fig 5.65: Time = 1 second

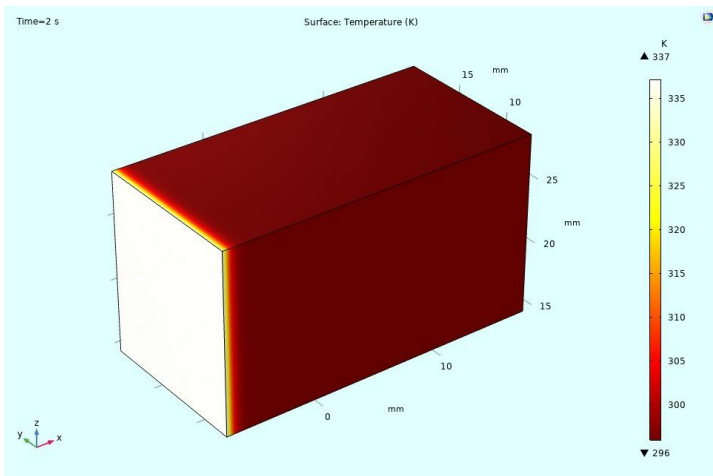


Fig 5.66: Time = 2 seconds

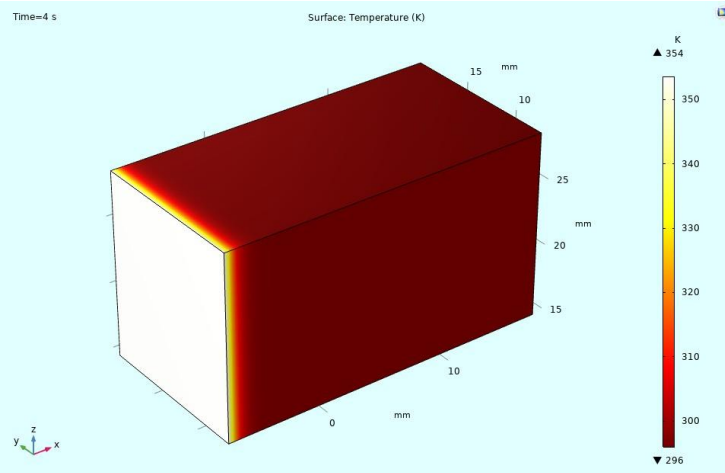


Fig 5.67: Time = 4 seconds

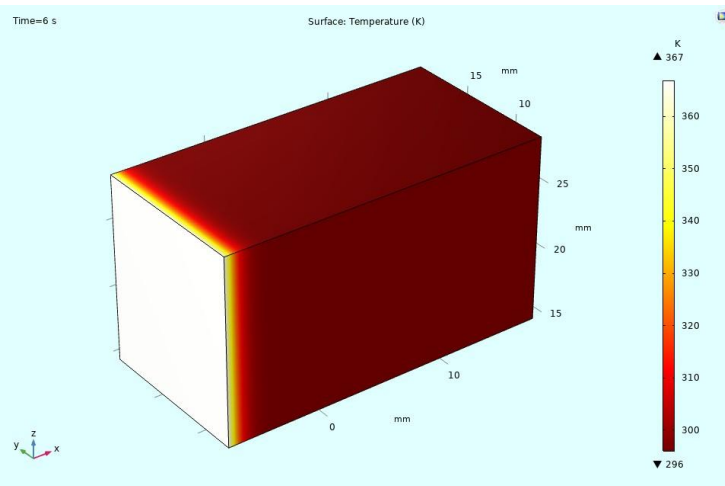


Fig 5.68: Time = 6 seconds

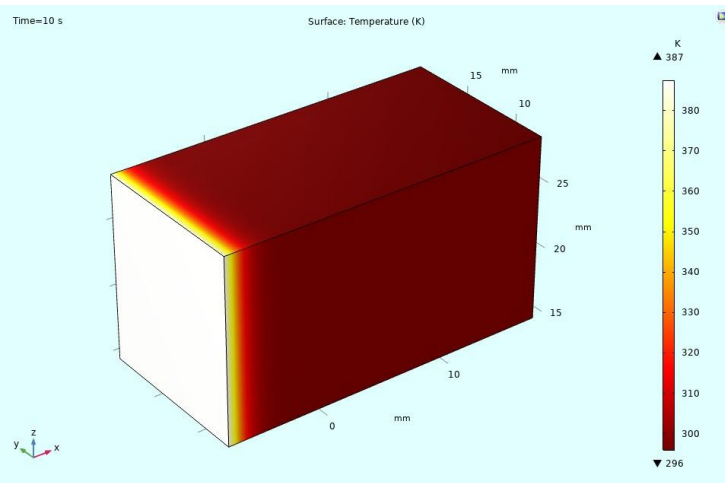


Fig 5.69: Time = 10 seconds

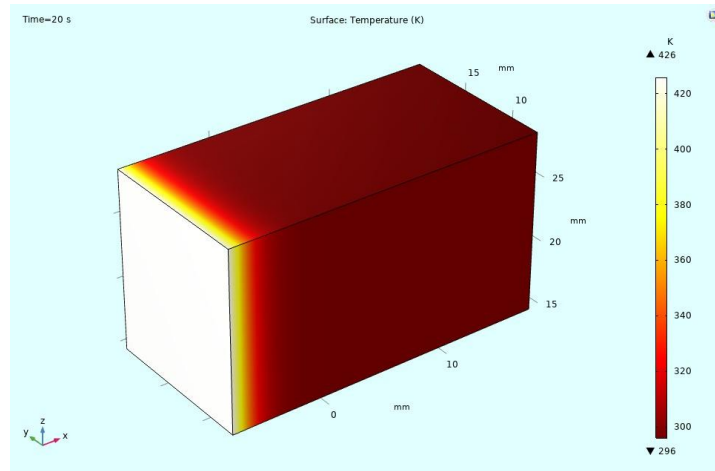


Fig 5.70: Time = 20 seconds

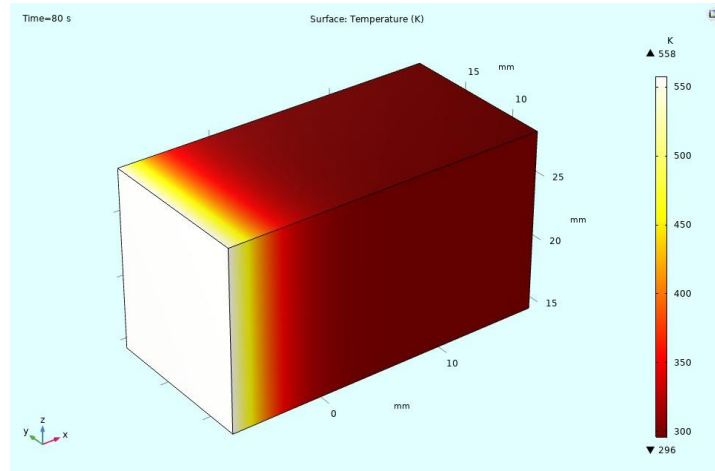


Fig 5.71: Time = 80 seconds

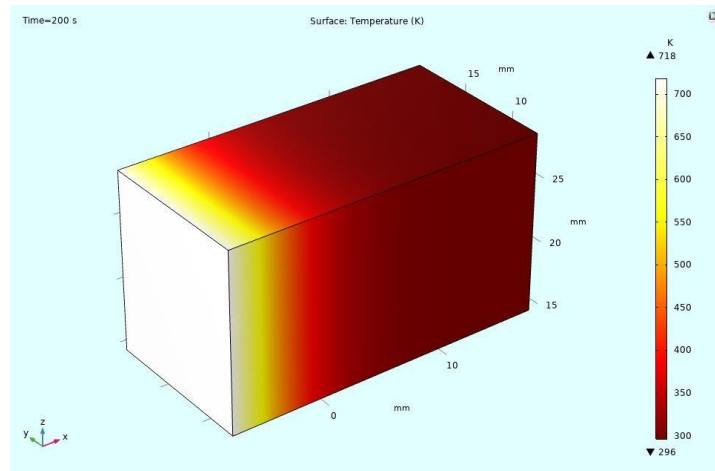


Fig 5.72: Time = 200 seconds

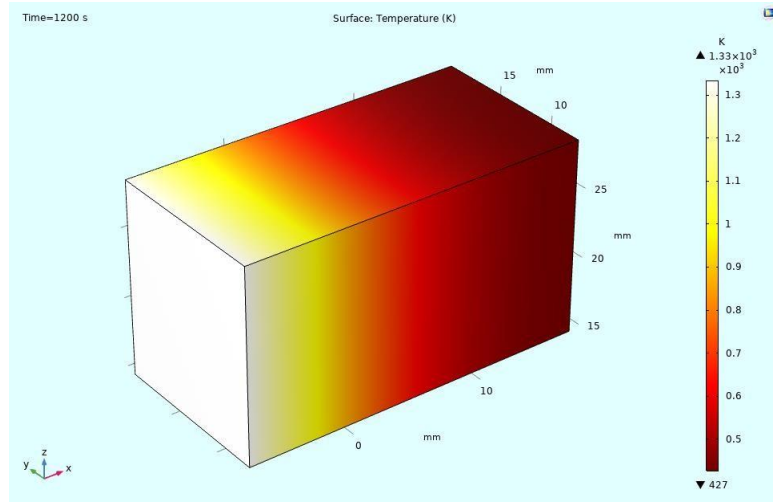


Fig 5.73: Time = 1200 seconds

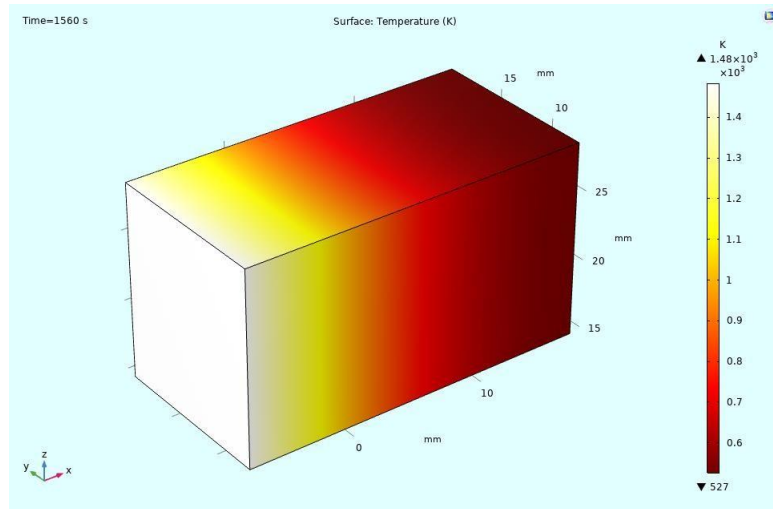


Fig 5.74: Time = 1560 seconds

- **Iso Surface Temperature View**

Here Iso Surface Contour plots are used to see how the Heat is transferred over the period, where the results are displayed on a set of colored surfaces where the results quantity is constant.

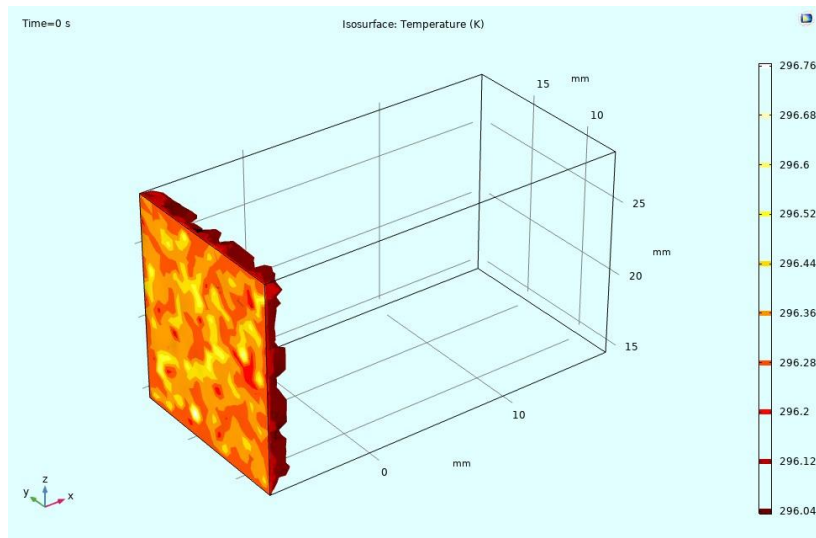


Fig 5.75: Time = 0 second

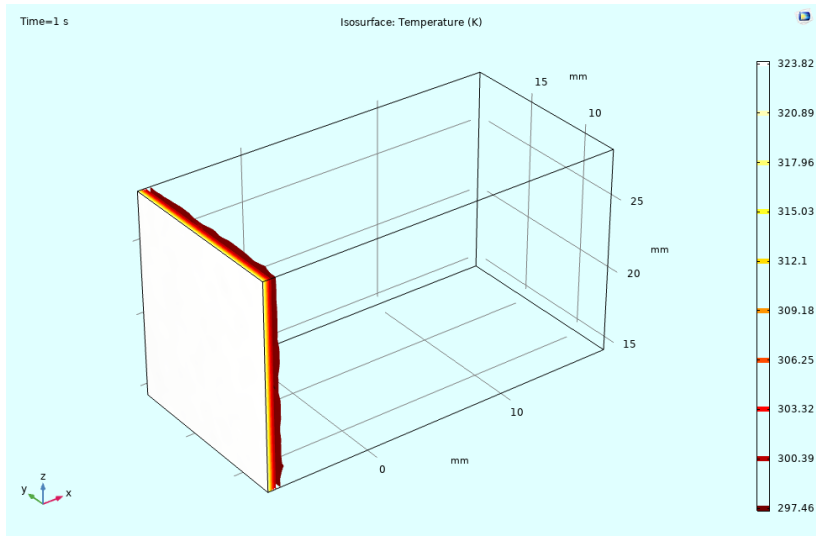


Fig 5.76: Time = 1 second

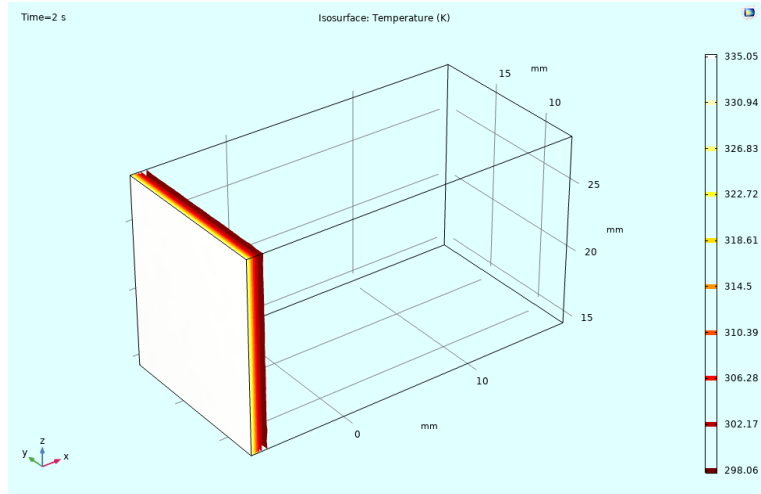


Fig 5.77: Time = 2 seconds

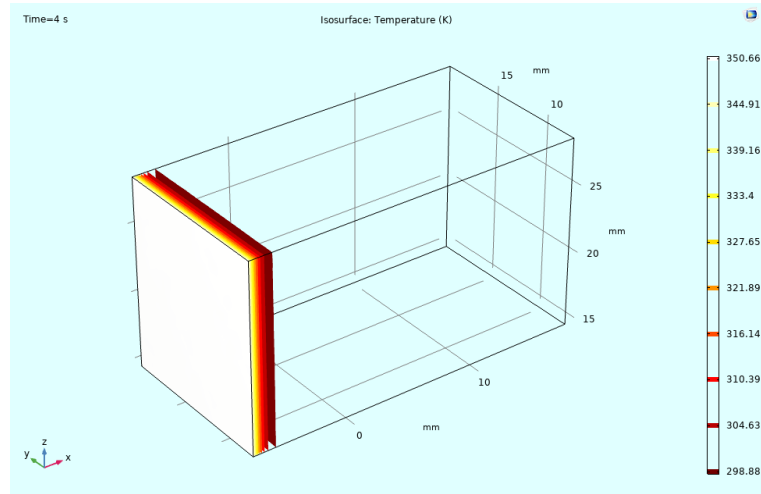


Fig 5.78: Time = 4 seconds

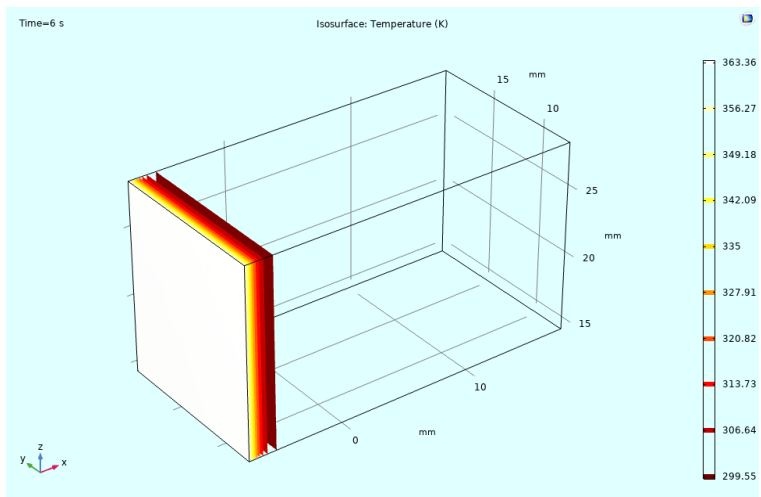


Fig 5.79: Time = 6 seconds

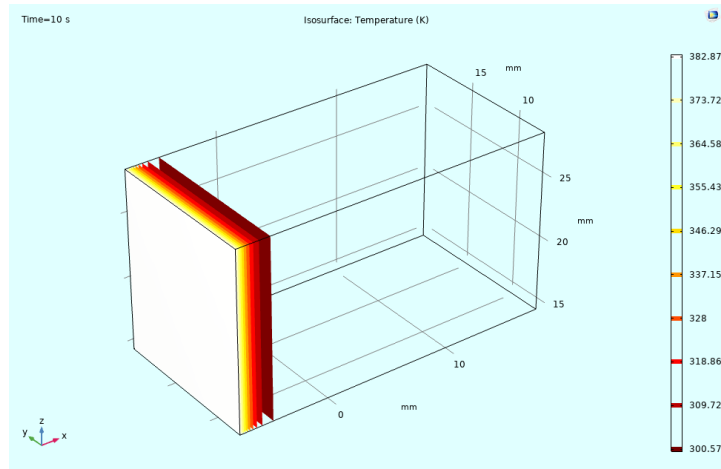


Fig 5.80: Time = 10 seconds

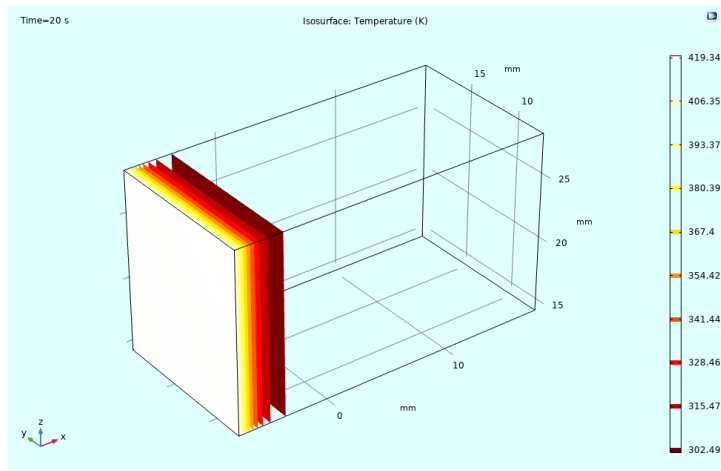


Fig 5.81: Time = 20 seconds

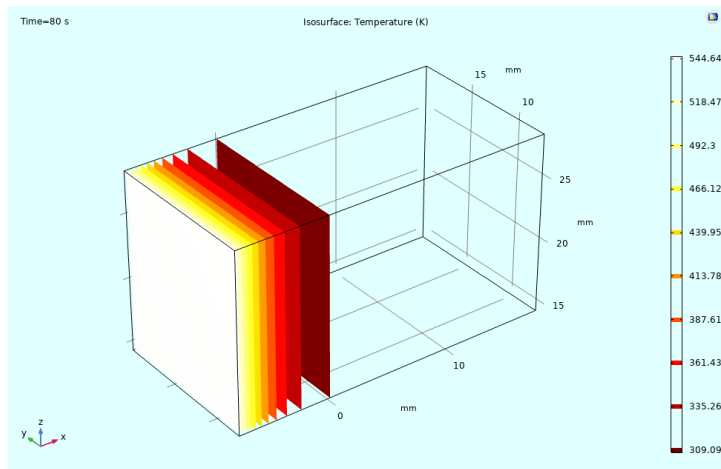


Fig 5.82: Time = 80 seconds

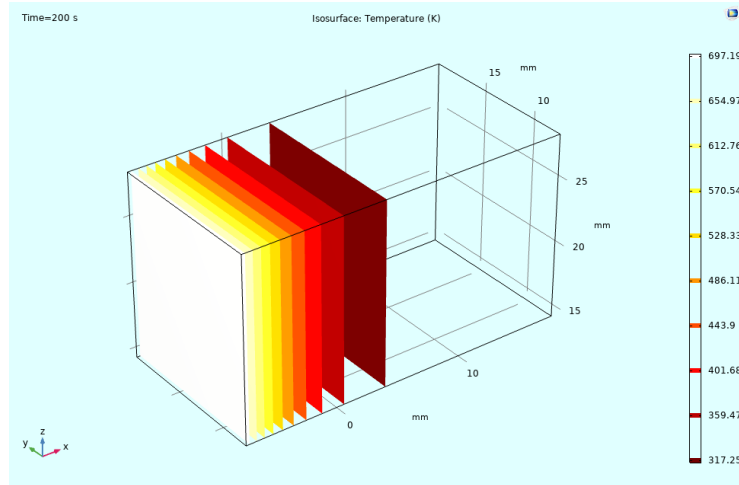


Fig 5.83: Time = 200 seconds

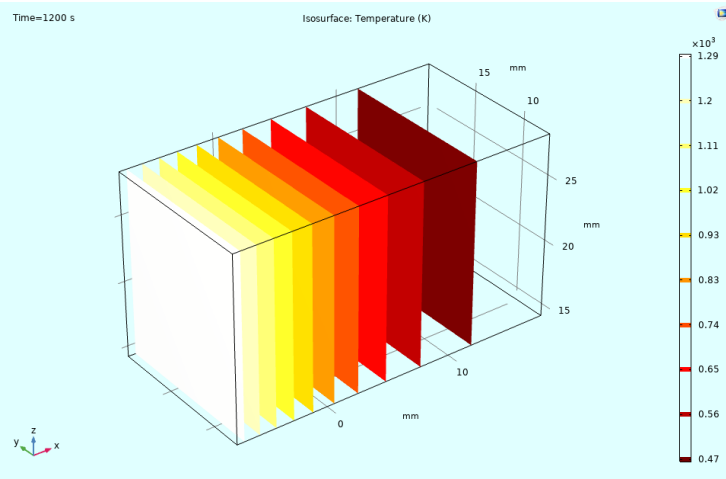


Fig 5.84: Time = 1200 seconds

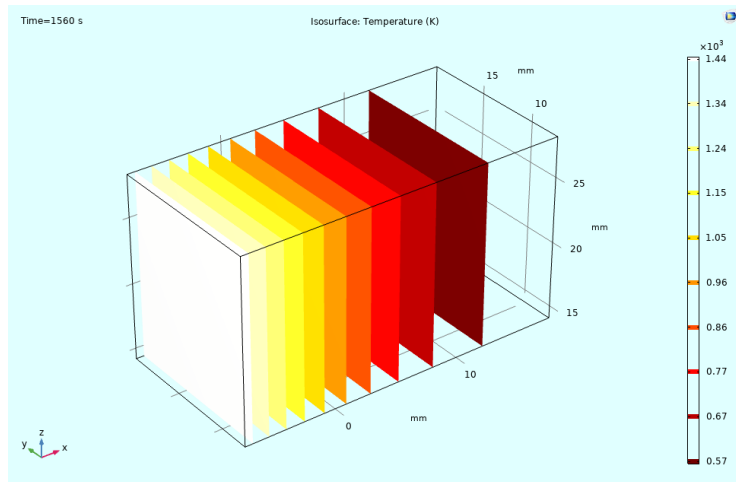


Fig 5.85: Time = 1560 seconds

- HEAT TRANSFER FROM A SINGLE PROTOTYPE TO BASEPLATE

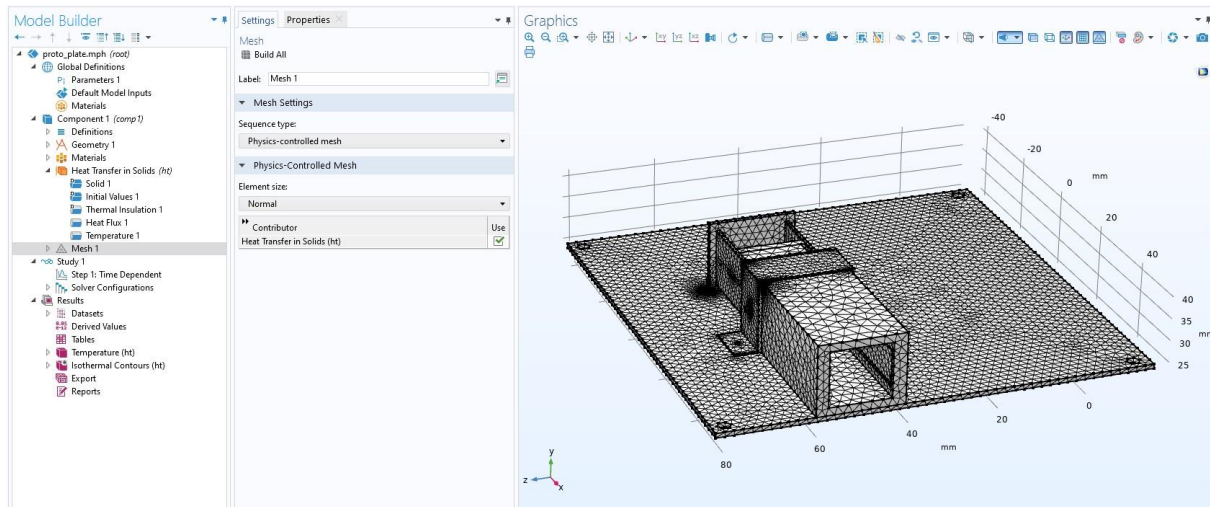


Fig 5.86: Meshing of Prototype and baseplate

The mesh consisted of 72685 domain elements, 32209 boundary elements, and 3101 edge elements.

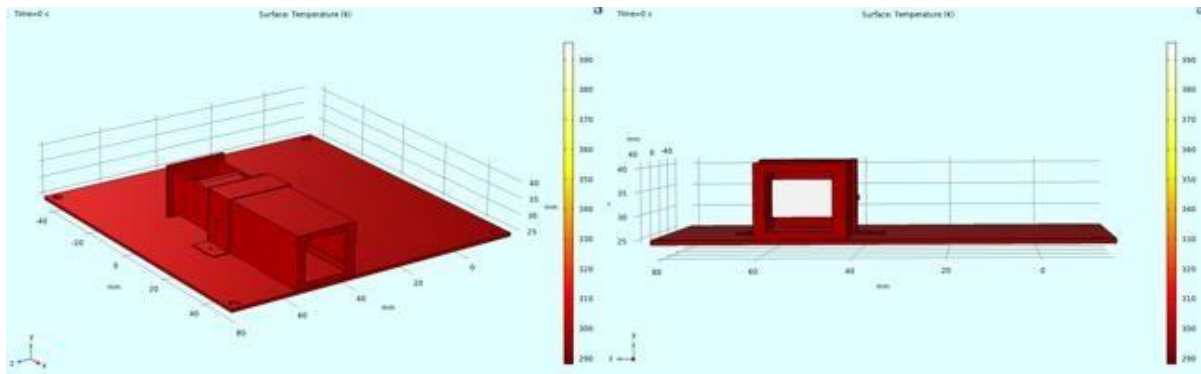


Fig 5.87: Time = 0 seconds

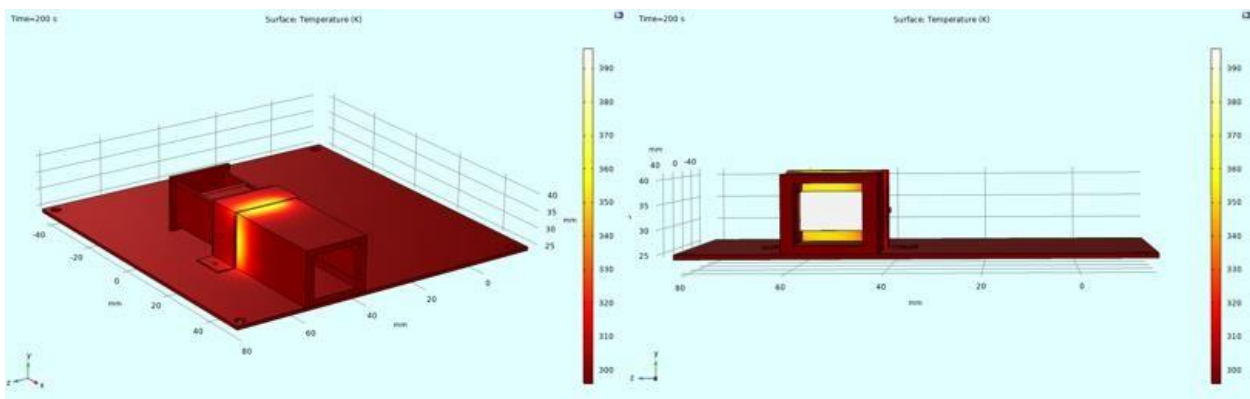


Fig 5.88: Time = 200 seconds

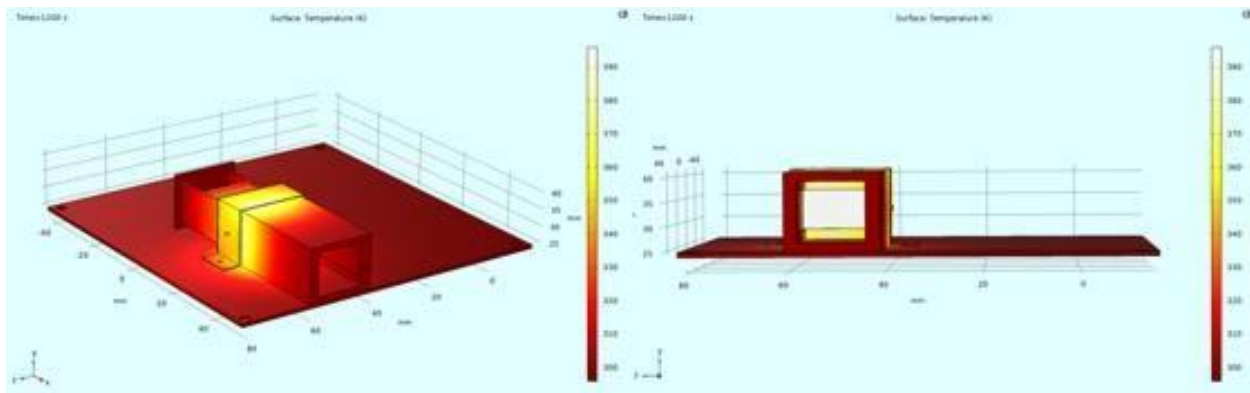


Fig 5.89: Time = 1200 seconds

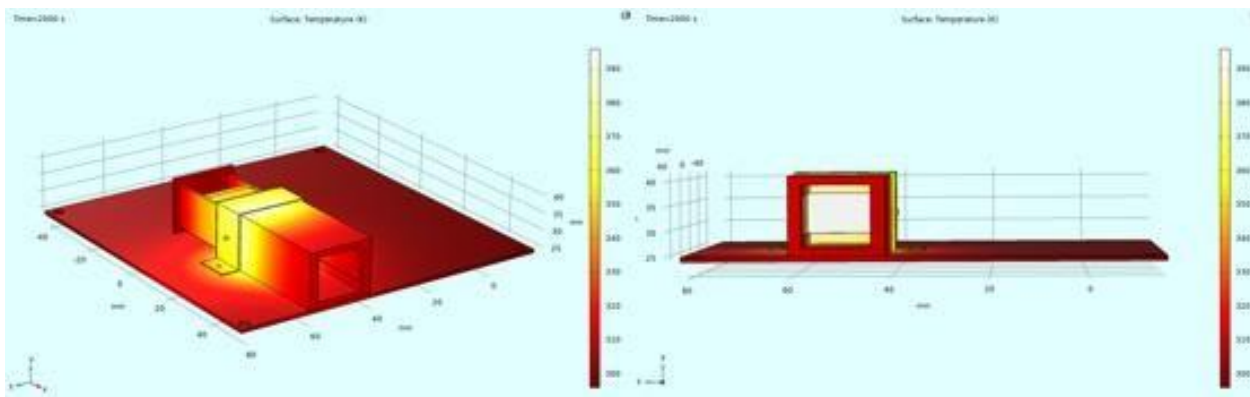


Fig 5.90: Time = 2000 seconds

- Heat Transfer of 4 prototypes on baseplate

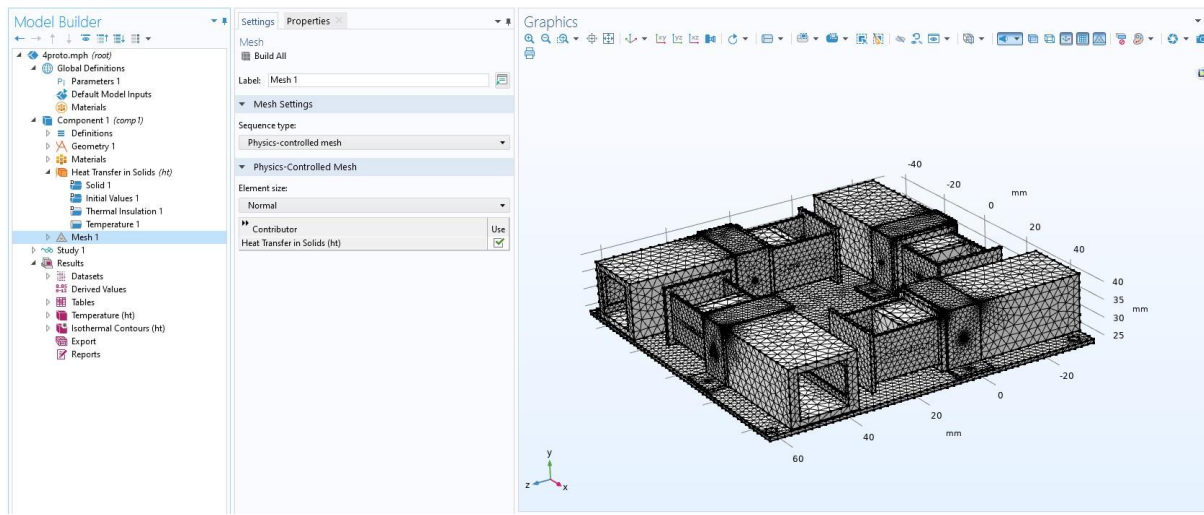


Fig 5.91 Meshing of 4 prototypes on baseplate

Complete mesh consisted of 182371 domain elements, 74558 boundary elements, and 9582 edge elements.

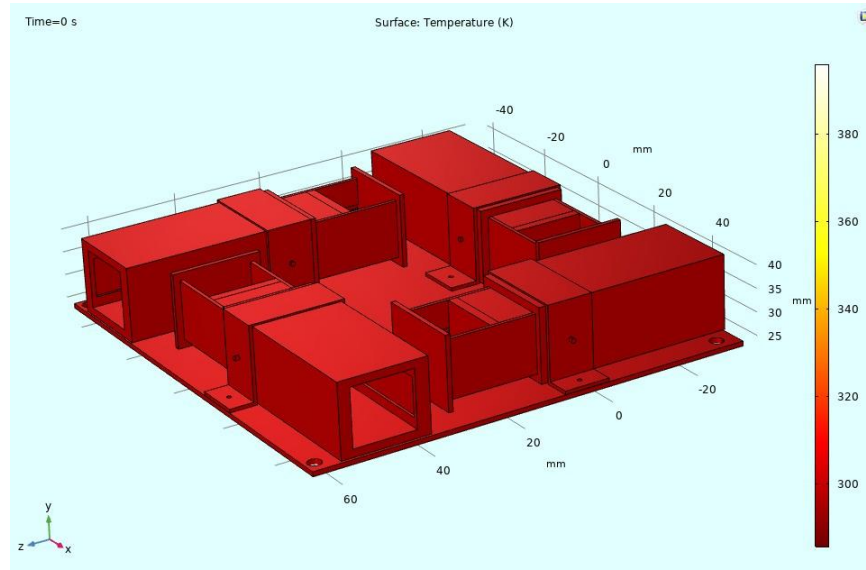


Fig 5.92: (4 Prototype) Time = 0 seconds

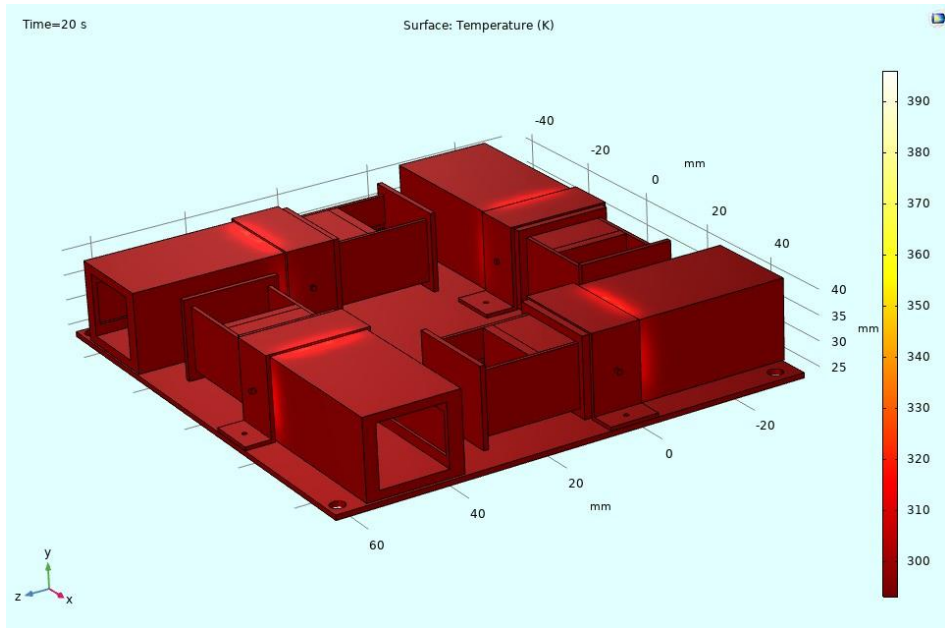


Fig 5.93: (4 Prototype) Time = 20 seconds

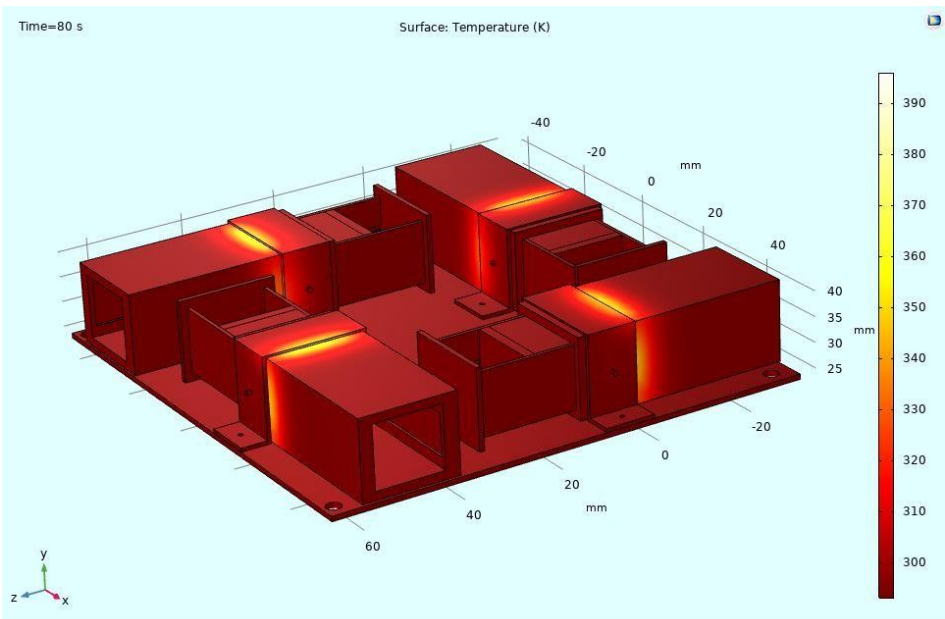


Fig 5.94: (4 Prototype) Time = 80 seconds

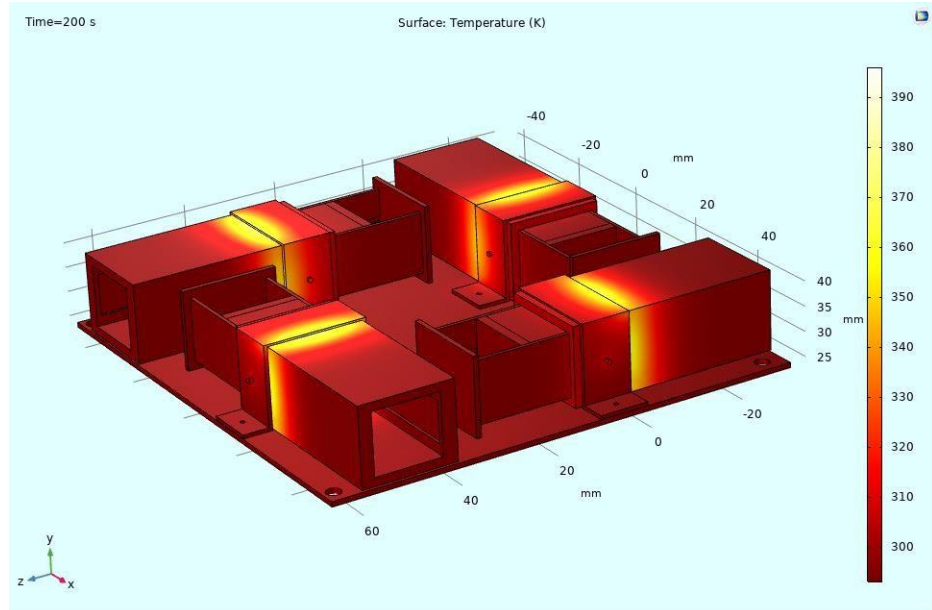


Fig 5.95: (4 Prototype) Time = 200 seconds

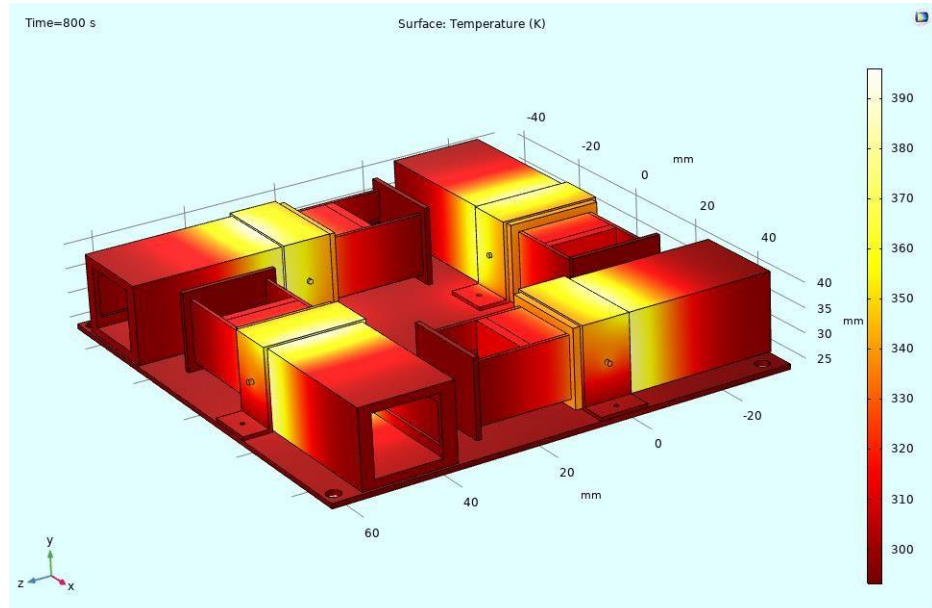


Fig 5.96: (4 Prototype) Time = 800 seconds

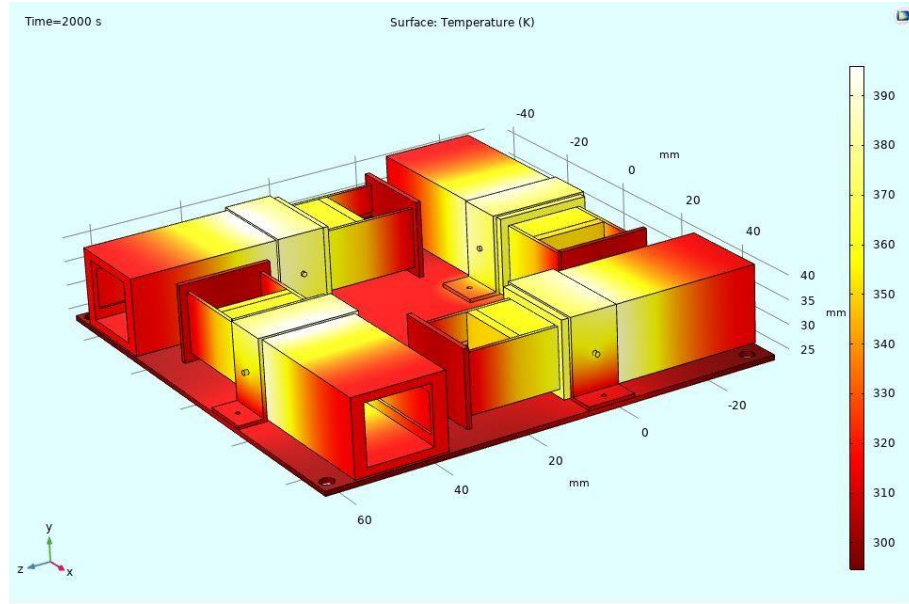


Fig 5.97: (4 Prototype) Time = 1200 seconds

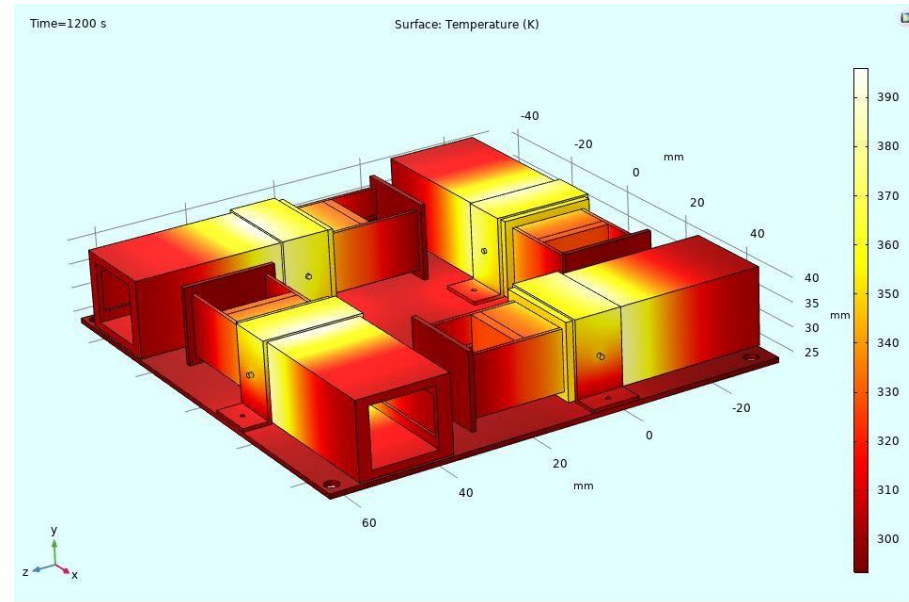


Fig 5.98: (4 Prototype) Time = 2000 seconds

## 5.4 STK INTEGRATION

Before importing the CubeSat model into the AGI STK software. The CAD model had to be imported into blender to convert the CAD model into COLLADA(.dae), as STK natively reads COLLADA (.dae) files. COLLADA is a popular open standards-based format that can be exported from many 3D editing applications (e.g., 3D Studio Max, Maya, Softimage, Blender, and Google SketchUp) and model converters,

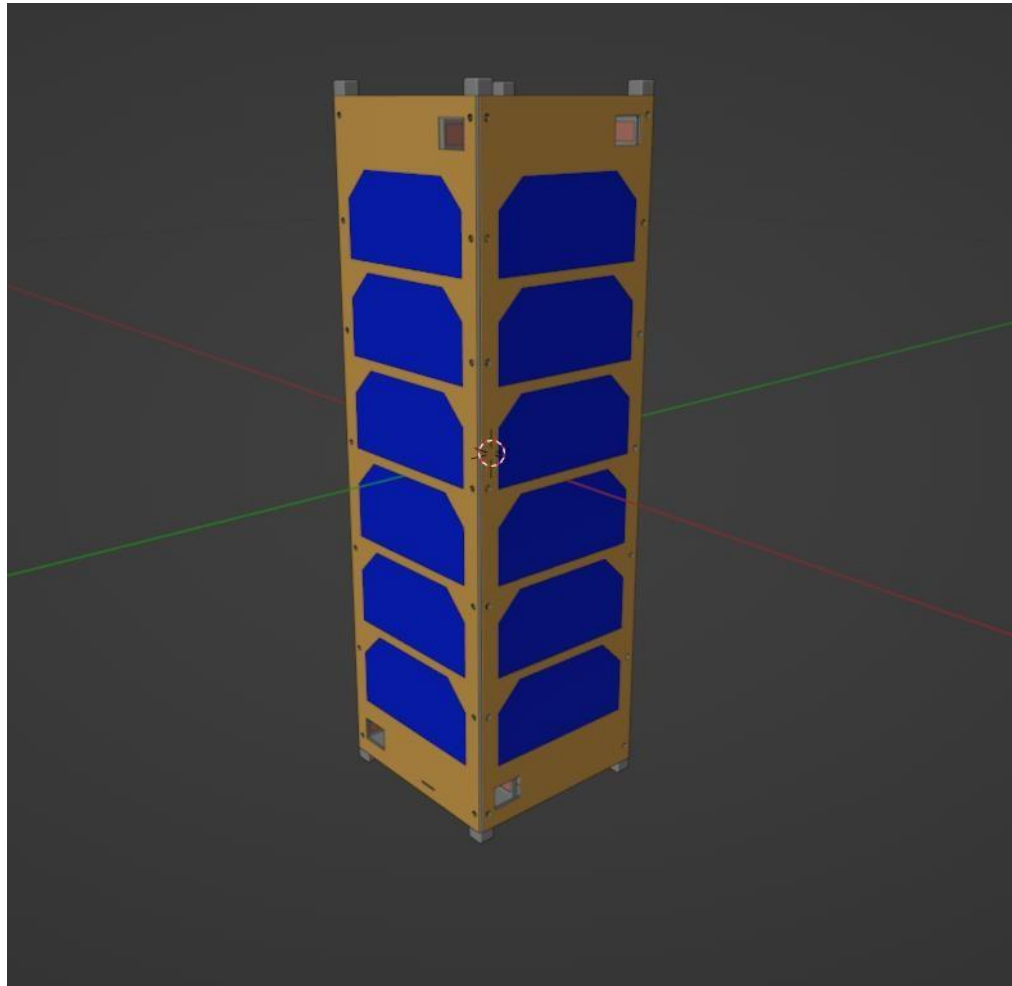


Fig 5.99: Final rendered CAD model of CubeSat with prototypes in Blender

Proper component parenting is crucial for correct articulations attitude adjustments. For example, if a solar array is not parented to the main body of a satellite and the main body rotates (i.e. any attitude adjustment in STK) then the arrays will not rotate with the rest of the spacecraft. In the case of solar panels to work properly in STK we have to create separate solar cells and place them on the panels.

## 5.4.1 SOLAR PANEL GROUPS

Creating solar panel groups is a requirement for the STK Solar Panel Tool to work correctly. With the current setup the solar panel tool would consider all outward facing polygons on each solar panel, including the back and side faces. To fix this an object must be created to represent just the solar cells.

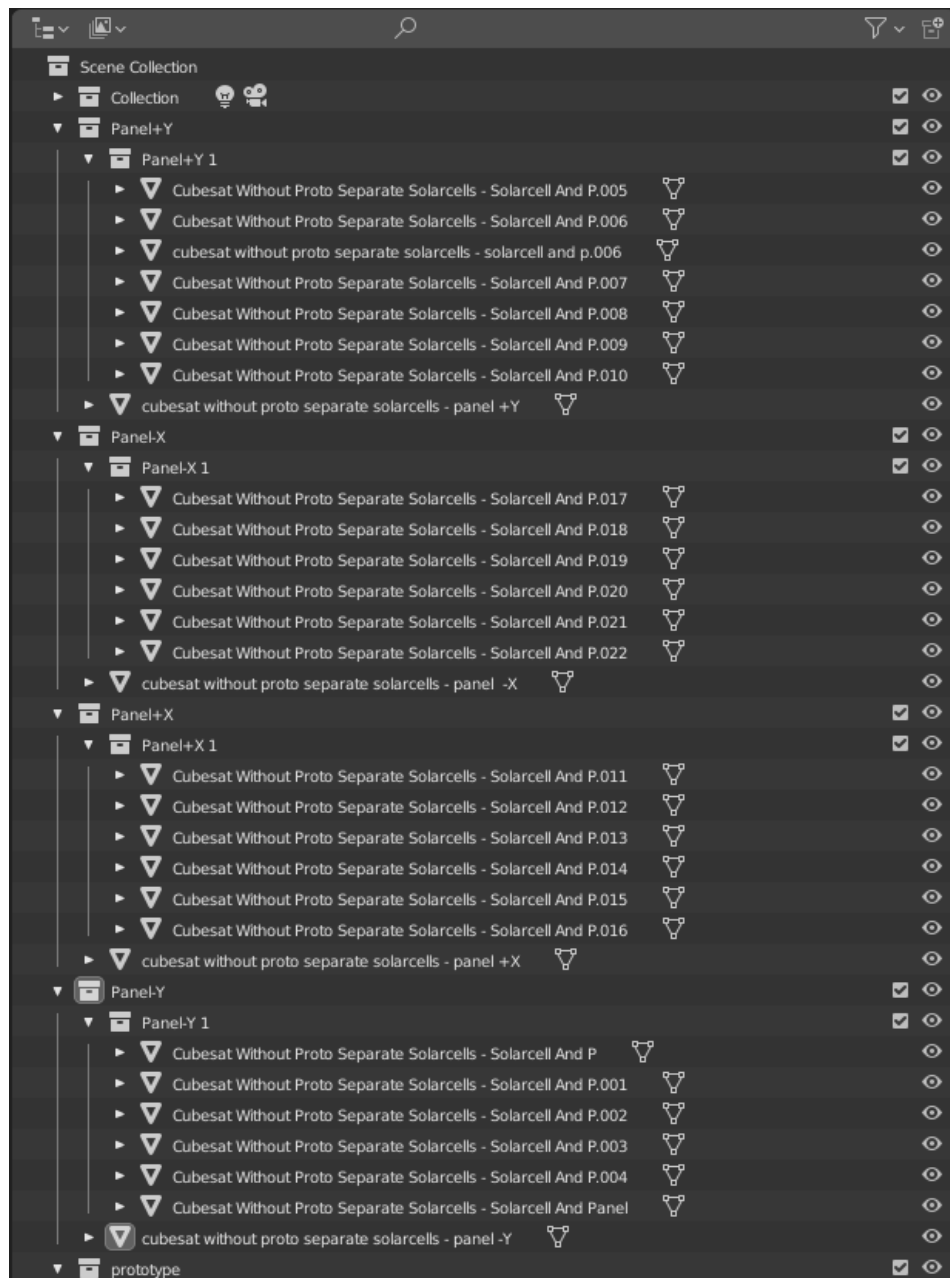


Fig 5.100: Solar cells grouping in Blender

## 5.4.2 CREATING ANCILLARY FILES

The Collada file (.dae) defines the model geometry and node names, while the ancillary file (.anc) is the driving code behind all articulations, sensor attach points, and solar panels in STK. For the ancillary file to work correctly it must be in the same directory as the Collada file. Unfortunately, the ancillary file must be written by hand but luckily the format is always the same and a basic template can be used as a guide.

A master ancillary file was used in this case provided by AGI. For this to work we need Notepad++.

Open the CubeSat.dae and rename the master ancillary file to CubeSat.anc and open the file in Notepad++. In the Collada file suppress all sections except for visual scenes.

Under the Visual Scenes section documents all objects in the assembly and how they are related to each other. What really matters in this section is the node name for each component, since the nodes will be the only part being referenced by the ancillary file.

If you look at line 5179 of the Collada file, you will see the node information for the Cubesat\_Without\_Proto\_Separate\_Solarcells. The node name will be exactly the same as the name given in Blender. If you put spaces in your names they will be replaced with underscores.



```
5179 <node id="#Cubesat_Without_Proto_Separate_Solarcells_-_Solarcell_And_Panel" name="Cubesat Without Proto Separate Solarcells - Solarcell And Panel" type="NODE">
5180   <matrix sid="transform">-0.9999983 -0.001867381 0 0.1314326 0 5.38676e-9 -1 0.3154435 0.001867381 -0.9999983 5.38676e-9 0.2344198 0 0 0 1</matrix>
5181   <instance_geometry url="#Cubesat_Without_Proto_Separate_Solarcells_-_Solarcell_And_Panel-mesh" name="Cubesat Without Proto Separate Solarcells - Solarcell And Panel">
5182     <bind_material>
5183       <technique_common>
5184         <instance_material symbol="Solarpanel_blue-material" target="#Solarpanel_blue-material"/>
5185       </technique_common>
5186     </bind_material>
5187   </instance_geometry>
5188 </node>
5189 <node id="#Cubesat_Without_Proto_Separate_Solarcells_-_Solarcell_And_P_004" name="Cubesat Without Proto Separate Solarcells - Solarcell And P.004" type="NODE">
5190   <matrix sid="transform">-0.9999983 -0.001867381 0 0.1314326 0 5.38676e-9 -1 0.3154435 0.001867381 -0.9999983 5.38676e-9 0.2344198 0 0 0 1</matrix>
5191   <instance_geometry url="#Cubesat_Without_Proto_Separate_Solarcells_-_Solarcell_And_P_004-mesh" name="Cubesat Without Proto Separate Solarcells - Solarcell And P.004">
5192     <bind_material>
5193       <technique_common>
5194         <instance_material symbol="Solarpanel_blue-material" target="#Solarpanel_blue-material"/>
5195       </technique_common>
5196     </bind_material>
5197   </instance_geometry>
5198 </node>
5199 <node id="#Cubesat_Without_Proto_Separate_Solarcells_-_Solarcell_And_P_003" name="Cubesat Without Proto Separate Solarcells - Solarcell And P.003" type="NODE">
5200   <matrix sid="transform">-0.9999983 -0.001867381 0 0.1314326 0 5.38676e-9 -1 0.3154435 0.001867381 -0.9999983 5.38676e-9 0.2344198 0 0 0 1</matrix>
5201   <instance_geometry url="#Cubesat_Without_Proto_Separate_Solarcells_-_Solarcell_And_P_003-mesh" name="Cubesat Without Proto Separate Solarcells - Solarcell And P.003">
5202     <bind_material>
5203       <technique_common>
5204         <instance_material symbol="Solarpanel_blue-material" target="#Solarpanel_blue-material"/>
5205       </technique_common>
5206     </bind_material>
5207   </instance_geometry>
5208 </node>
```

Fig 5.101: Collada file opened in Notepad++

Once we open the Ancillary file go under the solar panels group and add in the nodes from the Collada file to the desired nodes. Here you can see an example of Plus Y solar panel groups and there were six solar cells assigned to that panel.

The solar panel efficiency was set to 28 as to obtain realistic power values from the solar panels.

```
80 SOLAR PANEL GROUPS:  
81 Solar Panel Groups are components defined as solar panels and assigned an  
82 efficiency value. This is useful when running the STK solar panel tool.  
83 <solar_panel_groups>  
84     <solar_panel_group efficiency = "28" name = "Plus_Y">  
85         <assigned_nodes>  
86             Cubesat_Without_Proto_Separate_Solarcells__Solarcell_And_P_010  
87             Cubesat_Without_Proto_Separate_Solarcells__Solarcell_And_P_009  
88             Cubesat_Without_Proto_Separate_Solarcells__Solarcell_And_P_008  
89             Cubesat_Without_Proto_Separate_Solarcells__Solarcell_And_P_007  
90             Cubesat_Without_Proto_Separate_Solarcells__Solarcell_And_P_006  
91             Cubesat_Without_Proto_Separate_Solarcells__Solarcell_And_P_005  
92         </assigned_nodes>  
93     </solar_panel_group>  
94     <solar_panel_group efficiency = "28" name = "Minus_Y">  
95         <assigned_nodes>  
96             Cubesat_Without_Proto_Separate_Solarcells__Solarcell_And_Panel  
97             Cubesat_Without_Proto_Separate_Solarcells__Solarcell_And_P  
98             Cubesat_Without_Proto_Separate_Solarcells__Solarcell_And_P_001  
99             Cubesat_Without_Proto_Separate_Solarcells__Solarcell_And_P_002  
100            Cubesat_Without_Proto_Separate_Solarcells__Solarcell_And_P_003  
101            Cubesat_Without_Proto_Separate_Solarcells__Solarcell_And_P_004  
102        </assigned_nodes>  
103    </solar_panel_group>  
104    <solar_panel_group efficiency = "28" name = "Plus_X">  
105        <assigned_nodes>  
106            Cubesat_Without_Proto_Separate_Solarcells__Solarcell_And_P_011  
107            Cubesat_Without_Proto_Separate_Solarcells__Solarcell_And_P_012  
108            Cubesat_Without_Proto_Separate_Solarcells__Solarcell_And_P_013  
109            Cubesat_Without_Proto_Separate_Solarcells__Solarcell_And_P_014  
110            Cubesat_Without_Proto_Separate_Solarcells__Solarcell_And_P_015  
111            Cubesat_Without_Proto_Separate_Solarcells__Solarcell_And_P_016  
112        </assigned_nodes>  
113    </solar_panel_group>  
114    <solar_panel_group efficiency = "28" name = "Minus_X">  
115        <assigned_nodes>  
116            Cubesat_Without_Proto_Separate_Solarcells__Solarcell_And_P_017  
117            Cubesat_Without_Proto_Separate_Solarcells__Solarcell_And_P_018  
118            Cubesat_Without_Proto_Separate_Solarcells__Solarcell_And_P_019  
119            Cubesat_Without_Proto_Separate_Solarcells__Solarcell_And_P_020  
120            Cubesat_Without_Proto_Separate_Solarcells__Solarcell_And_P_021  
121            Cubesat_Without_Proto_Separate_Solarcells__Solarcell_And_P_022  
122        </assigned_nodes>
```

Fig 5.102: Solar Panels group and assigned nodes

### 5.4.3 IMPLEMENTATION IN STK

For the model to look and work properly in STK the Collada, ancillary, and all texture images must be in the same directory.

Open a new scenario in STK and create a new satellite. In the satellite properties, navigate to the 3D graphics->Model page. Under model click the ellipsis to browse for the model file and open the Collada file from the tutorial folder. You do not need to load the ancillary file. It will automatically be loaded as long as the file name is the same as the Collada file and in the same directory.

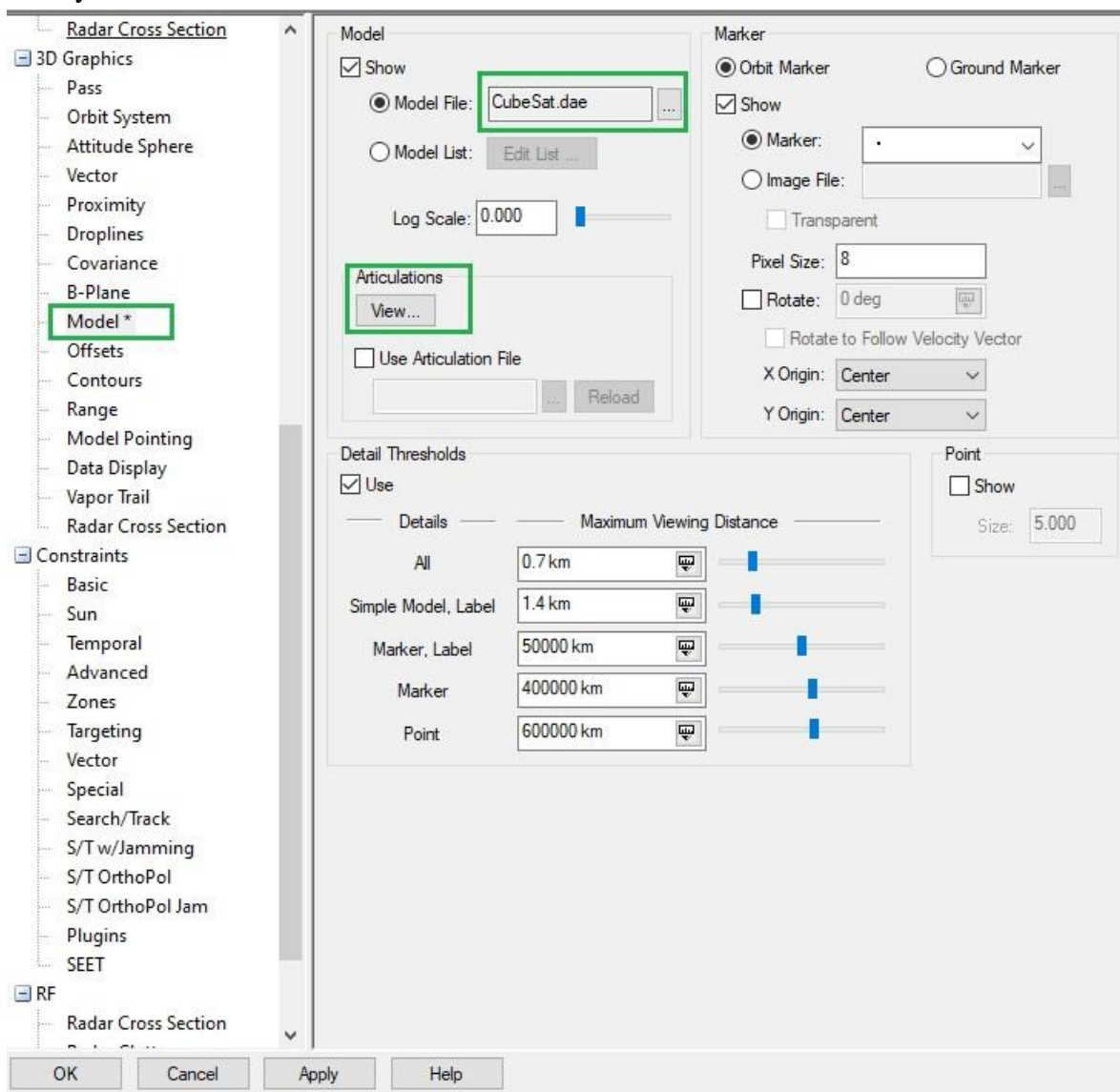


Fig 5.103: CubeSat model implementation in STK

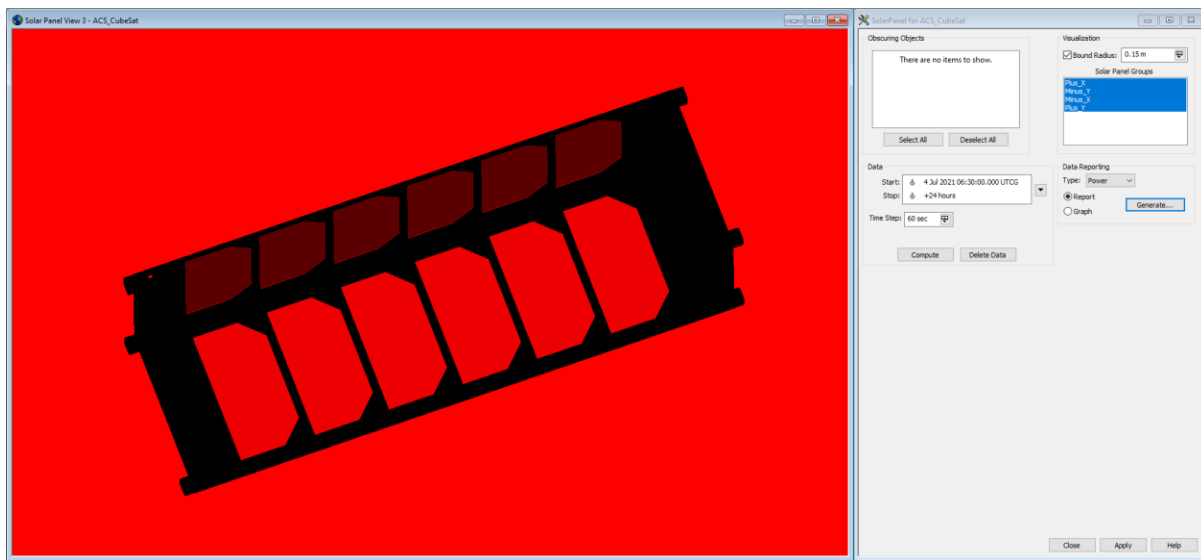


Fig 5.104: Solar Panel Tool in STK

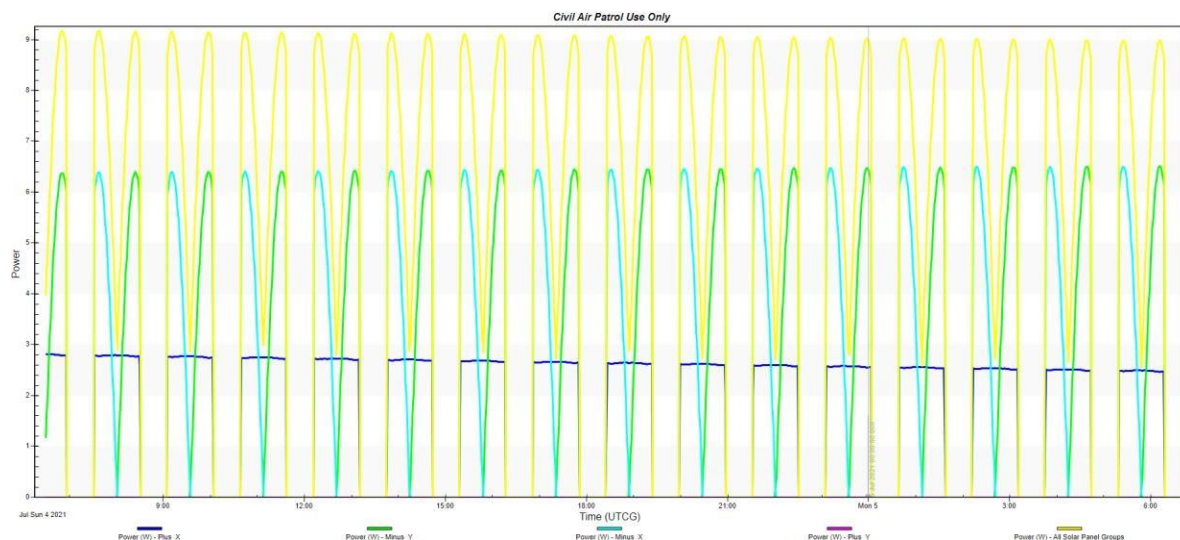


Fig 5.105: Solar Panel Power Profile

- Power(w)- Plus X
- Power(w)- Minus X
- Power(w)- Plus Y
- Power(w)- Minus X
- Power(w)- All Solar Panel Group

The maximum power produced by all the solar panels was around 9.117 W, the solar panels Minus X and Minus Y produced the most power compared to other two panel groups.

The maximum power produced by Minus Y panel was around 6.513 (W) on 5 Jul 2021 06:11:00.000, whereas Minus X panel produced maximum power of around 6.512 (W) on 5 Jul 2021 05:25:00.000.

The power produced by Plus X panel was maximum at the beginning which was about 2.813 (W) on 4 Jul 2021 06:30:00.000 but the power remained constant during the period where the panel was not eclipsed. The power range was about 2.813 (W) – 2.787 (W).

The Minus X panel was in the dark all the time so that panel didn't produce any sort of power.

Table 5.7:All Solar panel group power generated in watts

Time (UTCG)	Power (w)	Solar Intensity
4 Jul 2021 06:30:00.000	3.973	1.000000
4 Jul 2021 06:40:00.000	7.623	1.000000
4 Jul 2021 06:51:00.000	9.173	1.000000
4 Jul 2021 06:57:00.000	0.000	0.000000
4 Jul 2021 07:30:00.000	0.000	0.000000
4 Jul 2021 07:40:00.000	9.084	1.000000
4 Jul 2021 07:50:00.000	7.056	1.000000
4 Jul 2021 08:00:00.000	3.175	1.000000
4 Jul 2021 09:00:00.000	0.000	0.000000
4 Jul 2021 10:00:00.000	9.077	1.000000

4 Jul 2021 11:00:00.000	5.909	1.000000
4 Jul 2021 12:00:00.000	0.000	0.000000
4 Jul 2021 13:00:00.000	8.879	1.000000
4 Jul 2021 14:00:00.000	8.003	1.000000
4 Jul 2021 16:00:00.000	7.454	1.000000
4 Jul 2021 18:00:00.000	0.000	0.000000
4 Jul 2021 20:00:00.000	8.796	1.000000
4 Jul 2021 22:00:00.000	3.174	1.000000
5 Jul 2021 00:00:00.000	8.980	1.000000
5 Jul 2021 03:00:00.000	8.708	1.000000
5 Jul 2021 06:17:00.000	8.555	1.000000

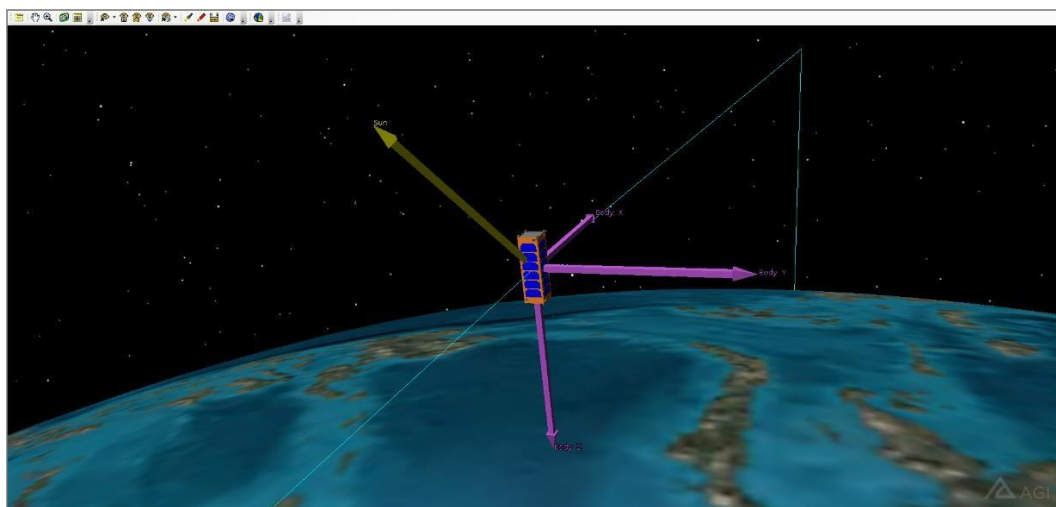


Fig 5.106: CubeSat model with its body axes and a vector pointing the Sun

The power profiles change with respect to the inclination of the satellite

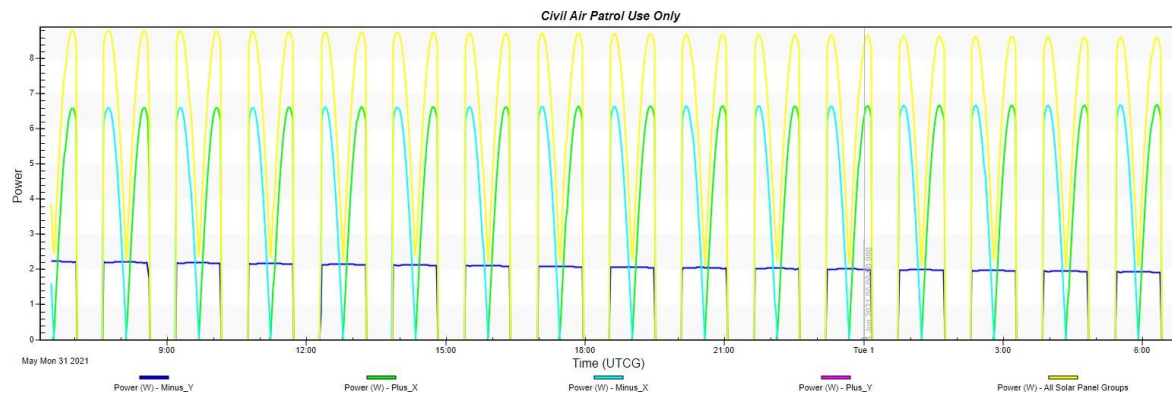


Fig 5.107: Power Profile at  $20^\circ$  inclination

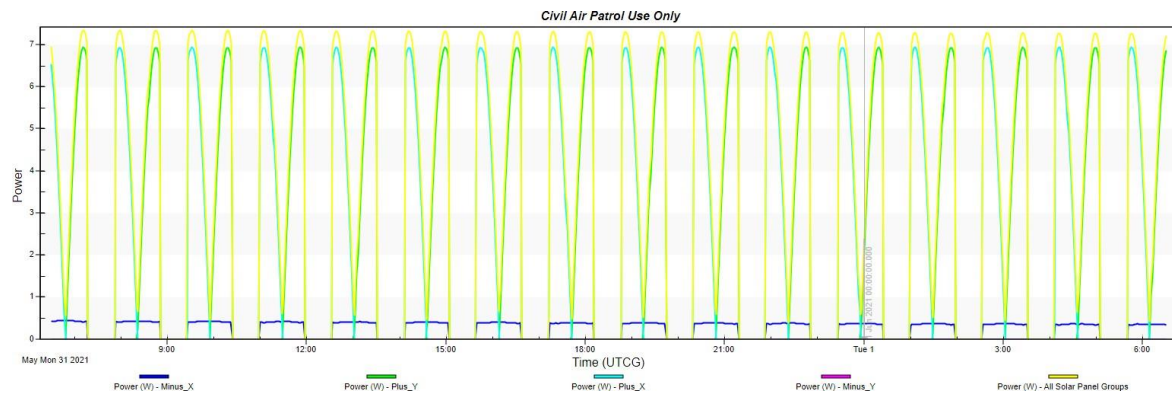


Fig 5.108: Power Profile at  $0^\circ$  inclination

### 5.4.3.1 Orbit Transfer using STK Astrogator

In this case it is assumed that the satellite was launched into the orbit using P-POD from the ISS and the main purpose was to raise its orbit and show that it is possible to achieve it for a CubeSat.

Since we used Hohmann transfer to increase its orbit and it is an impulsive type maneuver the following results were obtained

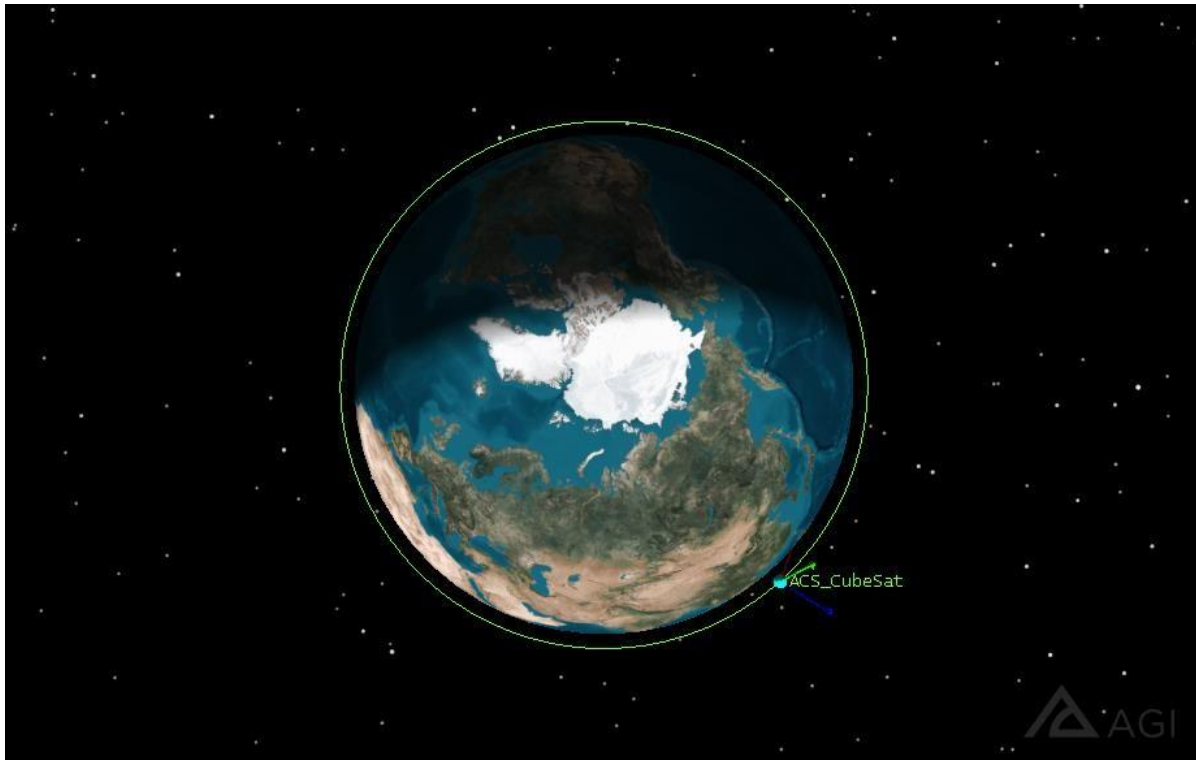


Fig 5.109: Initial orbit

The green line indicates the initial orbit and, in the figure, below we can see the white line which is indicating DV1 burn segment which was about 5.6 m/s and the initial burn segment had a radius of apoapsis constrain where in it reached the desired value of about 6841.14 km. The DV2 was about 288.363 m/s, also being an impulsive maneuver and the required velocities were unattainable by the CubeSat. For this reason, a finite burn segment was proposed and applied.

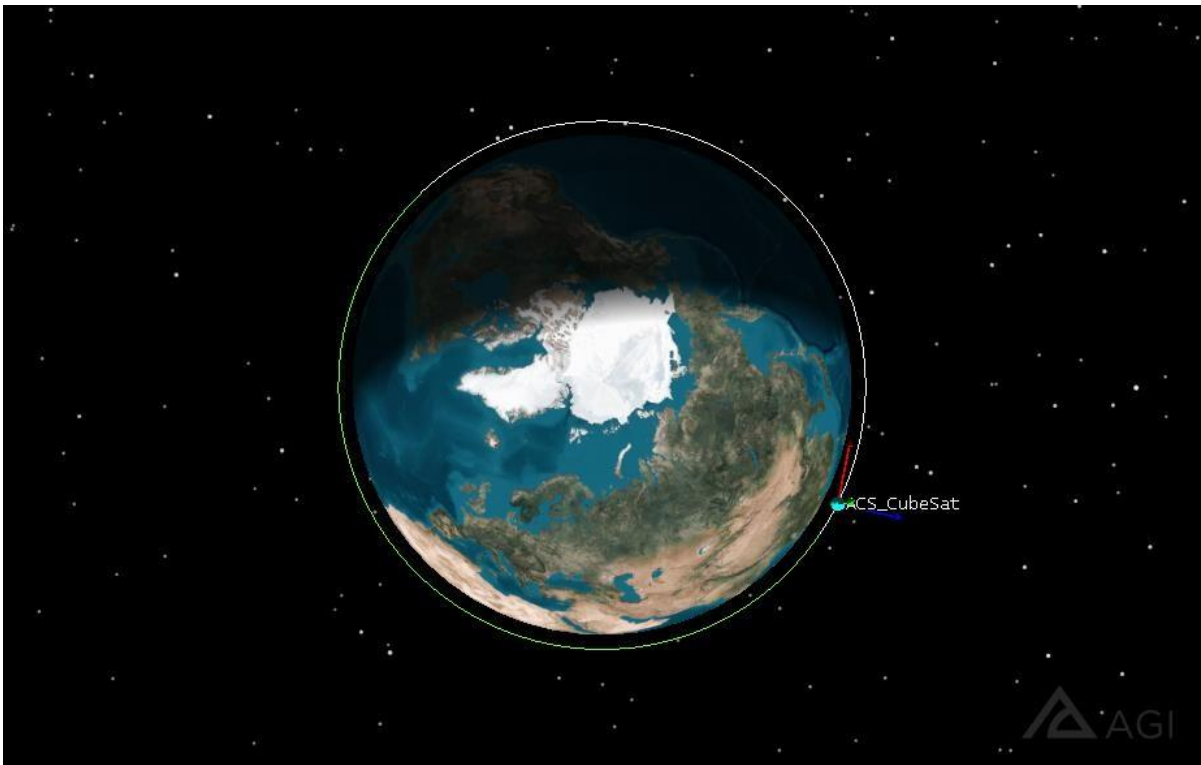


Fig 5.110: Transfer Orbit

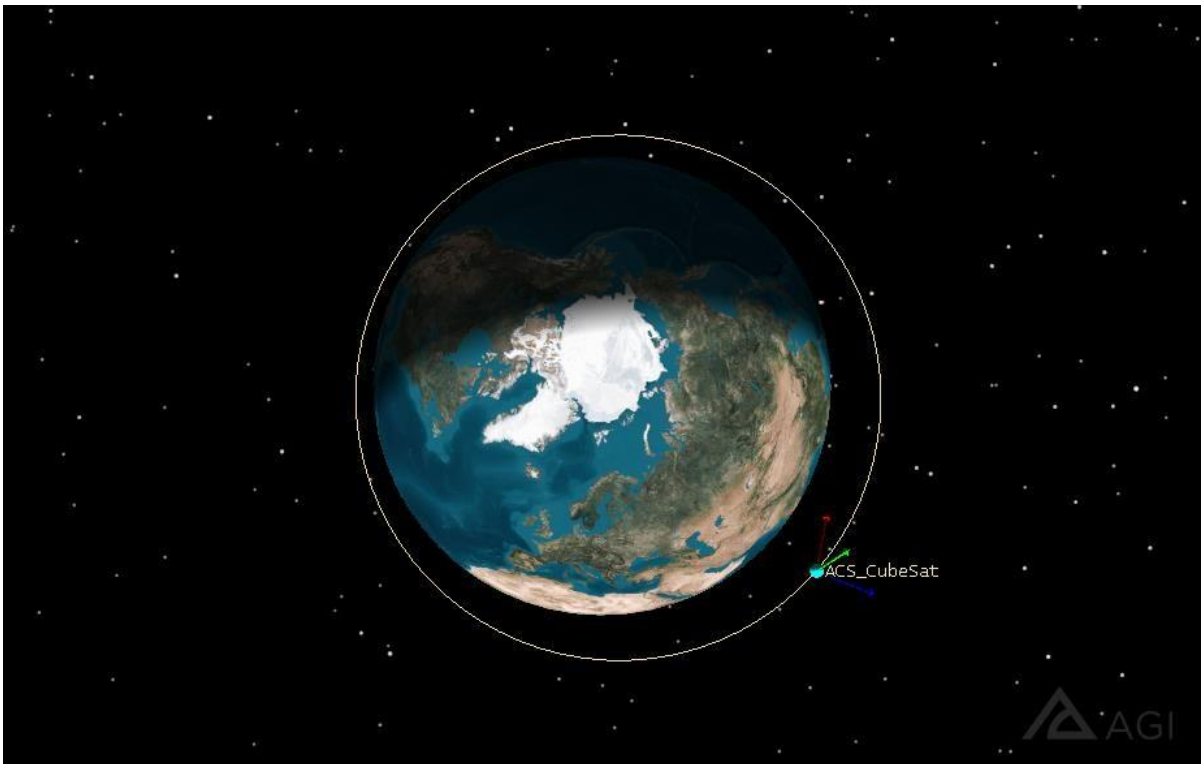


Fig 5.111: Final Orbit

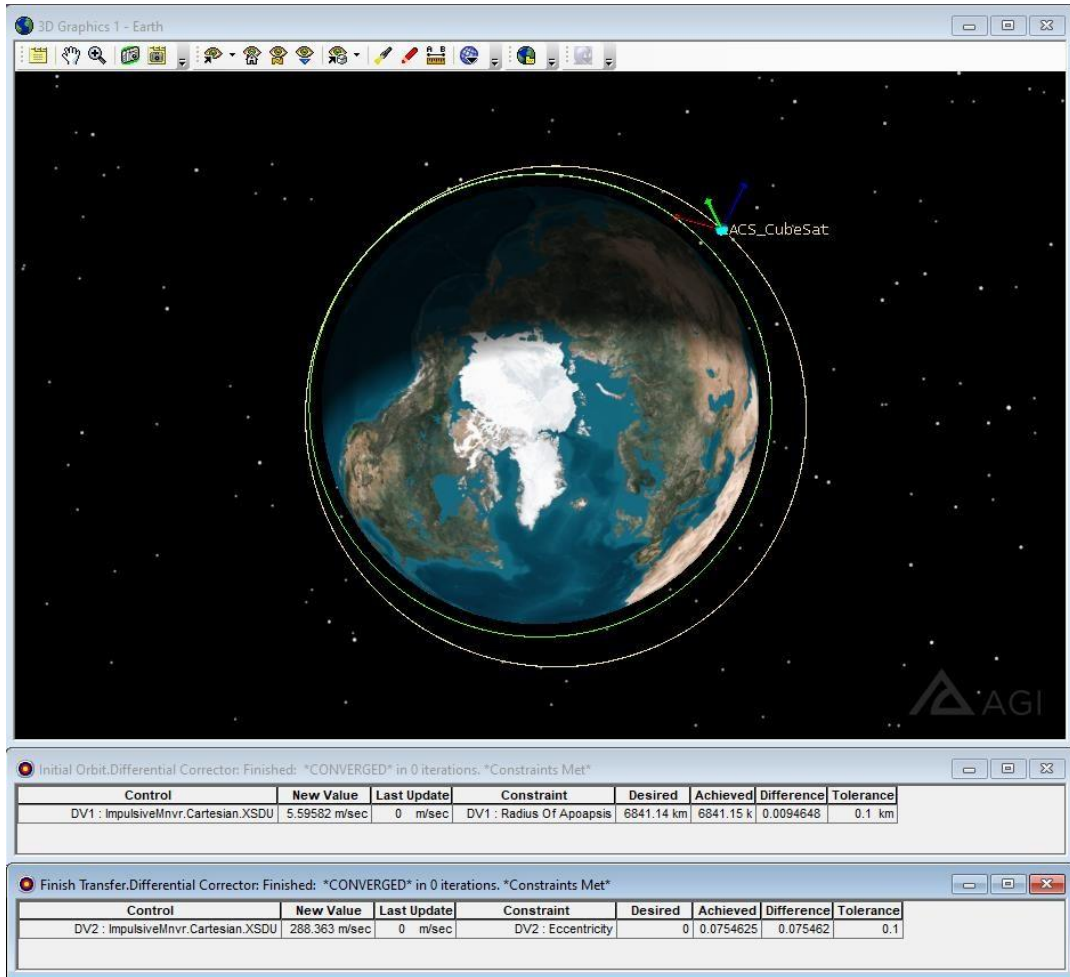


Fig 5.112: Hohmann Transfer

#### 5.4.3.2 Orbit Transfer using Finite manoeuvre type

The objective of the orbit transfer analysis is to define thrust vectors and their magnitudes required to travel from the ISS orbit to higher orbit to increase the lifetime of the CubeSat.

The engine being used must be manually defined within STK's component browser. Using the specifications of the Pulsed Plasma thruster obtained from electric analysis, the engine was defined as shown in figure below.

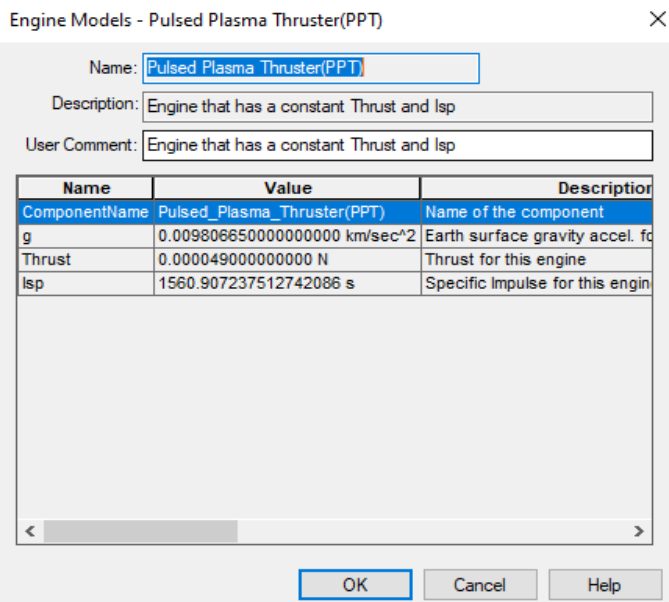


Fig 5.113: Engine Model: Pulsed Plasma Thruster

The other Parameters considered were as follows

Elements	Spacecraft Parameters	Fuel Tank	User Variables
Drag	Dry Mass: 5 kg Coefficient (Cd): 2.2 Area: 0.03 m <sup>2</sup>		Tank Pressure: 0 Pa Tank Volume: 4.2e-06 m <sup>3</sup> Tank Temperature: 393.15 K Fuel Density: 2200 kg/m <sup>3</sup> Fuel Mass: 40 g Maximum Fuel Mass: 160 g
Solar Radiation Pressure (Spherical)	Coefficient (Cr): 1 Area: 0.03 m <sup>2</sup>		
Radiation Pressure (Albedo/Thermal)	Coefficient (Ck): 1 Area: 0.03 m <sup>2</sup>		
GPS Solar Radiation Pressure	K1: 1 K2: 1		

Fig 5.114: Spacecraft parameters and Fuel tank

The coefficient of drag is set to 300 cm<sup>2</sup> since the CubeSat is oriented in high drag mode.

It was assumed that each thruster would have a fuel mass of about 20 grams, since there were 2 thruster on one side the fuel mass was set to 40 grams. Also, there were 8 thrusters in total, hence the maximum or total fuel mass is set to 160 grams.

Using the propagation sequence in Astrogator, a stopping condition is stated to define the automatic engine sequence such as the attitude, engine and propagator of every maneuver performed. The altitude, engine and propagator input values are shown in Figure below

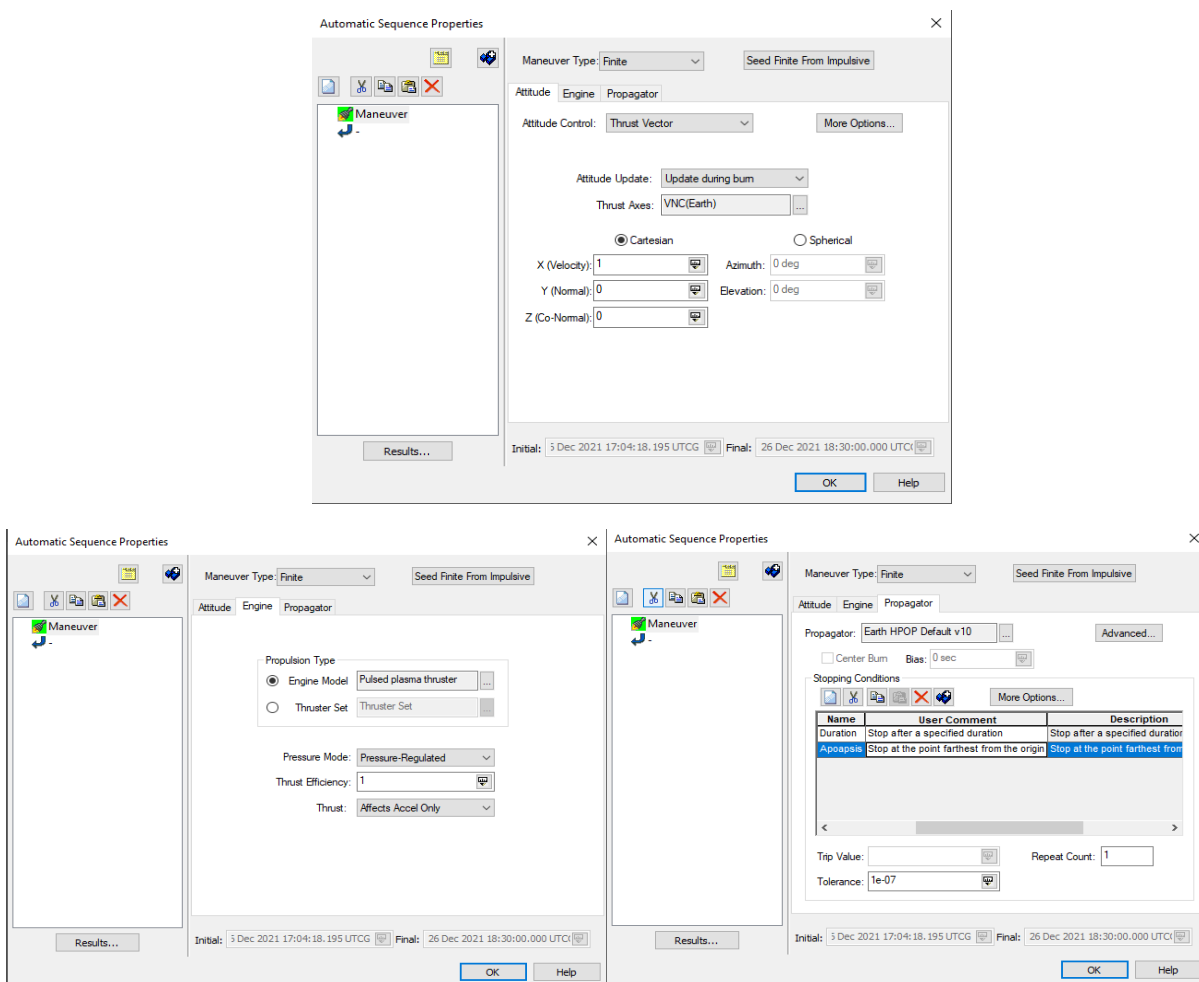


Fig 5.115: Thruster Attitude, Engine and Propagator

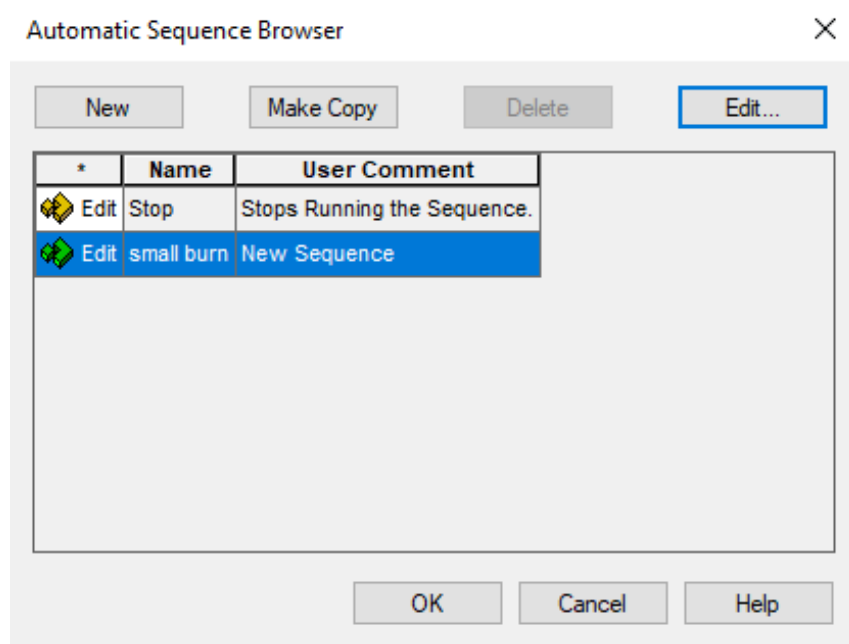


Fig 5.116: Stopping sequence

Once the engine auto sequences are set, the constraints for the propagation are set up. When the program runs the auto sequence to do the transfer, it requires stopping conditions namely the perigee and the apogee of the simulation's final orbit.

The initial state of CubeSat can be seen in figure below, there were two propagate segments called Apogee raise and Perigee raise

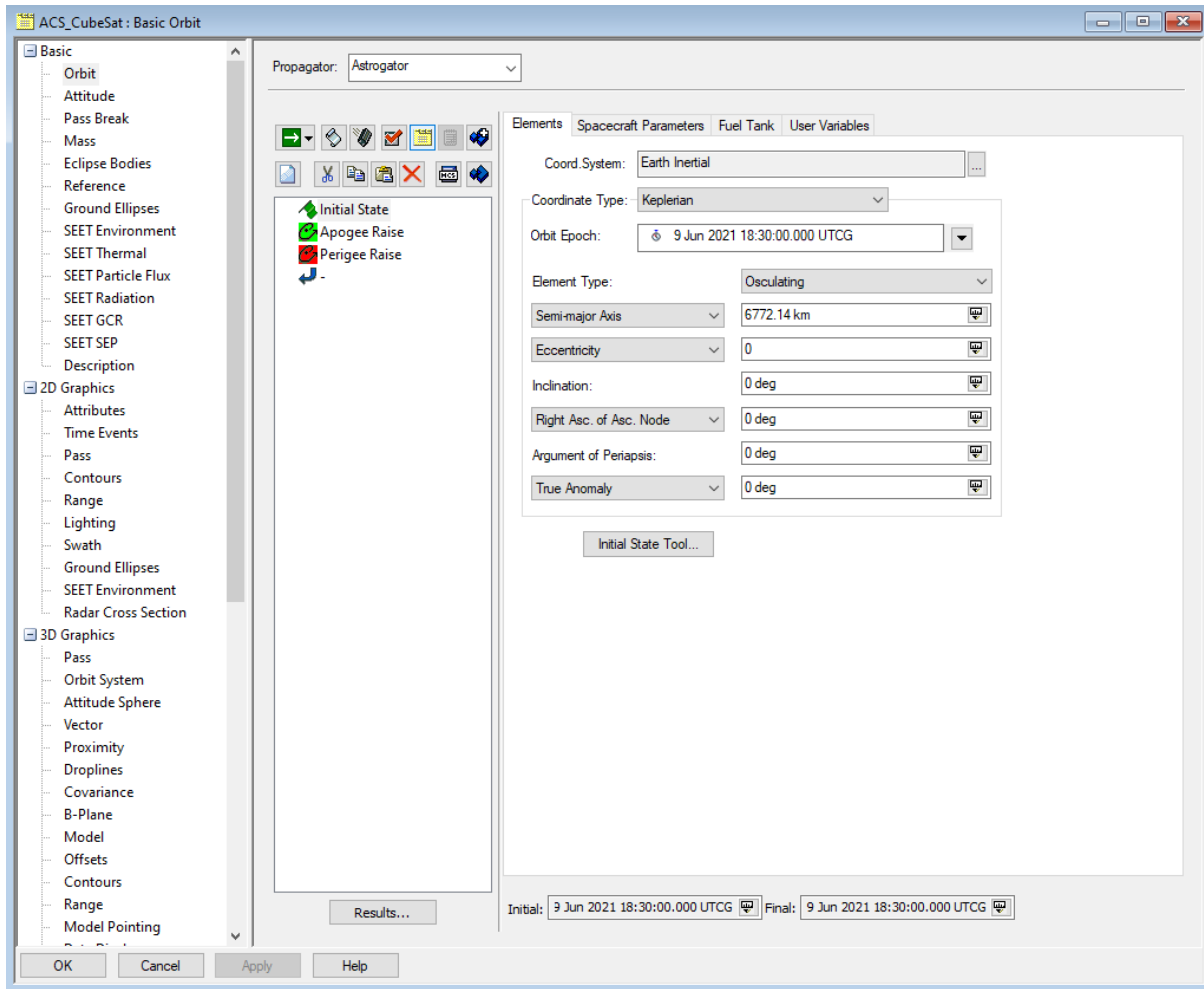


Fig 5.117: Initial State of CubeSat

Once the engine auto sequences are set, the constraints for the propagation are set up. When the program runs the auto sequence to do the transfer, it requires stopping conditions namely the perigee and the apogee of the simulation's final orbit.

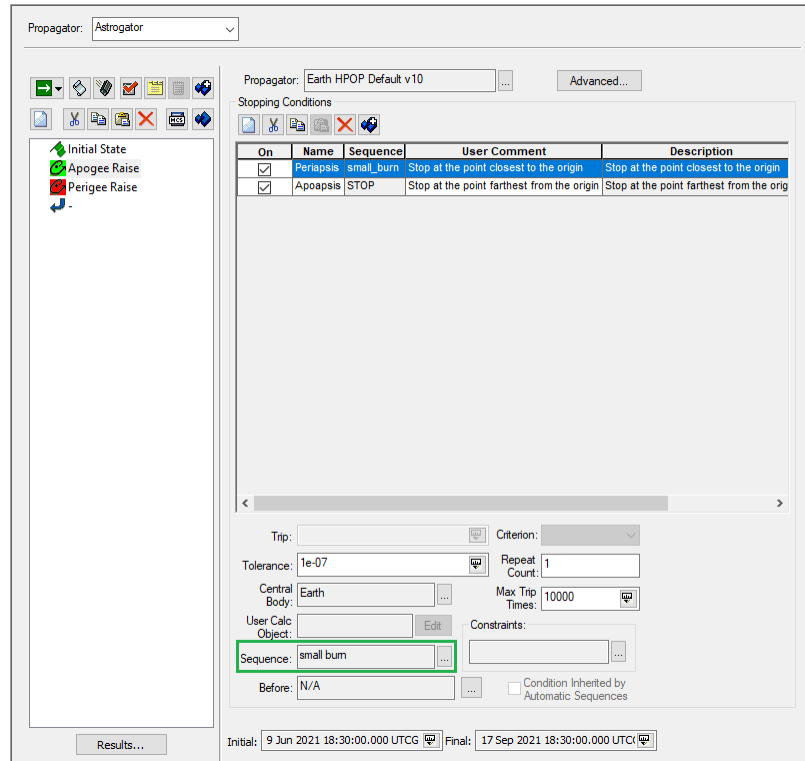


Fig 5.118: Apogee raise propagate segment options

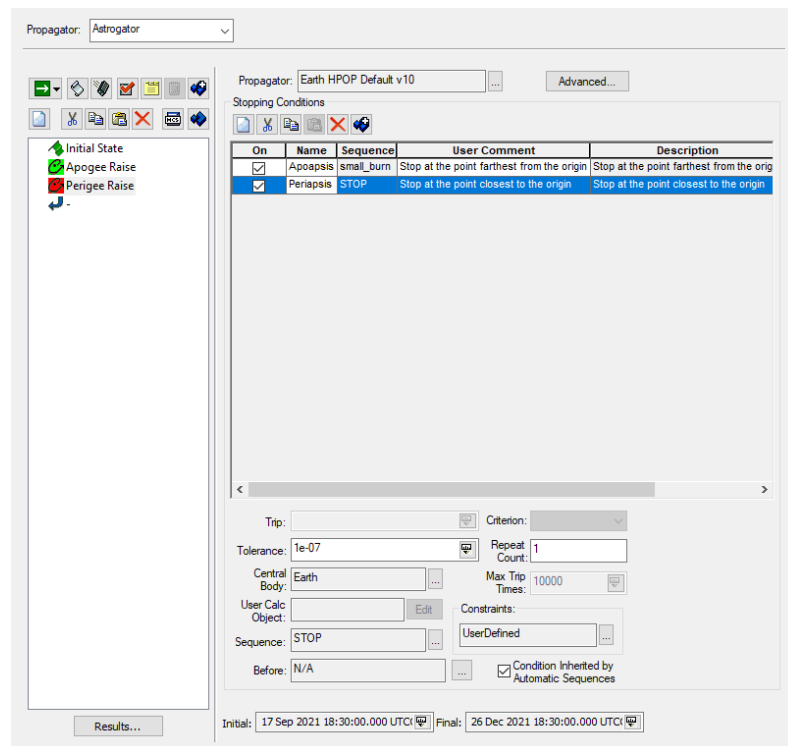


Fig 5.119: Perigee raise propagate segment options

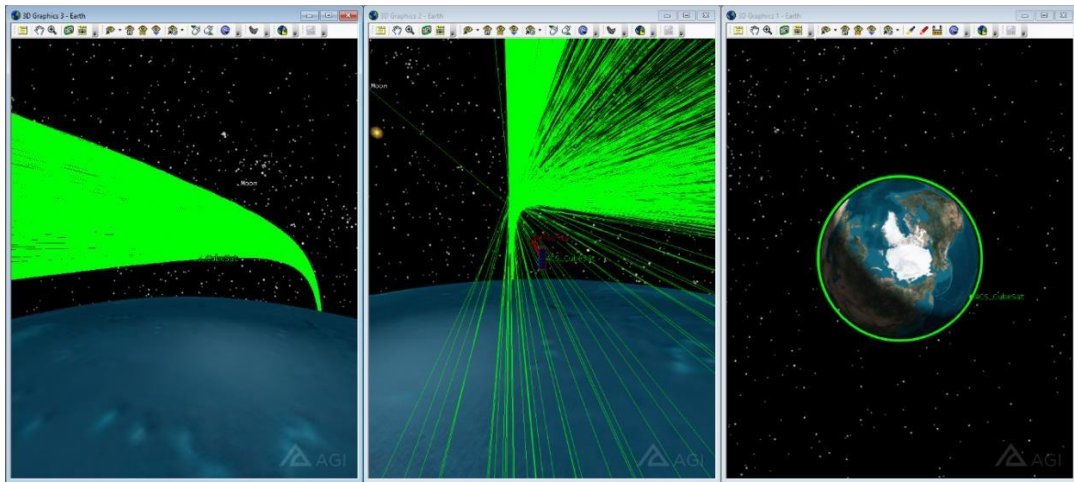


Fig 5.120: Apogee raise propagate segment

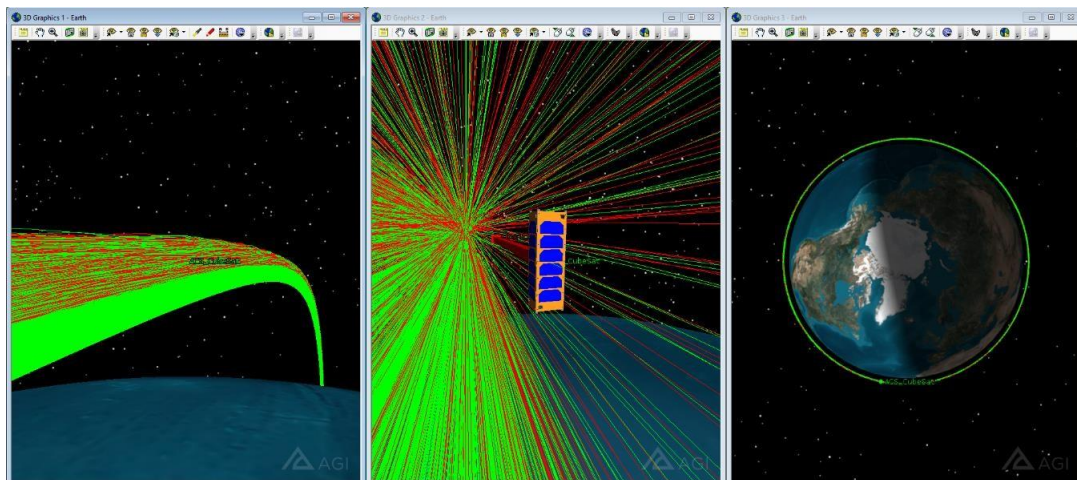


Fig 5.121: Perigee raise propagate segment

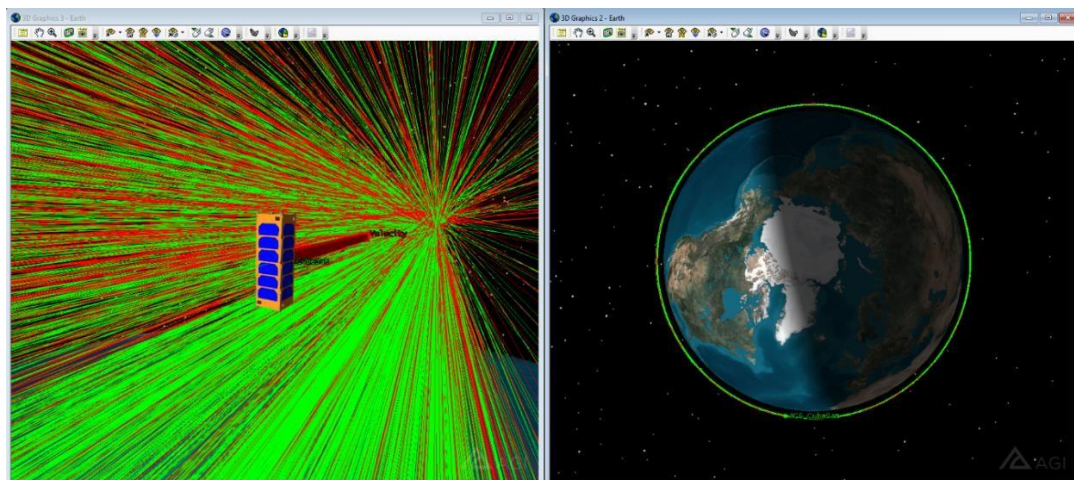


Fig 5.122: CubeSat iterations around Earth

### 5.4.3.3 Manoeuvre Summary

Table 5.8:Apogee Raise Maneouver Summary

<b>Maneuver Number</b>	<b>Segment</b>	<b>Start Time (UTCG)</b>	<b>Stop Time (UTCG)</b>	<b>Duration (sec)</b>	<b>Delta V (m/sec)</b>
<b>1</b>	small_burn	16:08.0	02:06.2	2758.191	0.026816
<b>2</b>	small_burn	48:14.9	34:20.0	2765.121	0.026883
<b>3</b>	small_burn	20:28.1	06:40.7	2772.668	0.026957
<b>4</b>	small_burn	52:43.8	39:04.9	2781.078	0.027038
<b>5</b>	small_burn	25:05.4	11:23.5	2778.093	0.027009
<b>6</b>	small_burn	57:34.5	43:49.2	2774.646	0.026976
<b>7</b>	small_burn	30:06.8	16:20.2	2773.411	0.026964
<b>8</b>	small_burn	02:40.1	48:53.4	2773.287	0.026963
<b>9</b>	small_burn	35:16.2	21:29.0	2772.752	0.026958
<b>10</b>	small_burn	07:49.4	54:02.3	2772.825	0.026958
<b>1544</b>	small_burn	39:11.4	25:52.3	2800.956	0.027306
<b>1545</b>	small_burn	12:34.4	59:10.7	2796.305	0.027261
<b>1546</b>	small_burn	45:53.3	32:25.8	2792.49	0.027224
<b>1547</b>	small_burn	19:08.4	05:43.0	2794.563	0.027244
<b>1548</b>	small_burn	52:25.9	39:09.2	2803.288	0.027329
<b>1549</b>	small_burn	25:51.2	12:42.6	2811.419	0.027408
<b>1550</b>	small_burn	59:17.5	30:00.0	1842.484	0.017962

Table 5.9: Perigee Raise Maneouver Summary

<b>Maneuver Number</b>	<b>Segment</b>	<b>Start Time (UTCG)</b>	<b>Stop Time (UTCG)</b>	<b>Duration (sec)</b>	<b>Delta V (m/sec)</b>
<b>1551</b>	small_burn	46:15.6	19:42.7	5607.093	0.054664
<b>1552</b>	small_burn	53:18.6	26:59.4	5620.794	0.054797
<b>1553</b>	small_burn	00:43.3	34:27.8	5624.464	0.054833
<b>1554</b>	small_burn	08:07.7	41:42.6	5614.902	0.05474
<b>1555</b>	small_burn	15:14.9	48:37.2	5602.254	0.054617
<b>1556</b>	small_burn	21:54.0	55:09.6	5595.523	0.054552
<b>1557</b>	small_burn	28:21.8	01:39.0	5597.177	0.054568
<b>1558</b>	small_burn	35:05.0	08:37.8	5612.845	0.054721
<b>1559</b>	small_burn	42:07.1	15:37.8	5610.707	0.0547
<b>2308</b>	small_burn	14:04.5	49:05.1	5700.692	0.055728
<b>2309</b>	small_burn	24:08.8	59:15.5	5706.673	0.055786
<b>2310</b>	small_burn	34:19.5	09:16.2	5696.784	0.05569
<b>2311</b>	small_burn	44:12.4	18:58.4	5686.042	0.055585
<b>2312</b>	small_burn	53:36.8	28:13.2	5676.363	0.055491
<b>2313</b>	small_burn	02:46.4	37:21.5	5675.134	0.055479
<b>2314</b>	small_burn	12:06.3	46:58.9	5692.547	0.055649
<b>2315</b>	small_burn	21:51.1	56:40.5	5689.37	0.055619

Table 5.10: Apogee raise statistics

<b>Apogee Raise Condition</b>	
<b>Global Statistics</b>	
<b>Total Duration</b>	4321215.773 s
<b>Total Est./Act. Finite Burn Duration</b>	4321215.773 s
<b>Total Delta V</b>	42.069578 m/s
<b>Total Fuel Used</b>	0.014 kg

Initial: 9<sup>th</sup> Jun 2021 18:30:00.000 UTCG

Final: 17<sup>th</sup> Sep 2021 18:30:00.000 UTCG

Table 5.11: Perigee raise statistics

<b>Perigee Raise Condition</b>	
<b>Global Statistics</b>	
<b>Total Duration</b>	4321339.640 s
<b>Total Est./Act. Finite Burn Duration</b>	4321339.640 s
<b>Total Delta V</b>	42.186729 m/s
<b>Total Fuel Used</b>	0.014 kg

Initial : 17 Sep 2021 18:30:00.000 UTCG

Final : 26 Dec 2021 18:30:00.000 UTCG

There were a total of 2315 finite burns which lasted roughly 6 months or around 8642555.413 seconds.

The Apogee raise segment took about 4321215.773 seconds which lasted from 9 Jun 2021 18:30:00.000 UTCG to 17 Sep 2021 18:30:00.000 UTCG.

Whereas the Perigee raise segment took about 4321339.640 seconds which was from 17 Sep 2021 18:30:00.000 UTCG to 26 Dec 2021 18:30:00.000 UTCG

The green lines indicate Apogee iterations and red lines indicates Perigee iterations.

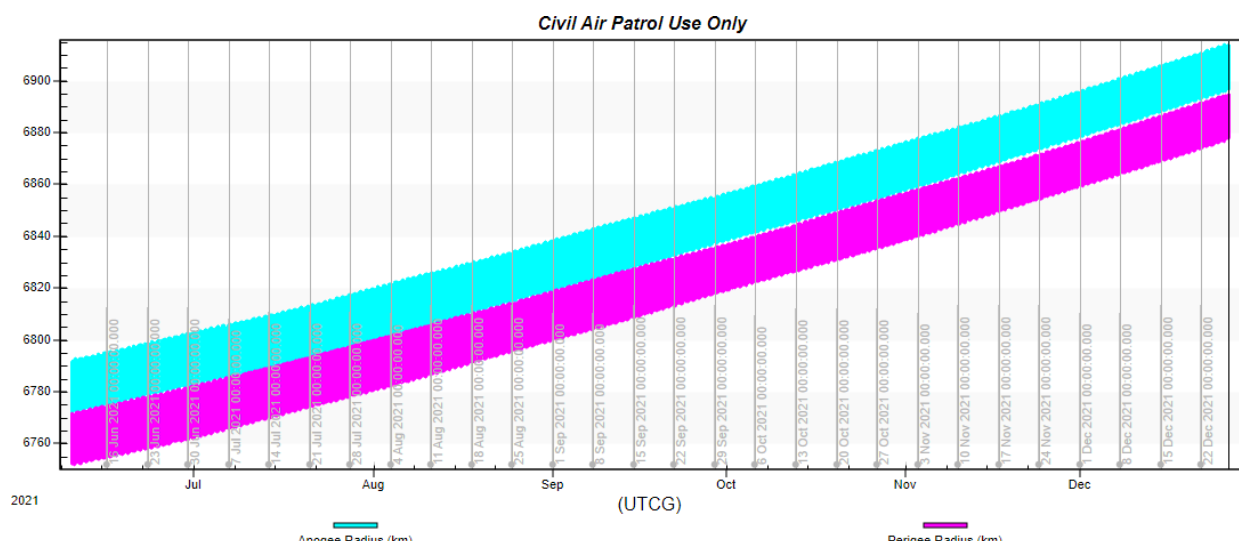


Fig 5.123: Apogee V/S Perigee radius Increment over time

#### 5.4.4 LIFETIME ANALYSIS

The Lifetime tool estimates the orbital lifetime of a satellite and provides the corresponding date of decay. It should be emphasized that although the Lifetime computations are based on sophisticated orbital theory and accurate environment models, the result is still an estimate.

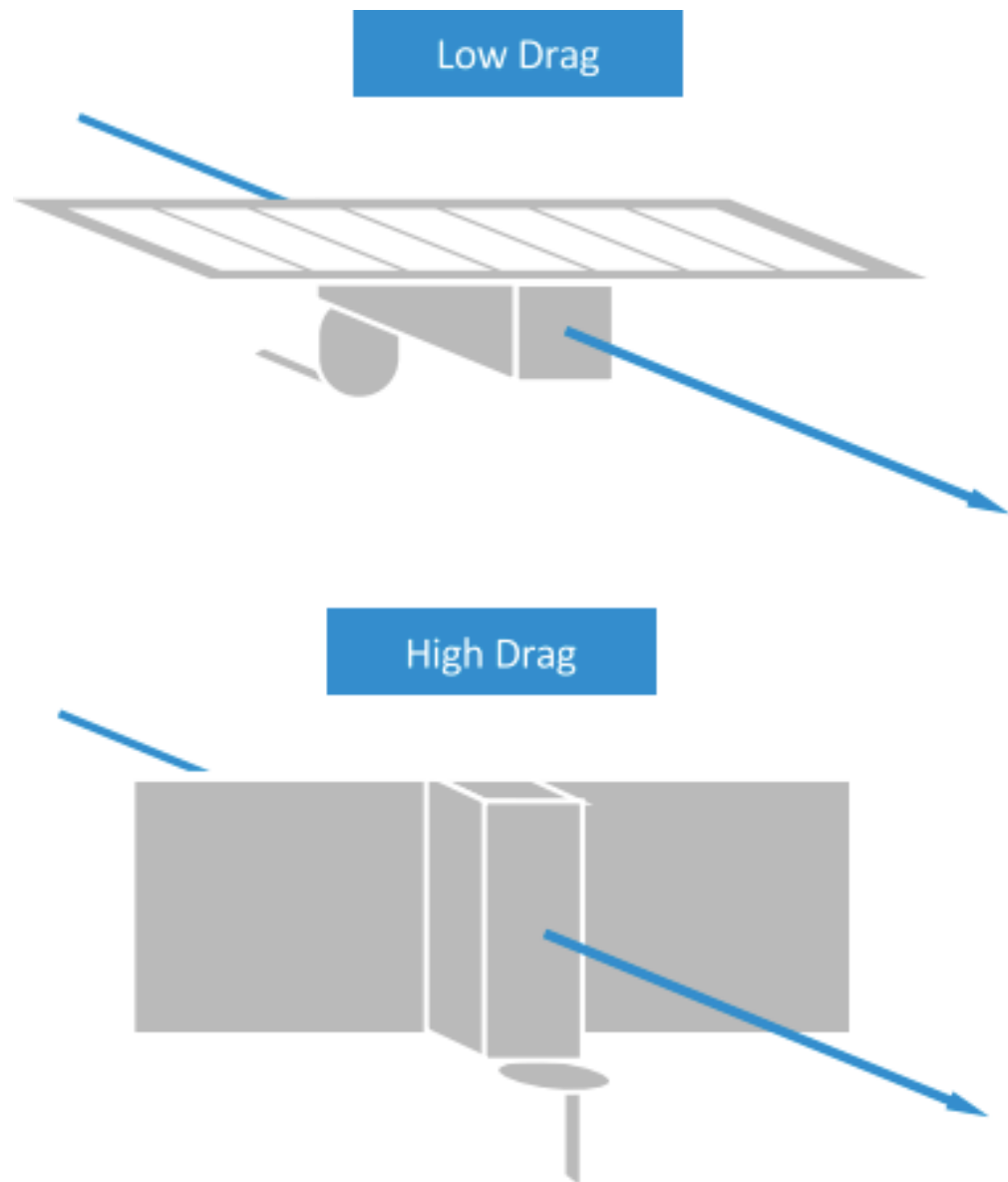


Fig 5.124: Low Drag V/S High Drag Configuration

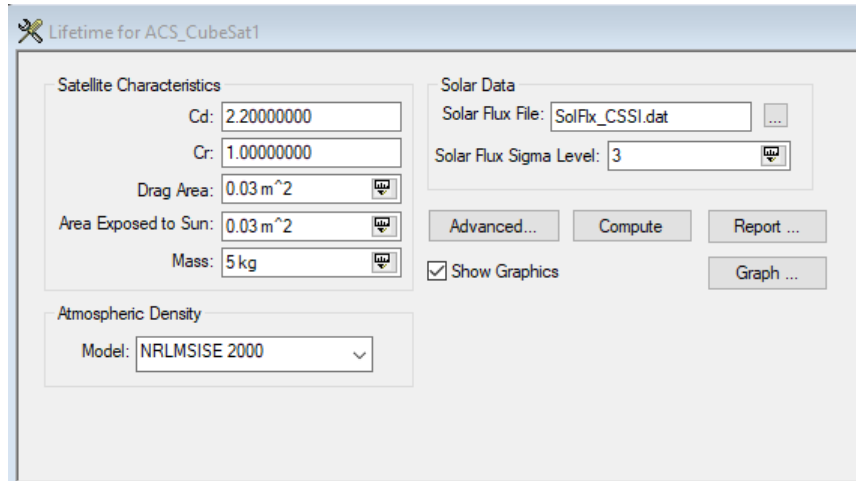


Fig 5.125: Lifetime Analysis tool in STK

Cd (Drag Coefficient): The satellite's drag coefficient, usually taken to be between 2.0 and 2.2.

Cr (Solar Radiation Pressure Coefficient): The satellite's SRP coefficient. A value of 0 indicates that the satellite is transparent to solar radiation; a value of 1 indicates that it is perfectly absorbing.

Drag area:  $30 \times 10 \text{ cm}^2$  (since it's a 3U CubeSat and it is in High drag configuration.)

Area exposed to Sun:  $30 \times 10 \text{ cm}^2$

Mass: 5kg

Atmospheric Density:

Model used was NRLMSISE 2000,

It is an Empirical density model developed by the US Naval Research Laboratory based on satellite data. Finds the total density by accounting for the contribution of N, N<sub>2</sub>, O, O<sub>2</sub>, He, Ar and H. Includes anomalous oxygen. 2000 version, valid range of 0-1000 km. This implementation always calls the gtd7d routine (in contrast to switching between it and gtd7) per the recommendation of Mike Picone, one of the code authors.

**Solar Flux File:** An ASCII file containing predicted values of solar flux and geomagnetic activity. The file may follow the format of CSSI long term predicts (.dat).

Solar Flux Sigma Level was set to 3 as the avg value.

Case 1: Considering a CubeSat is at an altitude of about 400 km

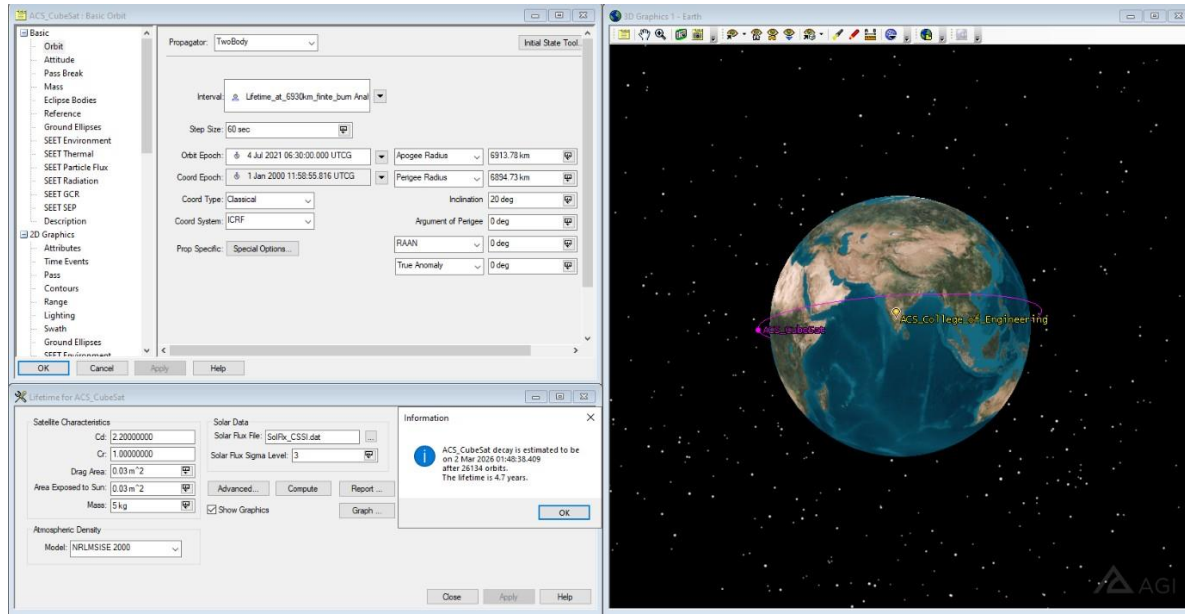


Fig 5.126: Lifetime of CubeSat at 400 km

Altitude: 400Km

Estimated Lifetime: 1.2 years

The CubeSat is estimated to decay on 12th September 2022 at 01:56:04.904 after 6855 orbits.

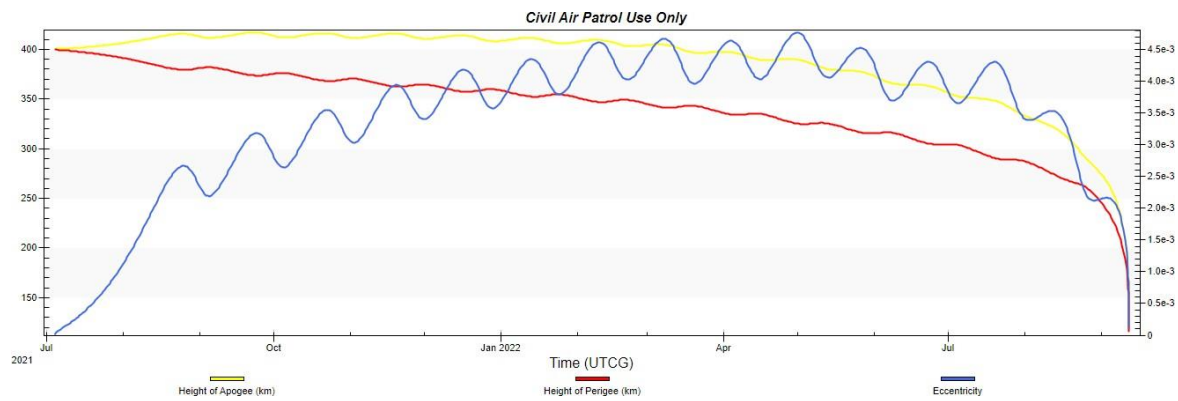


Fig 5.127: Lifetime graph of CubeSat at 400 km

Case 2 : Considering a CubeSat is at an altitude of about 450 km

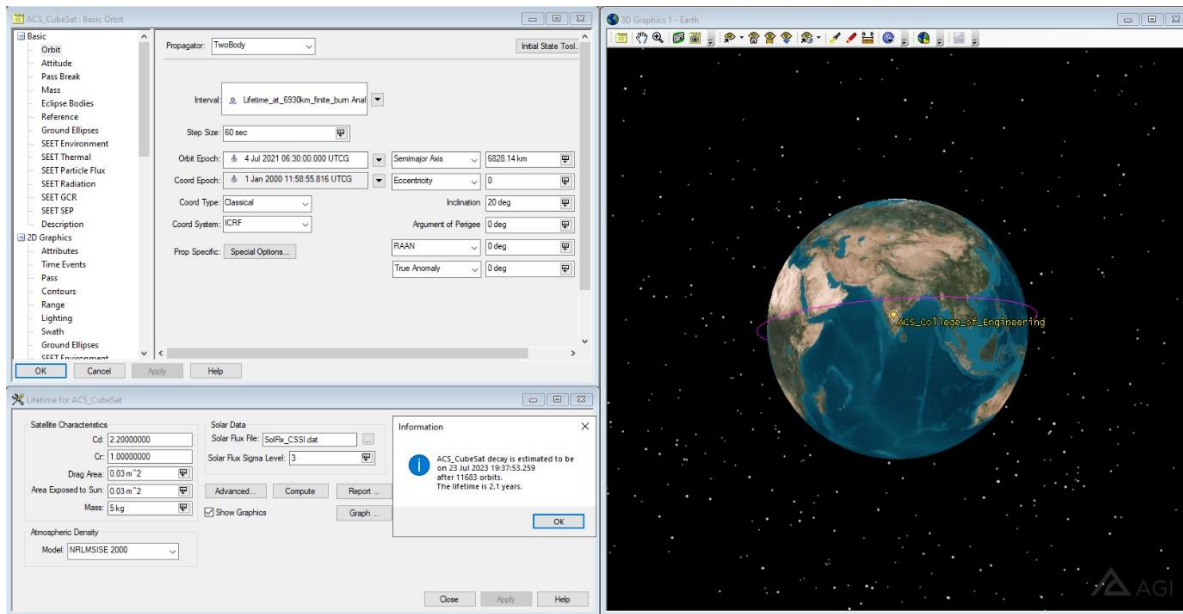


Fig 5.128: Lifetime of CubeSat at 450 km

Altitude: 450Km

Estimated Lifetime: 2.1 years

The CubeSat is estimated to decay on 23<sup>rd</sup> July 2023 at 19:37:53.259 after 11683 orbits.

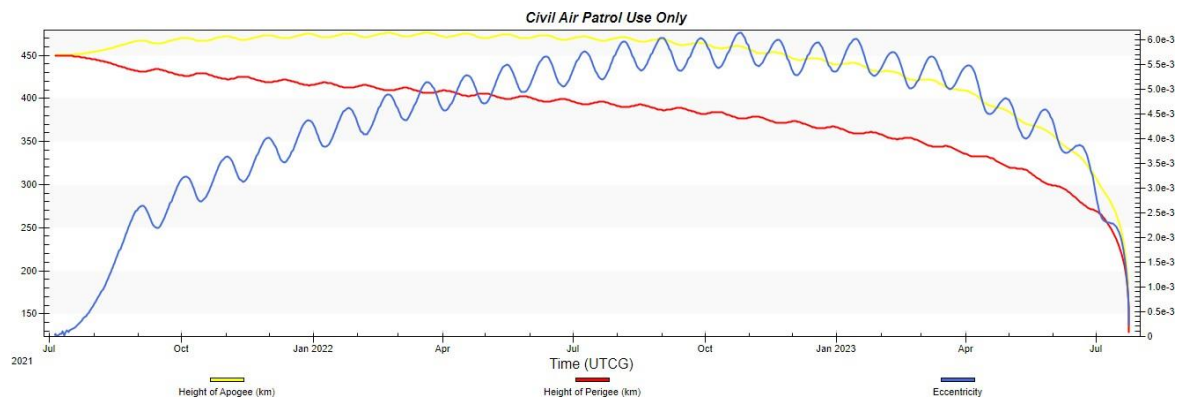


Fig 5.129: Lifetime graph of CubeSat at 450 km

Case 3: CubeSat after its orbital transfer i.e., using PPT to increasing the orbit

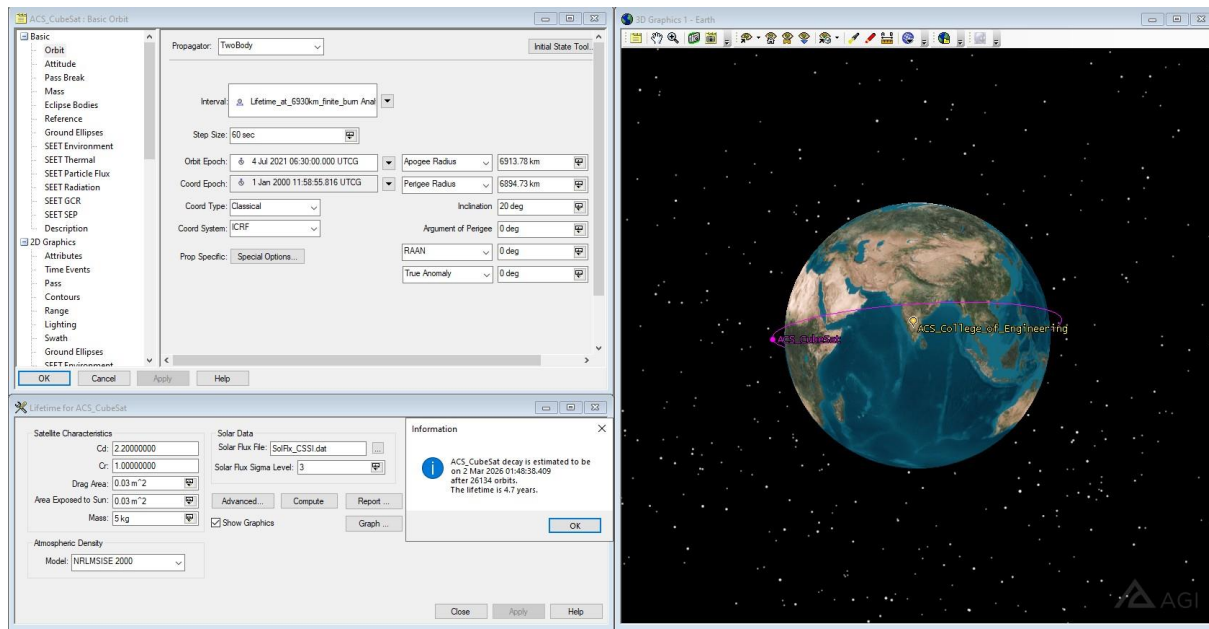


Fig 5.130: CubeSat after orbital transfer

Altitude: 515 km- 535 km

Estimated Lifetime: 4.7 years

The CubeSat is estimated to decay on 2<sup>nd</sup> March 2026 at 01:48:38.409 after 26134 orbits

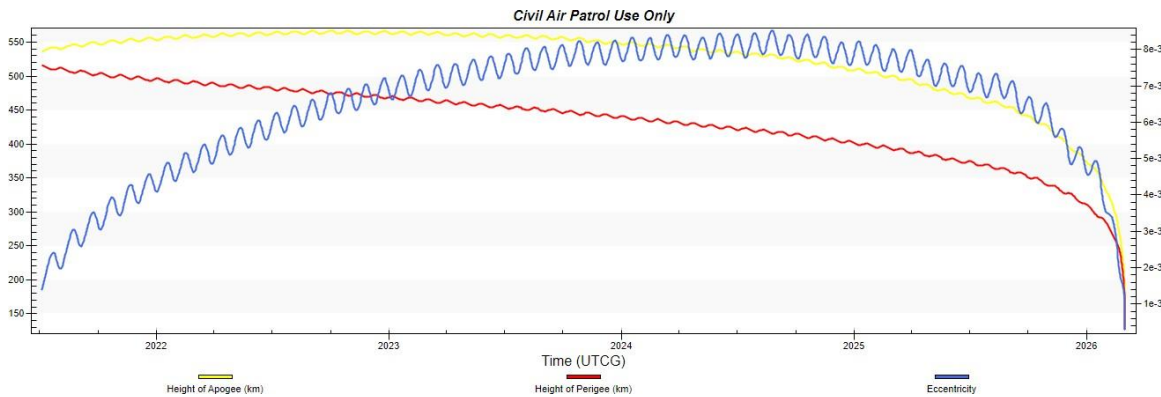


Fig 5.131: Lifetime graph of CubeSat after Orbit Transfer

### 5.4.5 SEET (Space Environment and Effect Tool)

This tool is used to determine the working temperature and Magnetic field interaction on the CubeSat. It can be found on the basic section of the satellite properties.

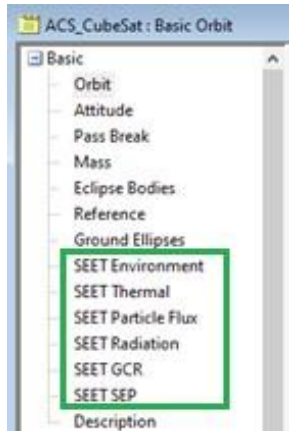


Fig 5.132: SEET Conditions

A screenshot of the 'Thermal Model' section. It contains the following parameters: Earth Albedo: 0.34, Material Emissivity: 0.82, Material Absorptivity: 0.75, Dissipation: 0 W, Cross-Sectional Area: 0.03 m<sup>2</sup>, Shape Model: Plate, and Normal Vector: ACS\_CubeSat Sun.

Fig 5.133: SEET Thermal model

A screenshot of the 'Magnetic Field Model' section. It includes: Main Field: IGRF, External Field: None, IGRF Update Rate: 1 day, and a 'South Atlantic Anomaly (SAA)' section with Channel: >23 MeV and Flux Level: Background + 3 Sigma.

Fig 5.134: Magnetic field model

In Magnetic field model the main model was chosen as IGRF( International Geomagnetic Reference Field) and all the other things were set as default.

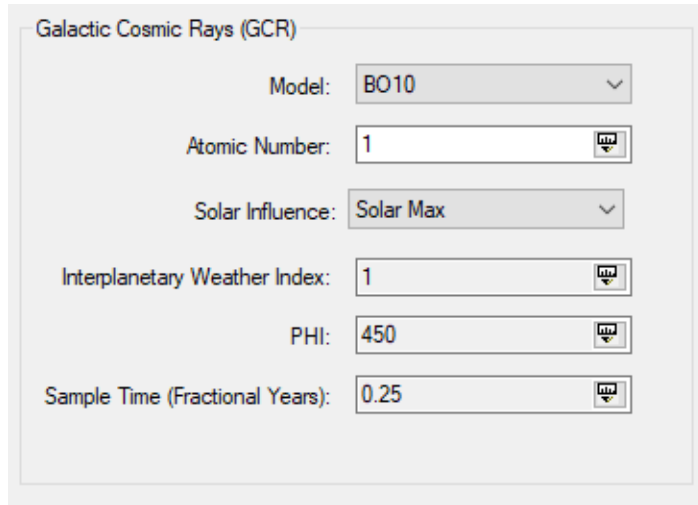


Fig 5.135: Galactic Cosmic Ray

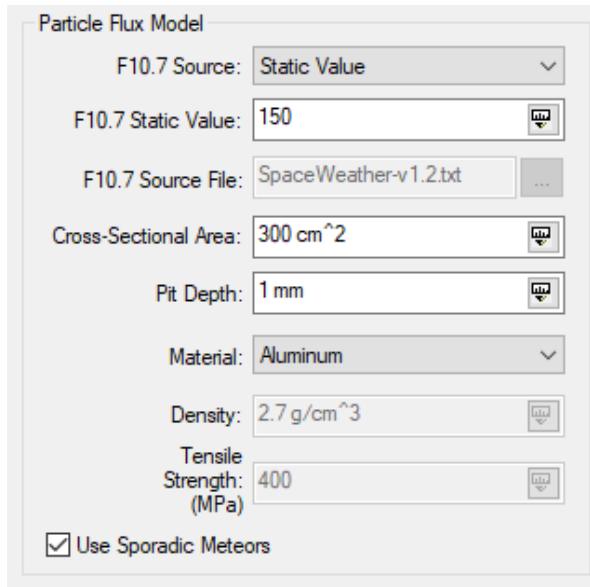


Fig 5.136: Particle Flux model

From these conditions, temperature and Magnetic Field of the CubeSat can be found.

In SEET thermal material absorptivity and emissivity typical values of Solar cells, silicon was used.

Using report manager and going into default installed styles, select satellite temperature and click on generate graph. Similarly select the Magnetic field (B Field V/S Total Intensity F) in the installed section and click on generate graph.

Table 5.10:Typical values of Solar cell used in Thermal model

Surface	Absorptance ( $\alpha$ )	Emittance ( $\varepsilon$ )	$\alpha/\varepsilon$
Polished beryllium	0.44	0.01	44.00
Goldized kapton (gold outside)	0.25	0.02	12.5
Gold	0.25	0.04	6.25
Aluminium tape	0.21	0.04	5.25
Polished aluminium	0.24	0.08	3.00
Aluminized kapton (aluminium outside)	0.14	0.05	2.80
Polished titanium	0.60	0.60	1.00
Black paint (epoxy)	0.95	0.85	1.12
Black paint (polyurethane)	0.95	0.90	1.06
—electrically conducting	0.95	0.80–0.85	1.12–1.19
Silver paint (electrically conducting)	0.37	0.44	0.84
White paint (silicone)	0.26	0.83	0.31
—after 1000 hours UV radiation	0.29	0.83	0.35
White paint (silicate)	0.12	0.90	0.13
—after 1000 hours UV radiation	0.14	0.90	0.16
Solar cells, GaAs (typical values)	0.88	0.80	1.10
Solar cells, silicon (typical values)	0.75	0.82	0.91
Aluminized kapton (kapton outside)	0.40	0.63	0.63
Aluminized FEP	0.16	0.47	0.34
Silver coated FEP (SSM)	0.08	0.78	0.10
OSR	0.07	0.74	0.09

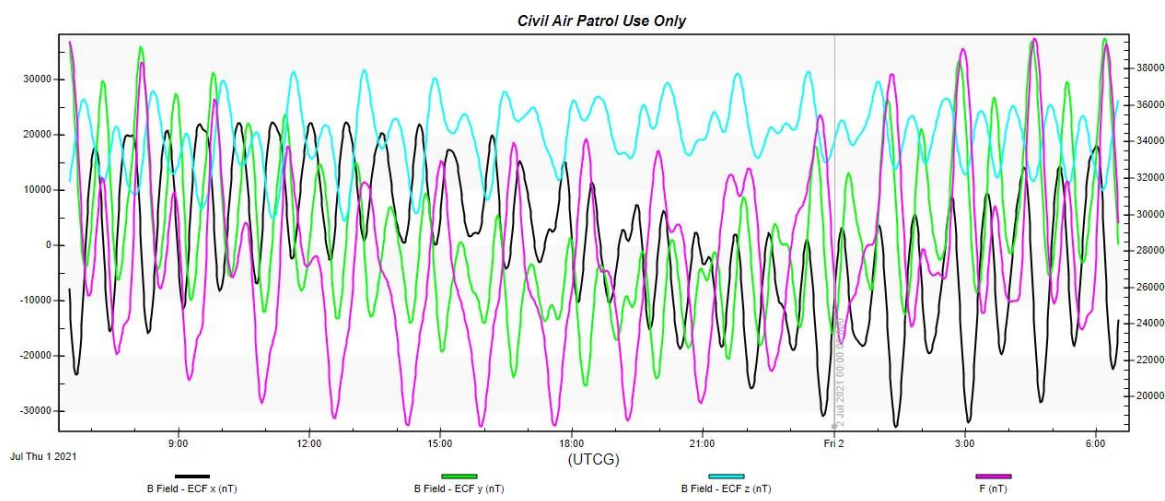


Fig 5.137: Magnetic Field (B Field V/S Total Intensity F)

#### 5.4.6 SATELLITE TEMPERATURE

The Maximum temperature was found to be 114.353 °C , whereas the Minimum temperature was about -80.546 °C. These values are under the operating temperatures which is from -100°C to 125°C.

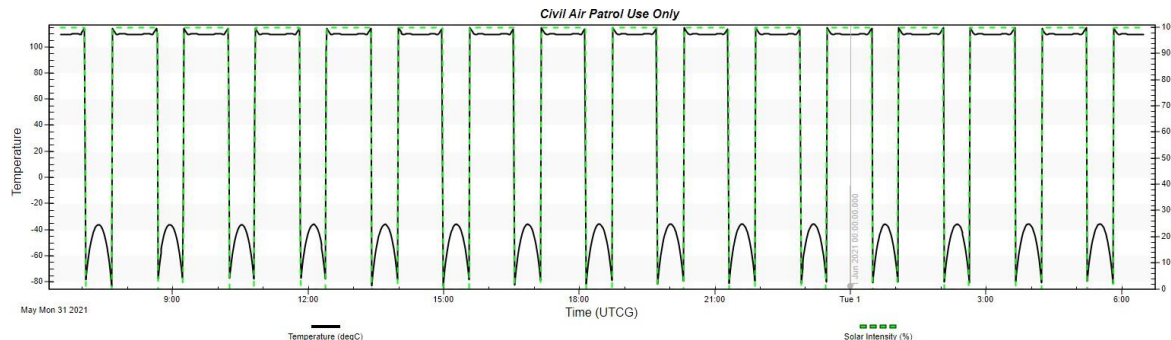


Fig 5.138: CubeSat Temperature

Table 5.11: Operating temperature and Survival temperature

Component/ System	Operating Temperature (C)	Survival Temperature (C)
Digital electronics	0 to 50	-20 to 70
Analog electronics	0 to 40	-20 to 70
Batteries	10 to 20	0 to 35
IR detectors	-269 to -173	-269 to 35
Solid-state particle detectors	-35 to 0	-35 to 35
Momentum wheels	0 to 50	-20 to 70
Solar panels	-100 to 125	-100 to 125

Table 5.12: Satellite temperature

Time (UTCG)	Temperature (deg C)	Solar Flux (W/m^2)	Solar Intensity (%)
<b>1 Jul 2021 06:30:00.000</b>	109.424	1320.695754	100.0000
<b>1 Jul 2021 06:40:00.000</b>	109.835	1320.719418	100.0000
<b>1 Jul 2021 06:56:00.000</b>	114.353	1320.718475	100.0000
<b>1 Jul 2021 07:06:00.000</b>	-54.795	1320.693636	0.0000
<b>1 Jul 2021 07:26:00.000</b>	-79.316	1320.634802	0.0000
<b>1 Jul 2021 08:00:00.000</b>	109.267	1320.676078	100.0000
<b>1 Jul 2021 08:30:00.000</b>	113.740	1320.715952	100.0000
<b>1 Jul 2021 09:00:00.000</b>	-75.089	1320.632743	0.0000
<b>1 Jul 2021 10:00:00.000</b>	110.381	1320.716922	100.0000
<b>1 Jul 2021 11:00:00.000</b>	109.617	1320.637794	100.0000
<b>1 Jul 2021 12:00:00.000</b>	-52.415	1320.652286	0.0000
<b>1 Jul 2021 13:00:00.000</b>	109.832	1320.703193	100.0000
<b>1 Jul 2021 14:00:00.000</b>	109.479	1320.611452	100.0000
<b>1 Jul 2021 15:00:00.000</b>	-56.460	1320.676621	0.0000
<b>1 Jul 2021 16:00:00.000</b>	109.428	1320.671790	100.0000
<b>1 Jul 2021 17:00:00.000</b>	112.598	1320.604943	100.0000
<b>1 Jul 2021 18:00:00.000</b>	113.731	1320.692292	100.0000
<b>1 Jul 2021 19:00:00.000</b>	109.346	1320.632905	100.0000
<b>2 Jul 2021 05:07:00.000</b>	-80.546	1320.663829	0.0000

## **5.5 CONCLUSION**

Pulsed Plasma Thrusters are a viable choice for a CubeSat's propulsion component because of their low power input, high specific impulse, and geometric scalability. A micro-PPT is even more appealing because to its tiny size, which allows for integration into a 3U CubeSat.

A PPT performance model (Laperierre et al. 2005,) and a PPT ablation model (Gatsonis et al, 2005; Stechmann 2007) was used to obtain the basic geometrical and performance characteristics of the micro-PPT. SolidWorks an Catia V5 was used for design, ANSYS for structural analysis (Modal and Random Vibrations), COMSOL for thermal design and analysis, and AGI:STK for propulsion and Orbital analysis.

### **Mechanical Design and Structural Analysis**

The mechanical design of the micro-PPT needed structural integrity in order to pass vibrational testing and retain the best practically achievable performance attributes.

SolidWorks was used to produce 3D models during the iterative design phase. The performance and ablation models offered performance parameters and geometrical aspects of the micro-PPT (Stechmann 2007).

Material selection was carried out in order to develop a micro-PPT capable of handling all essential loads and requirements. Vibrational testing was performed on materials that were added to the SolidWorks model. ANSYS was used to run a number of simulations to ensure structural integrity in the face of potential vibrational stresses. These loads were calculated using the NASA GEVS spaceflight verification document's worst-case scenario. Because the stresses and directional deformation caused by the loads were minimal, the design may proceed to space certification. The propulsion assembly's objective is to provide 3-axis yaw, pitch, and roll control of a 3U CubeSat.

### **Electrical Analysis**

The electrical analysis was necessary to obtain the Lorentz force which provides the thrust. A power distribution module and a marx circuit are used to charge the anode and cathode plates to a potential difference of 1500V.

The arc passing through the fuel causes it to ablate and sublimates and the heat of the arc changes the gas into plasma. The force of ablation causes the plasma to move between the charged electrodes thus completing the circuit. A 2T magnetic field is developed and the Lorentz force propels the plasma at an exhaust velocity of 13000m/s. Thus, from the Lorentz force formula:

$$\mathbf{F} = q(\mathbf{E} + \mathbf{V} \times \mathbf{B}) \quad (5.5)$$

The thrust thus obtained was 49uN. The specific impulse is computed as:

$$I_{sp} = F / ((dm/dt) g) \quad (5.6)$$

Where,

$$dm/dt = F/V \quad (5.7)$$

The value of the specific impulse obtained was 1561s.

### **Thermal Analysis**

Thermal Analysis was performed on the propellant and heat transfer from the spark ignition can be seen, COMSOL was used to perform the thermal analysis as it offers the best results for Simulation.

### **Propulsion and Orbital Analysis**

Orbit analysis was performed using the STK software. The propulsion subsystem is based on the Pulsed Plasma electromagnetic thruster.

It is able to perform an orbit transfer from the deployment from the ISS at an altitude of 400 km. It was able to successfully increase its orbit with an apogee of 535 km and a perigee of 515 km.

This total orbit transfer requires approximately 28g of propellant. Once the CubeSat reaches its desired orbit its lifetime increased to 4.7 years and it was expected to decay after 26134 orbits around the Earth.

For comparison without propulsion system our analysis shows that the CubeSat would decay in 1.2 years after just 6855 orbits around the Earth.

## References

1. Burton, R.L., 2010. Pulsed plasma thrusters. Encyclopedia of Aerospace Engineering.
2. Igarashi, M., Kumagai, N., Sato, K., Tamura, K., Takegahara, H., Okamoto, H., Wakizono T. and Hashimoto, H., 2001. Performance improvement of pulsed plasma thruster for micro satellite. *27th IEPC*.
3. Zhang, Z., Ling, W.Y.L., Tang, H., Cao, J., Liu, X. and Wang, N., 2019. A review of the characterization and optimization of ablative pulsed plasma thrusters. *Reviews of Modern Plasma Physics*, 3(1), pp.1-41.
4. Eslava, S., Marchetto, J. and Scougal, E., 2014. Design of a Micro-Pulsed Plasma Thruster for a 3U CubeSat. *Worcester Polytechnic Inst., Major Qualifying Project Rept. NAG-1302, Worcester, MA*.
5. Hoskins, W. and Cassady, R., 2000. Applications for pulsed plasma thrusters and the development of small PPTs for microspacecraft. In *36th AIAA/ASME/SAE/ASEE Joint Propulsion Conference and Exhibit* (p. 3434).
6. Chen, E., 2006. Gas-Fed Pulsed Plasma Thrusters: From Spark Plugs to Laser Initiation.
7. Markusic, T.E., Cassibry, J.T. and Thio, Y.C.F., 2002. *Design of a high-energy, two-stage pulsed plasma thruster*. AIAA.
8. Dali, H., Wansheng, Z. and Xiaoming, K., 2008. Operation analysis of pulsed plasma thruster. *Acta Astronautica*, 62(6-7), pp.404-409.
9. Wu, Z., Sun, G., Huang, T., Liu, X., Xie, K. and Wang, N., 2018. Optimization of the energy distribution in ablative pulsed plasma thrusters. *AIAA Journal*, 56(8), pp.3024-3034.
10. Zeng, L., Wu, Z., Sun, G., Huang, T., Xie, K. and Wang, N., 2019. A new ablation model for ablative pulsed plasma thrusters. *Acta Astronautica*, 160, pp.317-322.
11. Scougal, E.A., Marchetto, J.D. and Eslava, S.A., 2014. Design of a micro-Pulsed Plasma Thruster for a 3U CubeSat.
12. Wu, Z., Sun, G., Huang, T., Liu, X., Xie, K. and Wang, N., 2018. Optimization of the energy distribution in ablative pulsed plasma thrusters. *AIAA Journal*, 56(8), pp.3024-3034.

13. Nawaz, A., Albertoni, R. and Auweter-Kurtz, M., 2010. Thrust efficiency optimization of the pulsed plasma thruster SIMP-LEX. *Acta Astronautica*, 67(3-4), pp.440-448.
14. Peradzyński, Z., Makowski, K. and Kurzyna, J., 2019. Early stage of the discharge in ablative pulsed plasma thrusters. *Plasma Sources Science and Technology*, 28(2), p.024001.
15. Hoskins, W. and Cassady, R., 2000. Applications for pulsed plasma thrusters and the development of small PPTs for microspacecraft. In *36th AIAA/ASME/SAE/ASEE Joint Propulsion Conference and Exhibit* (p. 3434).
16. Design and Analysis of a 6U CubeSat and Mission by Snyder., Benjamin J., Andreani., Tristan P., Beerbower., Edward J., Clavijo., Roberto., Joy., Samuel Preston., Lee., Gavin S., Valero Araujo., Jeremiah W.
17. <https://help.agi.com/stk/index.htm#training/txhohmann.htm?TocPath=Training%257CLevel%25203%2520-%2520Focused%257CFeature%2520Specific%257C%252033>
18. [https://help.agi.com/stk/index.htm#training/Astro\\_AutoSequence.htm](https://help.agi.com/stk/index.htm#training/Astro_AutoSequence.htm)
19. Benson, Scott, and John Frus. "Advanced pulsed plasma thruster electrical components." *37th Joint Propulsion Conference and Exhibit*. 2001.
20. Scharlemann, C., et al. "Pulsed plasma thruster variations for improved mission capabilities." *36th AIAA/ASME/SAE/ASEE Joint Propulsion Conference and Exhibit*. 2000.
21. Shaw, Peter, and Vaios Lappas. "Modeling of a pulsed plasma thruster; simple design, complex matter." *Space Propulsion Conference*. 2010.
22. Northway, Paige, et al. "Pulsed plasma thruster gains in specific thrust for CubeSat propulsion." *53rd AIAA/SAE/ASEE Joint Propulsion Conference*. 2017.
23. Huang, Tiansun, et al. "Study on propellant utilization in pulsed plasma thrusters." *Acta Astronautica* 182 (2021): 578-586.
24. Myers, Roger, et al. "Pulsed plasma thruster technology for small satellite missions." (1995).